TECHNICAL SUPPORT DOCUMENT FOR VERSION 6 OF THE COMMUNITY MULTISCALE AIR QUALITY MODEL

October 2026

U.S. Environmental Protection Agency
Office of Air and Radiation
Air Quality Assessment Division
Methods and Model Development Branch
Research Triangle Park, North Carolina

List of Tables 2
List of Figures 3
Acronyms 7
Acknowledgement 9
1. Introduction 9
2. CMAQ version 6.0 Summary of Updates 10
2.1 Chemical Mechanisms 11
2.2 Natural Emissions 13
2.3 Dry Deposition 14
2.4 Meteorology and Urban Mixing 16
3. Model Configuration 16
3.1 Model Domains 17
3.2 Meteorological Inputs 17
3.3 Emission Inputs 18
3.4 Initial and Boundary Conditions 19
3.5 Model Science Option Settings 19
4. Evaluation 20
4.1 Ozone Evaluation 22
4.2 $PM_{2.5}$ Evaluation 32
5. Model Version Intercomparison 49
5.1 Seasonal Ozone Comparison for CMAQv5.5 and CMAQv6.0 50
5.2 Seasonal $PM_{2.5}$ Comparison for CMAQv5.5 and CMAQv6.0 54
6. Incremental Testing of Significant Model Updates 58
6.1 Chemistry vs. Non-chemistry Increments 59
6.2 Emissions Incremental Testing 62
6.3 Dry Deposition Incremental Testing 76
6.4 Meteorology and Urban Mixing Incremental Testing 78
7. Appendix 83
7.1 Summary of Model Performance Statistics 83
References 95

List of Tables

Table 4-1 Hemispheric (108NHEMI domain) CMAQ model configurations.....21
Table 4-2 CONUS (12US1 domain) CMAQ model configurations. 22
Table 7-1 Performance statistics for $PM_{2.5}$ at AQS Sites in 2022 using CMAQv6.0 CB6R5 with 2022he emissions consistent with 2022v2 air quality modeling platform.....84
Table 7-2 Performance statistics for $PM_{2.5}$ SO_4^{2-} at CSN Sites in 2022 using CMAQv6.0 CB6R5 with 2022he emissions consistent with 2022v2 air quality modeling platform.....85
Table 7-3 Performance statistics for $PM_{2.5}$ SO_4^{2-} at IMPROVE Sites in 2022 using CMAQv6.0 CB6R5 with 2022he emissions consistent with 2022v2 air quality modeling platform.....86
Table 7-4 Performance statistics for $PM_{2.5}$ NO_3^- at CSN Sites in 2022 using CMAQv6.0 CB6R5 with 2022he emissions consistent with 2022v2 air quality modeling platform.....87
Table 7-5 Performance statistics for $PM_{2.5}$ NO_3^- at IMPROVE Sites in 2022 using CMAQv6.0 CB6R5 with 2022he emissions consistent with 2022v2 air quality modeling platform.....88
Table 7-6 Performance statistics for $PM_{2.5}$ OC at CSN Sites in 2022 using CMAQv6.0 CB6R5 with 2022he emissions consistent with 2022v2 air quality modeling platform.....89
Table 7-7 Performance statistics for $PM_{2.5}$ OC at IMPROVE Sites in 2022 using CMAQv6.0 CB6R5 with 2022he emissions consistent with 2022v2 air quality modeling platform.....90
Table 7-8 Performance statistics for $PM_{2.5}$ EC at CSN Sites in 2022 using CMAQv6.0 CB6R5 with 2022he emissions consistent with 2022v2 air quality modeling platform.....91
Table 7-9 Performance statistics for $PM_{2.5}$ EC at IMPROVE Sites in 2022 using CMAQv6.0 CB6R5 with 2022he emissions consistent with 2022v2 air quality modeling platform.....92
Table 7-10 Performance statistics MDA8 O_3 at AQS Sites in 2022 using CMAQv6.0 CB6R5 with 2022he emissions consistent with 2022v2 air quality modeling platform.....93
Table 7-11 Performance statistics for MDA8 O_3 at CASTNET Sites in 2022 using CMAQv6.0 CB6R5 with 2022he emissions consistent with 2022v2 air quality modeling platform.....94

List of Figures

Figure 3-1 Model domain and vertical grid structure. (a) Northern hemisphere (108NHEMI domain) with CONUS (12US1) domain shaded in grey. (b) Vertical layer structure for 44- and 35-layer configurations used for the 108NHEMI and 12US1 simulations, respectively. Figure from Mathur et al. (2017), Figure 2. 17
Figure 4-1 Monthly average ozone from 2022 northern hemisphere simulations for CB6R5M with and without aerosol nitrate photolysis and for CRACMM3M (also includes aerosol nitrate photolysis) compared to ozonesonde observations averaged by latitude bands and separated by model layers. 23
Figure 4-2. Seasonally averaged vertical profiles of pairwise model-measurement matches for CMAQv5.5 and CMAQv6.0 northern hemisphere simulations for CRACMM3M and CB6R5M and In-service Aircraft for a Global Observing System (IAGOS). The number of vertical profiles with valid ozone data in each altitude bin is listed on the right axis. There are more than 300 soundings with valid data in each season. 24
Figure 4-3 Monthly mean MDA8 ozone AQS observations and paired monthly mean model values at observation sites, separated by region. Table 4-2 provides more details on these simulations. 26
Figure 4-4 Performance statistics by simulation (along x-axis) and region (along y-axis) for MDA8 ozone from May – September at AQS monitoring sites. Region abbreviations refer to the following NOAA climate regions: NW=Northwest, W=West, SW=Southwest, NRP=Northern Rockies and Plains, S=South, UMW=Upper Midwest; OV=Ohio Vally, NE=Northeast, SE=Southeast. Table 4-2 provides more details on these simulations. 28
Figure 4-5 Winter (DJF) average MDA8 ozone bias at AQS sites for 12US1 simulations with CMAQv6.0 with CRACMM3 (top left), CMAQv5.5 with CRACMM2 (bottom left), CMAQv6.0 with CB6R5 (top right), and CMAQv5.5 with CB6R5 (bottom right). 29
Figure 4-6 Spring (MAM) average MDA8 ozone bias at AQS sites for 12US1 simulations with CMAQv6.0 with CRACMM3 (top left), CMAQv5.5 with CRACMM2 (bottom left), CMAQv6.0 with CB6R5 (top right), and CMAQv5.5 with CB6R5 (bottom right). 30
Figure 4-7 Summer (JJA) average MDA8 ozone bias at AQS sites for 12US1 simulations with CMAQv6.0 with CRACMM3 (top left), CMAQv5.5 with CRACMM2 (bottom left), CMAQv6.0 with CB6R5 (top right), and CMAQv5.5 with CB6R5 (bottom right). 31
Figure 4-8 Fall (SON) average MDA8 ozone bias at AQS sites for 12US1 simulations with CMAQv6.0 with CRACMM3 (top left), CMAQv5.5 with CRACMM2 (bottom left), CMAQv6.0 with CB6R5 (top right), and CMAQv5.5 with CB6R5 (bottom right). 32
Figure 4-9 Weekly averaged CMAQ predicted AOD for CMAQ version 5.5 and version 6.0 for the year 2022. Modeled predictions were compared to measurements at ground-based AERONET monitoring sites. 35
Figure 4-10 Annual mean bias in CMAQ predicted $PM_{2.5}$ for versions 5.5 and version 6.0 for the year 2022. Modeled $PM_{2.5}$ was compared to $PM_{2.5}$ measured at AQS monitoring sites. 36
Figure 4-11 Seasonal mean bias in $PM_{2.5}$ by NOAA Climate Region for a yearly simulation of 2022 on the 12US1 CONUS Domain. Modeled $PM_{2.5}$ was compared with measurements from AQS monitoring network. 37
Figure 4-12 Annual mean speciated $PM_{2.5}$ concentrations across all monitors for the CSN network (a, c) and the IMPROVE network (b, d) compared with CMAQv5.5 and CMAQv6.0 predicted speciated $PM_{2.5}$ from CRACMM (a, b) and CB6 (c, d) model runs. 38

Figure 4-13 Annual mean bias in CMAQ predicted SO_4 for version 5.5 and version 6.0 for the year 2022. Modeled SO_4 was compared to SO_4 measured at IMPROVE, CSN, and CASTNET monitoring sites. 39
Figure 4-14 Seasonal mean bias in SO_4 by NOAA Climate Region for a yearly simulation of 2022 on the 12US1 CONUS Domain. Modeled SO_4 was compared with filter measurements from the IMPROVE, CSN, and CASTNET monitoring network. 40
Figure 4-15 Predicted and observed $PM_{2.5}$ sulfur species concentrations in downtown Fairbanks, Alaska, during ALPACA 2022. 24-hr $PM_{2.5}$ SO_4 observations (every third day) are represented by black dots. The blue line represents predictions of $PM_{2.5}$ SO_4 and HMS with heterogeneous sulfur chemistry, while the red dashed-line is predicted $PM_{2.5}$ SO_4 without heterogeneous sulfur chemistry. 41
Figure 4-16 Annual mean bias in CMAQ predicted NO_3 for versions 5.5 and version 6.0 for the year 2022. Modeled NO_3 was compared to NO_3 measured at IMPROVE, CSN, and CASTNET monitoring sites. 42
Figure 4-17 Seasonal mean bias in NO_3 by NOAA Climate Region for a yearly simulation of 2022 on the 12US1 CONUS Domain. Modeled NO_3 was compared with filter measurements from the IMPROVE, CSN, and CASTNET monitoring network. 43
Figure 4-18 Annual mean bias in CMAQ predicted EC for versions 5.5 and version 6.0 for the year 2022. Modeled EC was compared to EC measured at IMPROVE and CSN monitoring sites. 44
Figure 4-19 Seasonal mean bias in EC by NOAA Climate Region for a yearly simulation of 2022 on the 12US1 CONUS Domain. Modeled EC was compared with filter measurements from the IMPROVE and CSN monitoring network....45
Figure 4-20 Annual mean bias in CMAQ predicted OC for versions 5.5 and version 6.0 for the year 2022. Modeled OC was compared to OC measured at IMPROVE and CSN monitoring sites. 46
Figure 4-21 Seasonal mean bias in OC by NOAA Climate Region for a yearly simulation of 2022 on the 12US1 CONUS Domain. Modeled OC was compared with filter measurements from the IMPROVE and CSN monitoring network....47
Figure 4-22 Annual mean bias in CMAQ predicted soil for versions 5.5 and version 6.0 for the year 2022. Modeled soil $PM_{2.5}$ was compared to soil $PM_{2.5}$ measured at IMPROVE and CSN monitoring sites. 48
Figure 4-23 Seasonal mean bias in soil by NOAA Climate Region for a yearly simulation of 2022 on the 12US1 CONUS Domain. Modeled soil was compared with filter measurements from the IMPROVE and CSN monitoring network....49
Figure 5-1 Seasonal mean ozone concentrations with BASEv55_HEMI_CB6R5M (left column), BASEv60_HEMI_CB6R5M (middle column), and the difference BASEv60_HEMI_CB6R5M – BASEv55_HEMI_CB6R5M (right column). 51
Figure 5-2 Seasonal mean ozone concentrations with BASEv55_HEMI_CRACMM2 (left column), BASEv60_HEMI_CRACMM3M (middle column), and the difference BASEv60_HEMI_CRACMM3M – BASEv55_HEMI_CRACMM2 (right column). 52
Figure 5-3 Seasonal average changes in ozone in CMAQv6.0 compared to CMAQv5.5 using CB6R5 for 12US1 domain. 53
Figure 5-4 Seasonal average changes in ozone in CMAQv6.0 compared to CMAQv5.5 using CRACMM for 12US1 domain. 54

Figure 5-5 Seasonal mean $PM_{2.5}$ concentrations with BASEv55_HEMI_CRACMM2 (left column), BASEv60_HEMI_CRACMM3M (middle column), and the difference BASEv60_HEMI_CRACMM3M – BASEv55_HEMI_CRACMM2 (right column). 56
Figure 5-6 Seasonal average changes in $PM_{2.5}$ in CMAQv6.0 compared to CMAQv5.5 using CB6R5 for 12US1 domain. 57
Figure 5-7 Seasonal average changes in $PM_{2.5}$ in CMAQv6.0 compared to CMAQv5.5 using CRACMM for 12US1 domain. 58
Figure 6-1 Seasonal average ozone in CMAQv5.5 base simulation (left column), changes in ozone using CRACMM3 for CMAQv6.0 compared to CRACMM2 for CMAQv5.5 (second from left column), changes from non-chemistry updates when using CRACMM2 with CMAQv5.5 and CMAQv6.0 (second from right column), and changes from updating the chemistry to CRACMM3 from CRACMM2 with CMAQv6.0 (right column). Changes shown here include changes both from boundary conditions generated from hemispheric CMAQ simulations using different versions (CMAQv5.5 and CMAQv6.0) and differences in the version of CMAQ used for the CONUS simulations (CMAQv5.5 and CMAQv6.0). 60
Figure 6-2. Seasonal average $PM_{2.5}$ concentrations in CMAQv5.5 base simulation (left column), total change in $PM_{2.5}$ using CRACMM3 for CMAQv6.0 compared to CRACMM2 for CMAQv5.5 (second from left column), changes from non-chemistry updates when using CRACMM2 with CMAQv5.5 and CMAQv6.0 (second from right column), and changes from updating the chemistry to CRACMM3 from CRACMM2 with CMAQv6.0 (right column). Changes shown here include changes both from boundary conditions generated from hemispheric CMAQ simulations using different versions (CMAQv5.5 and CMAQv6.0) and differences in the version of CMAQ used for the CONUS simulations (CMAQv5.5 and CMAQv6.0). 61
Figure 6-3 Monthly total PM emissions from windblown dust for the 108NHEMI domain. 63
Figure 6-4 Mean annual PM emissions from windblown dust from the No WBD Updates sensitivity (left) and difference in windblown dust emissions resulting from enabling CTM_BROWN_VEG (right). 64
Figure 6-5 Annual mean surface $PM_{2.5}$ concentration in the No WBD Updates sensitivity simulation (left) and difference in annual mean surface $PM_{2.5}$ concentration resulting from enabling CTM_BROWN_VEG (right). 65
Figure 6-6 Monthly total PM emissions from windblown dust for the 12US1 domain. 66
Figure 6-7 Mean annual PM emissions from windblown dust from the No WBD Updates sensitivity (left) and difference in windblown dust emissions resulting from enabling CTM_BROWN_VEG and implementing the NLCD landuse correction (right). 66
Figure 6-8 Annual mean surface $PM_{2.5}$ concentration in the No WBD Updates sensitivity simulation (left) and difference in annual mean surface $PM_{2.5}$ concentration resulting from enabling CTM_BROWN_VEG and implementing the NLCD landuse correction (right). 67
Figure 6-9 Soil bias for No WBD Updates sensitivity (left) and v6.0 BASE case (right) when compared to IMPROVE (circles) and CSN (triangles) observational networks. 68
Figure 6-10 Time series of average soil concentration over the observational networks in the geographical area shown in Figure 6-9. 68
Figure 6-11 F_{dl} (left) and F_{Ts} (right). The product of these two terms is used to estimate fertilizer adjustment factor (F_{adj}). 70
Figure 6-12 HEMI emissions of soil NO for CAMS, BDSNP, and SEGA. 71

Figure 6-13 Time series of soil NO emissions with different science options used in the 108NHEMI simulations.....71
Figure 6-14 CONUS domain soil NO emissions for BEIS, BDSNP, and SEGA.....72
Figure 6-15 Time series of soil NO emissions with different science options used in the 12US1 simulations.....72
Figure 6-16 BASE case annual average ozone from CAMS, and difference from BASE when using BDSNP or SEGA soil NO options. 73
Figure 6-17 BASE case summertime average ozone from BEIS, and difference from BASE when using BDSNP or SEGA soil NO options. 74
Figure 6-18 Normalized mean bias in 8-hr max O_3 by season and region for 12 km CONUS BASE with BEIS (left) and SEGA (right) soil NO. 74
Figure 6-19 June – August average NO_2 column for base model (top) and impact of new science option for model lightning NOx emission on NO_2 column (middle) and on surface MDA8 ozone (bottom). The base model lightning NOx emission option did not change between CMAQv5.5 and CMAQv6.0. 75
Figure 6-20 Seasonal average impact on surface layer MDA8 ozone due to STAGE updates for the 108NHEMI domain.....76
Figure 6-21 Seasonal average impact on surface layer MDA8 ozone due to STAGE updates for the 12US1 domain. 77
Figure 6-22 Seasonal average impact on surface layer $PM_{2.5}$ due to STAGE updates for the 108NHEMI domain.....77
Figure 6-23 Seasonal average impact on surface layer $PM_{2.5}$ due to STAGE updates for the 12US1 domain.....78
Figure 6-24 Cartoon depicting Kz_{min} calculations for urban, rural, and suburban grid cells (from left to right). The red boxes highlight the areas that will experience reduced mixing in CMAQ version 6.0, which occurs when the WRF PBL height is below the previously fixed value of 500 m. 79
Figure 6-25 Seasonal plots of mean ozone bias for the Base CB6 case (left) and Kz_{min} sensitivity test (right).....80
Figure 6-26 Seasonal plots of mean $PM_{2.5}$ bias for the Base CB6 case (left) and Kz_{min} sensitivity test (right).....80
Figure 6-27 Case study of Northeast $PM_{2.5}$ prediction (top) and bias (bottom) from Jan 12, 2022 through Jan 14, 2022. Lines represent the base configuration (blue), base configuration without Kz_{min} without updates (red), and KZU_CUSTOM equal to 2.0 (green). 81
Figure 6-28 $PM_{2.5}$ bias for January through March in the v6.0 base simulation (left), simulation with KZU_CUSTOM = 2.0 (middle), and the difference in bias (right). Cool colors in the rightmost panel indicate improved model performance. 81

Acronyms

AERONET	Aerosol Robotic Network
ALPACA	Alaskan Layered Pollution and Chemical Analysis
AOD	Aerosol optical depth
AQS	Air Quality System
BDSNP	Berkeley-Dalhousie Soil NOx Parameterization
BEIS	Biogenic Emissions Inventory System
CAA	Clean Air Act
CAMS	Copernicus Atmosphere Monitoring Service
CASTNET	Clean Air Status and Trends Network
CB6R5	Carbon Bond 6 revision 5
CMAQ	Community Multiscale Air Quality model
CO	Carbon monoxide
CONUS	Contiguous United States
CRACMM	Community Regional Atmospheric Chemistry Multiphase Mechanism
CSN	Chemical Speciation Network
DMS	Dimethyl sulfide
EC	Elemental carbon
EPA	Environmental Protection Agency
Fe	Iron
FINN	Fire Inventory from NCAR
GLM	Geostationary Lightning Mapper
H2O2	Hydrogen peroxide
HAP	Hazardous Air Pollutant
HCHO	Formadehyde
HMS	Hydroxymethanesulfonate
HONO	Nitrous acid
I/O API	Input/Output Applications Programming Interface
IAGOS	In-service Aircraft for a Global Observing System
IMPROVE	Interagency Monitoring of Protected Visual Environments
Kz	Vertical eddy diffusivity
MB	Mean bias
LAI	Leaf area index
MCIP	Meteorology Chemistry Interface Processor
MDA8	Maximum daily 8-hour average
MEGAN	Model of Emissions of Gases and Aerosols from Nature
Mn	Manganese
MOVES	Motor Vehicle Emissions Simulator
MPAS	Model for Prediction Across Scales
NAAQS	National Ambient Air Quality Standards
NEI	National Emissions Inventory
NH4	Ammonium

NLCD	National Land Cover Dataset
NMB	Normalized mean bias
NO	Nitric oxide
NO2	Nitrogen dioxide
NO3	Nitrate
NOAA	National Oceanic and Atmospheric Administration
NOx	Nitrogen oxides
NPV	Non-photosynthetically active vegetation
O2	Diatomic oxygen
O3	Ozone
OC	Organic carbon
OH	Hydroxyl radical
OPERA	Open (Quantitative) Structure-activity/property Relationship App
PBL	Planetary boundary layer
PM	Particulate matter
$PM_{2.5}$	Particulate matter with an aerodynamic diameter less than 2.5 micrometers
POA	Primary organic aerosol
ppb	Parts per billion
PV	Photosynthetically active vegetation
r	Pearson correlation coefficient
Ra	Aerodynamic resistance
RMSE	Root mean square error
Rst	Stomatal resistance
S(IV)	Sulfur with oxidation state of +4
SAPRC	Statewide Air Pollution Research Center mechanism
SEGA	Soil Emissions of Gases to the Atmosphere
SIP	State Implementation Plan
SLT	State, local, and tribal agencies
SO2	Sulfur dioxide
SO4	Sulfate
SOA	Secondary organic aerosol
STAGE	Surface Tiled Aerosol and Gaseous Exchange
TF HTAP	Task Force on Hemispheric Transport of Air Pollution
Tg	Teragrams
TSD	Technical Support Document
VOC	Volatile organic compound
WBD	Windblown dust
WRF	Weather Research and Forecasting model
WWLLN	World Wide Lightning Location Network

Acknowledgement

The first version of the Community Multi-scale Air Quality (CMAQ) model was developed by EPA's Office of Research and Development (ORD) in the late 1990s to help EPA and state, local, and Tribal air agencies meet Clean Air Act responsibilities. For more than 25 years, ORD staff have supported CMAQ science development in partnership with a broad user community. In 2025, following the reorganization of EPA, the responsibility to lead the development of the CMAQ model transitioned to the Office of State Air Partnerships (OSAP) in the Office of Air and Radiation (OAR). The development of CMAQv6.0 was initiated within ORD and completed by staff in OSAP. We acknowledge the significant time, effort, and scientific contributions from staff across EPA, including those in ORD, OSAP and the Office of Applied Science and Environmental Solutions (OASES), in making this release of CMAQ possible.

1. Introduction

Air quality management by state, local, and tribal agencies (SLTs) is informed by modeling assessments required under the Clean Air Act (CAA). For instance, State Implementation Plans (SIPs) for ozone and $PM_{2.5}$ include modeled attainment demonstrations that use photochemical air quality models to show attainment of National Ambient Air Quality Standards (NAAQS) by applicable attainment dates (US EPA, 2018). Since criteria air pollutants such as ozone and secondary $PM_{2.5}$ are not directly emitted but instead are formed through complex chemical and physical processes in the atmosphere, photochemical models must reliably parameterize detailed air pollution processes to inform air quality planning. Photochemical modeling systems must also reflect spatiotemporal heterogeneity in emission sources, meteorology, terrain, and other factors that influence pollutant concentrations.

To facilitate modeling assessments by SLTs required under the CAA, the U.S. Environmental Protection Agency (EPA) developed the Community Multiscale Air Quality (CMAQ) model. CMAQ is a state of the science, photochemical air quality model that simulates complex atmospheric processes to predict pollutant concentrations and their deposition back to Earth's surface (Byun and Schere, 2006). CMAQ incorporates first-principles of atmospheric science, multi-processor computing, and an open-source framework to address air quality management needs. CMAQ is available through a version-controlled GitHub repository (https://github.com/USEPA/CMAQ) that enables the user community to obtain the software code as well as contribute to code enhancements.

This Technical Support Document (TSD) accompanies the release of version 6.0 of the CMAQ model and documents the major model developments since the prior version, CMAQv5.5. Section 2 provides an overview of the CMAQ updates in version 6.0, while Section 3 describes the technical approach and model configurations used to assess version 6.0. Section 4 details the

evaluation of base modeling cases for CMAQv6.0 and CMAQv5.5 using observations from ambient monitoring networks and other sources. Section 5 provides model-to-model comparisons of CMAQv5.5 and CMAQv6.0. Section 6 describes incremental model testing that isolates the influence of individual model updates. Finally, the Appendix (Section 7) provides additional relevant information, including tables of model performance statistics based on consistent data and approach as used for U.S. EPA's recently released air quality modeling platform based on an earlier version of CMAQ (US EPA, 2026).

2. CMAQ version 6.0 Summary of Updates

CMAQ version 6.0 includes code and science updates across the entire system that improves the representation of atmospheric chemistry and the user experience. These include:

- Updates to the chemical mechanisms, including the Carbon Bond 6 revision 5 (CB6R5) mechanism and the Community Regional Atmospheric Chemistry Multiphase Mechanism (CRACMM). These updates include changes to the treatment of monoterpene oxidation, nitrate photolysis in the aerosol phase, and other processes that affect ozone and $PM_{2.5}$ formation and loss.
- Updates to the online calculation of windblown dust emissions, including the consideration of non-photosynthetic vegetation (aka "brown vegetation") in the calculation of dust emissions. This update is expected to reduce dust emissions in arid environments and improve the representation of $PM_{2.5}$ in those regions.
- A new parameterization of soil emissions of gases to the atmosphere (SEGA), including soil NO and HONO estimates for regional to global applications.
- Updates to the treatment of lightning NOx emissions, including the use of World Wide Lightning Location Network (WWLLN) strike data to inform the spatial and temporal distribution of lightning NOx emissions.
- Updates to the calculation of dry deposition, including updates to the Surface Tiled Aerosol and Gaseous Exchange (STAGE) and M3DRY dry deposition options.
- Updates to the treatment of urban mixing, including changes to the parameterization of urban heat island effects on pollutant dispersion.
- Other minor bug fixes.

The primary effects of these updates are to decrease ozone bias in spring and summer and decrease $PM_{2.5}$ dust-related bias, with the largest impacts in spring and in the western U.S. Across hemispheric and CONUS simulations, ozone is increased, primarily due to aerosol nitrate photolysis, much of which is transported into CONUS through boundary conditions from hemispheric runs. The increase in ozone concentrations results in improved performance in the western US, especially during spring, where the model historically had a low bias. In the eastern

US, where ozone was already biased high, model performance is degraded since ozone is further increased.

$PM_{2.5}$ changes are dominated by non-chemistry updates, especially windblown dust updates which correct a bug in land use categorization and consider the effect of non-photosynthetically active vegetation that substantially reduce soil/dust $PM_{2.5}$ thereby improving overprediction in arid regions. Chemistry updates in CRACMM3 can increase summer organic aerosol in forested regions, but these effects are generally smaller than dust-related decreases. Model performance comparisons indicate improved $PM_{2.5}$ performance where dust was previously overestimated, mixed regional and seasonal responses for sulfate and nitrate, modest NH_4 improvements in some seasons, minimal EC and OC changes between versions.

2.1 Chemical Mechanisms

CMAQv6.0 includes three families of chemical mechanisms:

- Community Regional Atmospheric Chemistry Multiphase Mechanism (CRACMM): CRACMM1 was introduced in CMAQv5.4 (Pye et al., 2023; Place et al., 2023; Wiser et al., 2023) and was updated in CMAQv5.5 as CRACMM2 (Skipper et al., 2024). CRACMM3 is introduced in CMAQv6.0 and includes several updates to CRACMM2 intended to improve the representation of gas-phase and aerosol chemistry in multiple environments (Pye et al., 2026b). In addition to the base CRACMM3 mechanism, CMAQv6.0 includes CRACMM3M with extended marine chemistry (Sarwar et al., 2026) and CRACMM3HAPS (Pye et al., 2026a), which includes additional Hazardous Air Pollutants (HAPs).
- Carbon Bond (CB): CB6R5 was originally released in 2020 (Yarwood et al., 2020) and was first implemented in CMAQ for version 5.4, and the CMAQ implementation has been further updated since its original inclusion.
- Statewide Air Pollution Research Center (SAPRC): SAPRC07 is originally described by Carter (2010a) and Carter (2010b). Implementation of SAPRC07 in CMAQ is described by Hutzell et al. (2012) and Xie et al. (2013).

CRACMM and CB6R5 mechanisms have been updated in CMAQv6.0, while the SAPRC07 mechanisms have been carried forward from CMAQv5.5 without modifications.

The following gas phase chemical mechanisms have been deprecated and removed from CMAQ as of version 6.0: cb6r3_ae7_aq, cracmm1_aq, cracmm1amore_aq, racm2_ae6_aq, and saprc07tic_aq7i_aqkmt2. Additionally, the acm_ae6_mp cloud module has been removed as it is no longer compatible with any chemical mechanism available in CMAQ.

2.1.1 Aerosol Nitrate Photolysis Parameterization

Aerosol nitrate photolysis has been implemented in both CRACMM3 and CB6R5 for CMAQv6.0. Field and laboratory studies suggest that aerosol nitrate can undergo photolysis, releasing NOx that was previously sequestered in particles ("renoxification") and promoting ozone formation. Aerosol nitrate photolysis has been added in CMAQv6.0 for the CB6R5 and CRACMM3 families of mechanisms and produces HONO and NO_2 with molar yields of 67% and 33% respectively, following the implementation of Sarwar et al. (2024). The photolysis frequency of aerosol nitrate is expressed as an enhancement factor relative to the photolysis frequency of nitric acid. The enhancement factor depends on the concentrations of sea salt and aerosol nitrate and has a range of 10 to 100 following Shah et al. (2023). The dependence on sea salt is due to the proposed mechanism of nitrate photolysis which involves halide ions (which have a known surface affinity) drawing sodium cations to the particle surface, which in turn attract nitrate anions which become susceptible to photolysis near the particle surface (Andersen et al., 2023).

More details on the effects of aerosol nitrate photolysis over the CONUS, including assessment of CONUS impacts due to changes in lateral boundary conditions vs. within the CONUS modeling domain have been described in Sarwar et al. (2025), and is shown in Section 5 in the framework of all CMAQv6.0 updates.

The addition of aerosol nitrate photolysis leads to increases in ozone throughout the northern hemisphere across all seasons. The largest increases are during the spring when seasonal photochemistry is near maximum and ozone lifetime is still relatively long leading to more long-range transport. The addition of aerosol nitrate photolysis in CMAQ leads to increased ozone simulation over CONUS, particularly over the western US and during spring, improving upon low biases.

2.1.2 Heterogenous Sulfur Chemistry

Updates to heterogeneous chemistry of sulfur species have also been incorporated into CRACMM3 and CB6R5. Several studies have suggested that heterogeneous sulfur chemistry in or on aqueous aerosols may contribute significant amounts of sulfur PM in locations characterized by high wintertime PM loading and SO_2 concentrations (e.g., Fairbanks, Alaska and the North China Plain). In such locations, the existing sulfate production pathways included in most models, namely SO_2 oxidation by OH in the gas phase and S(IV) oxidation by H_2O_2 and O_3 in cloud droplets and which are thought to account for the majority of secondary sulfate production globally, are not sufficiently active under cold and dark conditions to explain the observed levels of particulate sulfur. There have been suggestions that some of this observed "sulfate" may include hydroxymethanesulfonate (HMS) as well, a reversible adduct of SO_2 and formaldehyde (HCHO) formed and observed in the aqueous phase of atmospheric aerosols, fogs, and cloud droplets. Adding the heterogeneous formation of sulfate and HMS in aerosol water to CMAQ improves model underprediction of particulate sulfur during the ALPACA field

campaign (Simpson et al., 2024) conducted in and around the Fairbanks, Alaska, $PM_{2.5}$ nonattainment area in January-February 2022.

Several heterogeneous sulfur reactions were added to both the CRACMM3M and CB6R5M chemical mechanisms. The methodology builds upon the approach outlined by Farrell et al. (2025) and includes the formation of particulate sulfate from SO_2 oxidation by H_2O_2, O_3, methylhydroperoxide, peroxyacetic acid, O_2 (Fe^{3+}, Mn^{2+} catalyzed), NO_2 and HNO_4 and HMS formation and loss from reactions of SO_2 and HCHO in aerosol water.

The largest impacts of the model update can be found over eastern China and over Fairbanks, AK in the winter. Impacts on monthly average concentrations over CONUS (12US1) tend to be minimal.

2.1.3 Additional CRACMM Updates

Besides the addition of aerosol nitrate photolysis and updates to heterogeneous sulfur chemistry, additional updates in CRACMM3 include:

- Adding chlorine chemistry to base CRACMM (Sarwar et al., 2026),
- Updating the aging reactions for semi- and intermediate-volatility oxygenated reactive organic carbon species (Pye et al., 2026b),
- Updating formation of highly oxygenated organic molecules from monoterpenes (Pye et al., 2026b),
- Adding peroxy radical reaction rate temperature dependence (Wennberg et al., 2018),
- Adding photolysis of monoterpene secondary organic aerosol (SOA) (Vannucci et al., 2024; Pye et al., 2026a),
- Updating benzaldehyde chemistry (Jenkin et al., 2003), and
- Updating Henry's Law constants to match OPERA values (Mansouri et al., 2018).

Overall, the updates to aerosol nitrate photolysis (Section 2.1.1) dominate the changes in ozone associated with updates in CRACMM3 compared to CRACMM2. CRACMM3 updates generally tend to increase $PM_{2.5}$, particularly in forested areas during summer months. The increased $PM_{2.5}$ is primarily due to increases in SOA resulting from monoterpene chemistry updates.

2.2 Natural Emissions

2.2.1 Windblown Dust

Windblown dust (WBD) in CMAQ is a significant and natural source of particulate matter (PM), both locally generated and transported. WBD is almost always enabled for hemispheric configurations of CMAQ, but large overestimates of WBD in recent versions of the model often necessitated disabling WBD for the CONUS domain. Version 6.0 of CMAQ introduces changes

that allow WBD to be enabled for all domains. We note here that simulations using CMAQv5.5 presented in sections below have WBD enabled in the CONUS domain.

The first change is a correction to the National Land Cover Dataset (NLCD) land use categorization within CMAQ. Previously, some shrubland was incorrectly categorized as barren land, leading to an overestimate of dust when using NLCD inputs for land use. Since NLCD is only available for North America, this bug did not affect hemispheric simulations. The second change is a new option to consider photosynthetically- and non-photosynthetically active vegetation (PV and NPV), following the process described by Huang and Foroutan (2022).

2.2.2 Soil Emissions of Gases to the Atmosphere (SEGA)

The SEGA module is a new science update in CMAQv6.0 that estimates soil emissions of nitric oxide (NO) and nitrous acid (HONO), broadly following the Berkeley-Dalhousie Soil NOx Parameterization (BDSNP) (Hudman et al., 2012) with several modifications. It uses updated temperature and soil moisture response functions informed by more recent laboratory and field studies, updates canopy reduction treatments, and includes pulsing from soil moisture and freeze–thaw cycles. Emission factors are based on updated global observations, including enhanced contributions from biocrusts in arid regions. SEGA uses land use-specific, in-line emission factors for any modeling domain. Fertilizer-related emissions are represented through an empirical timing function dependent on soil temperature and daylength, with reduced seasonality toward the tropics.

2.2.3 Lightning NOx Emissions

Inclusion of lightning NOx at a global scale is important for realistic simulation of surface level ozone (Finney et al., 2016). Estimates of global lightning NOx emission totals range from 2 – 8 Tg each year (Schumann and Huntrieser, 2007) with some recent estimates exceeding the high end of the range (e.g., Nault et al. (2017)). Lightning NOx is predominantly emitted aloft, where it efficiently forms ozone. Over CONUS, surface level impacts of lighting NOx on ozone air quality tend to be largest in the high elevation regions of the western US and across the southern regions of the US.

CMAQ has two options for estimating lightning NOx emissions which are based on ground network data or a combination of ground network and satellite data. The second option is new to CMAQv6.0. The first method is based on adjusted strike count data from ground-based networks like the National Lightning Detection Network (NLDN) or the World Wide Lightning Location Network (WWLLN) (Kang et al., 2022). The second option uses lightning strike count and energy information from a combination of WWLLN and satellite-based GOES R-series Geostationary Lightning Mapper (GLM) within its field regard (Kang et al., 2026).

2.3 Dry Deposition

Two dry deposition options are available in CMAQ:

- M3DRY bi-directional deposition module (Pleim and Ran, 2011; Pleim et al., 2019; Pleim et al., 2022), and
- Surface Tiled Aerosol and Gaseous Exchange (STAGE) advanced dry deposition module (Bash et al., 2026).

Starting with CMAQv6.0, the dry deposition option is selected at runtime rather than at compile time, as was the case in previous versions. For both M3DRY and STAGE, "relative reactivity" parameters have been updated for volatile organic compounds (VOCs) and CO. Relative reactivity is a parameterization to represent the bulk resistance of deposition to vegetation and soil due to condensation (e.g., low vapor pressure organic compounds) or heterogeneous surface reactions (e.g., oxidation). The relative reactivity affects deposition to plant cuticles, dry ground, and snow in both M3DRY and STAGE.

The CMAQv6.0 update to relative reactivity uses a method for organic trace gases which is based on Raoult's Law and is analogous to the partitioning of semi-volatile gases to organic aerosols. The method is described by Bash et al. (2026) (see Supplement section S1 of reference). This update also changes the minimum specified relative reactivity from 1.0 to 0.01 to better reflect the relative reactivity calculated by the new method. This update tends to reduce the deposition of most organic species and reduces the deposition of CO. This update increases seasonal average ozone mixing ratios up to 1 ppb in testing for the northern hemisphere and has negligible impacts on $PM_{2.5}$.

In addition to the changes to relative reactivity parameters, the STAGE deposition module has been further updated. The following updates for STAGE are included in CMAQv6.0:

- Bugfix: Tiled deposition to snow covered land was modeled as resistances in series but should have been in parallel, which was corrected.
- Changes to tiling parameterization for aerodynamic and stomatal resistances.
- Corrections to tiled leaf area index (LAI) that better represent parameterizations in coastal areas.
- Added HCHO bidirectional exchange process and changed canopy water content to include impact of micro-wetness on all soluble species (as previously implemented in Skipper et al. (2024)).
- Tiled stomatal resistance (R_{st}) is scaled by land use type based on the minimum stomatal resistance and better represents the driving meteorological model.
- Tiled aerodynamic resistance (R_a) is now parameterized as $R_a = Pr_oU/u_*^2$ and stability corrections are implicitly included by applying Byun et al. (1999) Equations 12-30, 12-40, 12-42, and 12-46.
- Changes to dry bare soil resistance to include an additional diffusive resistance to the wet part of the dry soil.
- Changes to wet resistance calculation to account for differences in deposition when temperatures are above freezing vs. below freezing.

Overall, the STAGE updates decrease ozone over northern latitudes in winter, spring, and fall. STAGE updates slightly decrease $PM_{2.5}$ on average.

2.4 Meteorology and Urban Mixing

Meteorology in CMAQ is commonly provided by the WRF model, either through online coupling or meteorological input files. WRF provides meteorological variables that describe the atmosphere, including temperature, wind, surface fluxes, radiation, precipitation, and turbulence. The Meteorology Chemistry Interface Processor (MCIP) prepares the meteorological outputs from WRF for CMAQ when using offline coupling and requires periodic updates to ensure that the meteorological data is properly formatted and compatible with the latest version of CMAQ. In CMAQv6.0, MCIP has received minor updates including the following: expanded urban land use categories, support for time independent I/O API files, corrections for Mercator projection issues, and documentation.

CMAQ can directly access the meteorological data from WRF without the need for MCIP (two-way coupling), and a new unified coupling approach has been developed for version 6.0 to support coupling with both WRF and the Model for Prediction Across Scales (MPAS). The unified coupler and MCIP updates do not affect model results, except in niche applications, and the changes should not be noticeable to most users.

CMAQv6.0's most significant meteorological update revises near-surface vertical diffusion in cold conditions. Minimum vertical eddy diffusivity (Kz_{min}), which sets a lower limit on mixing, strongly affects nighttime NOx, ozone, and PM in stable conditions. Because urban heat island effects and anthropogenic heating are often underrepresented in WRF, earlier CMAQ versions applied an urban-weighted Kz_{min} effect through the bottom 500 m of the atmosphere, even when WRF reported a much lower PBL height.

Motivated by Desai et al. (2024), CMAQv6.0 now applies urban-weighted Kzmin only up to WRF's PBL height. This improves CMAQ–WRF consistency but reduces nighttime mixing in cold conditions, which can increase near-surface precursors, pollutants, and oxidants. A new option is available that allows users to customize the mixing floor in specific situations where the new Kz_{min} behavior causes performance issues. Section 6.4 describes effect of the mixing update on PM and demonstrates an application of the new KZU_CUSTOM option.

3. Model Configuration

For assessment of CMAQv6.0 and incremental updates, we evaluate simulations of model year 2022 for consistency with EPA's 2022 air quality modeling platform (US EPA, 2026). One minor difference with the 2022 platform, beyond the core model components, is that the simulations

use an earlier version of anthropogenic emissions for the CONUS modeling domain due to availability of these emissions data at the time the simulations were initiated (see Section 3.3). Differences between the emission cases are minor, and model performance statistics are provided in the Appendix for a CMAQv6.0 simulation using the same emissions and evaluation approach as for the 2022 platform (see Section 7.1).

3.1 Model Domains

Two modeling domains are used: a northern hemisphere domain and a CONUS domain. The northern hemisphere domain uses 108 km horizontal grid spacing (187 by 187 grid cells) and has 44 vertical layers extending from the surface to 50 hPa. The northern hemisphere domain is commonly referred to as the 108NHEMI domain. The CONUS domain uses 12 km horizontal grid spacing (299 x 459 grid cells) and has 35 vertical layers extending from the surface to 50 hPa. The 12 km CONUS domain is commonly referred to as the 12US1 domain. The two model domains and their vertical layer structures are shown in Figure 3-1.

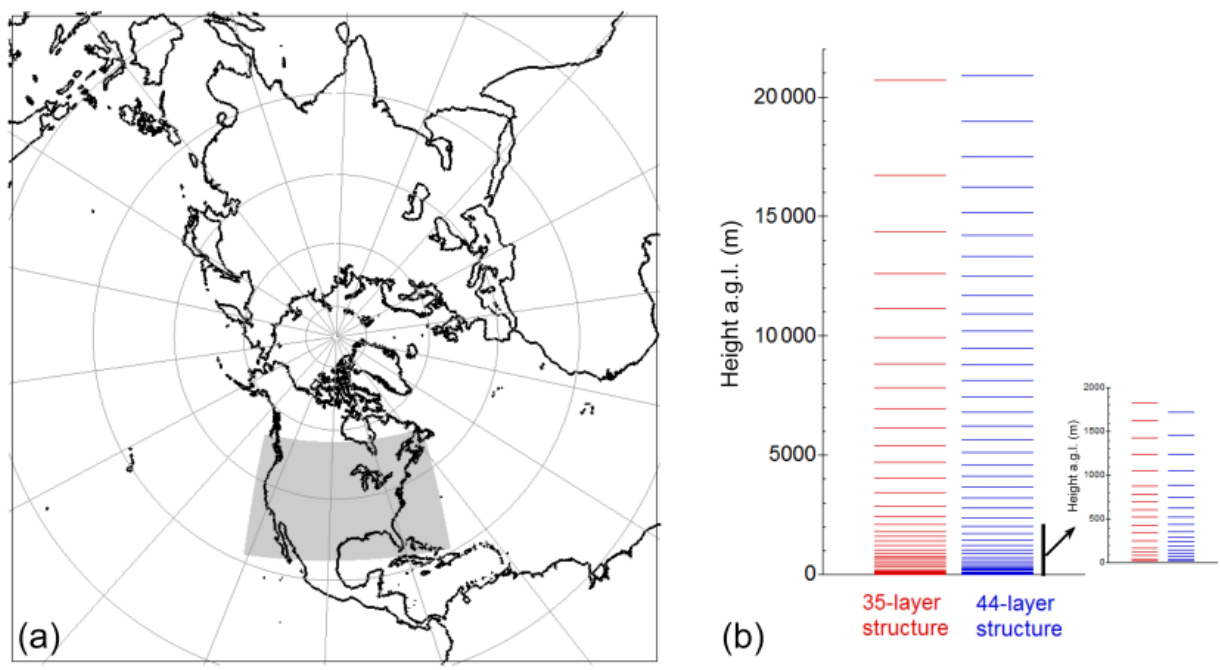

Figure 3-1 Model domain and vertical grid structure. (a) Northern hemisphere (108NHEMI domain) with CONUS (12US1) domain shaded in grey. (b) Vertical layer structure for 44- and 35-layer configurations used for the 108NHEMI and 12US1 simulations, respectively. Figure from Mathur et al. (2017), Figure 2.

3.2 Meteorological Inputs

Meteorological inputs for CMAQ for both the 108NHEMI and 12US1 domains are from the WRF model version 4.4.2 (Skamarock et al., 2019). MCIP (Otte and Pleim, 2010) version 5.3.3

is used to prepare CMAQ-ready meteorological inputs from WRF outputs for both domains. WRF was run for the full years of 2021 and 2022 for the 108NHEMI domain to allow for CMAQ spin-up of up to one full year for this domain to reduce the influence of initial conditions. For the 12US1 domain, WRF was run for the last ten days of December 2021 and the full year of 2022 to allow for ten days of CONUS CMAQ model spin up. For details on the configuration and evaluation of WRF simulations, refer to the 2022 WRF modeling TSD (US EPA, 2024).

3.3 Emission Inputs

Anthropogenic emissions for the US, Canada, and Mexico for both the 108NHEMI and 12US1 domains are based on the 2022 emissions modeling platform. The specific version of 2022 emissions modeling platform is referred to as "2022hd", where 2022 is the year modeled, "h" represents that it was based on the 2020 National Emissions Inventory (NEI), and "d" represents that it was the fourth version of a 2020 NEI-based platform. The 2022hd platform was a draft version in between versions 1 and 2 of the 2022 platform (US EPA, 2025a, b). The 2022hd platform was used for stakeholder review leading to the final version 2 platform. The 2022hd platform was selected because it was the most recent version of the 2022 emissions modeling platform that was available at the time that CMAQv6.0 evaluation simulations were initiated.

Anthropogenic emissions for the rest of the northern hemisphere are based on the Task Force on Hemispheric Transport of Air Pollution (TF HTAP) version 3.1 emissions inventory (Crippa et al., 2023).

Fire emissions for the 12US1 domain are based on the 2022 emissions modeling platform and are described in detail in the emissions TSDs referenced above. Fire emissions for the 108NHEMI domain are from Fire Inventory from NCAR (FINN) v2.5 (Wiedinmyer et al., 2023) outside of North America. Within North America, the same source of fire emissions as used for the 12US1 simulations was used for the 108NHEMI simulations.

Natural emissions are from the sources indicated in the list below. In cases where the source of natural emissions differs between the 108NHEMI and 12US1 simulations, the sources for both domains are provided separately. In cases where the source of natural emissions is the same for both domains, one source is indicated.

- Biogenic VOC
    - 108NHEMI: From Copernicus Atmosphere Monitoring Service (CAMS) based on Model of Emissions of Gases and Aerosols from Nature (MEGAN) version 2.1 (Guenther et al., 2012) as described by Sindelarova et al. (2014)
    - 12US1: Biogenic Emissions Inventory System (BEIS) online in CMAQ
- Soil NOx
    - 108NHEMI: From CAMS (CAMS, 2018)
    - 12US1: BEIS online in CMAQ
- Lightning NOx

    - Based on WWLLN strike data (Kang et al., 2022; Kang et al., 2026)
- Windblown dust
    - CMAQ online module (Foroutan et al., 2017)
- Sea spray
    - CMAQ online module (Kelly et al., 2010; Gantt et al., 2015)
- Marine halogens and dimethyl sulfide (DMS)
    - CMAQ online module (Sarwar et al., 2015; Zhao et al., 2021; Sarwar et al., 2023)

3.4 Initial and Boundary Conditions

For the 108NHEMI simulations, initial and boundary conditions are set to "clean" tropospheric background values as described by Mathur et al. (2017). For the 12US1 simulations, initial condition files and hourly boundary condition files are generated based on hourly 3D concentration output files from corresponding 108NHEMI simulations using the ICON and BCON preprocessors distributed with the CMAQ codebase.

3.5 Model Science Option Settings

The settings of some key model science options used in the base modeling configuration are described below:

- Chemical mechanism:
    - 108NHEMI: Hemispheric simulations were performed using CRACMM2 and CB6R5M for CMAQv5.5 and using CRACMM3M and CB6R5M for CMAQv6.0 (mechanisms with an appended "M" include extended halogen chemistry relevant in the marine environment). CB6R5 simulations are configured with non-volatile primary organic aerosol (POA) and without potential combustion SOA.
    - 12US1: CONUS simulations were performed using CRACMM2 and CB6R5 for CMAQv5.5 and using the CRACMM3 and CB6R5 for CMAQv6.0. CB6R5 simulations are configured with non-volatile primary organic aerosol (POA) and without potential combustion SOA.
- Dry deposition: Both the 108NHEMI and 12US1 simulations described here used the STAGE dry deposition option (Bash et al., 2026). The STAGE aerosol deposition option based on Emerson et al. (2020) was used.
- Ammonia bi-directional flux: Not enabled for 108NHEMI simulations. Enabled for 12US1 simulations.
- Stratospheric ozone by potential vorticity scaling: Enabled for 108NHEMI simulations as described in (Xing et al., 2016). Not enabled for 12US1 simulations.

4. Evaluation

Section 2 highlighted scientific updates and bug fixes included in the CMAQv6.0 release, and Section 3 described the model configuration to be used for the evaluation of CMAQv6.0. Section 4 presents an evaluation of model updates between base configurations of CMAQv5.5 and CMAQv6.0 for each mechanism separately against surface-based and airborne in situ measurements. Section 5 presents model version intercomparison for assessment of broad spatial and temporal features that may not be evident through comparisons with observations, while Section 6 presents the impacts of individual model updates.

To demonstrate the effects of model updates on $PM_{2.5}$ and ozone CMAQ simulation results, we compare base model configurations of CMAQv5.5 and CMAQv6.0 releases. Between CMAQv5.5 and CMAQv6.0, updates to chemistry were made to both the CRACMM and CB6 chemical mechanisms. We evaluate the updates between base configurations of CMAQv5.5 and CMAQv6.0 for each mechanism separately. The different configurations of chemical mechanisms and boundary conditions considered are summarized in Table 4-1 (hemispheric simulations) and Table 4-2 (CONUS simulations). The hemispheric simulations use chemical mechanisms with detailed halogen chemistry that is relevant in the marine environment and potentially other environments (Sarwar et al., 2012; Sarwar et al., 2019; Sarwar et al., 2026). These mechanisms are differentiated from the base mechanisms by adding an "M" (M stands for marine) to the base mechanism name (e.g., CB6R5 vs. CB6R5M and CRACMM3 vs. CRACMM3M). The base mechanisms contain more condensed halogen chemistry compared to the detailed halogen chemistry and are typically used for regional scale modeling. The choice of detailed vs. condensed halogen chemistry is intended to balance the need to better represent halogen chemistry with the need for computationally efficient simulations.

Previous evaluation of the CMAQv5.5 base model (US EPA, 2026) identified substantial biases of simulated ozone over CONUS, most notably in spring and early summer over the southwest US. A chemistry module update adding nitrate photolysis in the aerosol aqueous phase resulted in a large increase of ozone from CMAQv5.5 and CMAQv6.0. Ozone formed via this process is slow, but global in nature, accumulating ozone in the remote atmosphere far downwind of nitrogen oxide sources that is then transported at hemispheric scales, with largest surface impacts in regions with elevated terrain and subtropical high pressure.

It is important to include this update enhancing nitrate photolysis in the aerosol aqueous phase in the global or hemispheric model used to generate boundary conditions for the domains of interest. We demonstrate this point by comparing CMAQv5.5 and CMAQv6.0 CONUS simulations driven by hemispheric boundary conditions using the same model version to one where a CMAQv6.0 CONUS simulation uses the CMAQv5.5 108NHEMI results as boundary conditions. Comparing these three CONUS runs, the results (Section 4.1) show that much of the difference between CMAQv6.0 and CMAQv5.5 ozone simulation is due to the version of the

model used for the boundary conditions and less so for the version of the model used in the CONUS or nested simulation.

For $PM_{2.5}$, regional and seasonal model performance issues have been previously noted in the 2022v1 regulatory platform (US EPA, 2026). Many of those issues remain and are not mitigated by updates to CMAQv6.0 from CMAQv5.5. One notable update, both on a hemispheric and regional scale over CONUS is the update to the inline windblown dust emissions module. Briefly, landuse updates, consistent with literature implementations, are used to improve the characterization of non-photosynthetically active vegetation in arid environments and their effect in mitigating dust emissions. As a result, simulated $PM_{2.5}$ and the dust component are lower in CMAQv6.0 relative to CMAQv5.5, most notably in arid environments and seasons with high winds (e.g., springtime in the southwest US). The model updates in CMAQv6.0 within the CONUS domain mitigate gross biases in CMAQv5.5 simulation over the west and southwest US during spring.

Effects of CMAQ model updates from version 5.5 to version 6.0 are assessed using a multiscale modeling framework. The multiscale modeling framework used here entails running the model at the hemispheric scale followed by running the model at the 12 km CONUS scale using lateral boundary conditions generated from outputs of a corresponding hemispheric simulation. This framework allows for the assessment of updates that may affect large-scale background concentrations of pollutants (and thus boundary conditions for CONUS scale simulations) but that would not be apparent when running only a CONUS scale simulation in addition to updates that are influential over the CONUS domain itself.

For a given model configuration, the CMAQ version (5.5 or 6.0) and chemical mechanism family (CB6 or CRACMM) are consistent between the hemispheric and CONUS simulations. One exception in this analysis is the sensitivity test described above which uses boundary conditions from a hemispheric simulation using CMAQv5.5 to run a CONUS simulation using CMAQv6.0. This sensitivity test is used to assess differences in impacts affecting the CONUS modeling domain that are driven by updates that are important on the hemispheric scale compared to impacts that are driven by updates that are important at the CONUS scale.

Table 4-1 Hemispheric (108NHEMI domain) CMAQ model configurations.

Label	Version	Mechanism	BCs
BASEv55_HEMI_CB6R5M	v5.5	CB6R5M_AE7	Fixed (at Equator)
BASEv55_HEMI_CRACMM2	v5.5	CRACMM2	Fixed (at Equator)
BASEv60_HEMI_CB6R5M	v6.0	CB6R5M_AE7	Fixed (at Equator)
BASEv60_HEMI_CRACMM3M	v6.0	CRACMM3M	Fixed (at Equator)

Table 4-2 CONUS (12US1 domain) CMAQ model configurations.

Label	Version	Mechanism	BCs
BASEv55_12US1_CB6R5	v5.5	CB6R5_AE7	BASEv55_HEMI_CB6R5M
BASEv55_12US1_CRACMM2	v5.5	CRACMM2	BASEv55_HEMI_CRACMM2
BASEv60_12US1_CB6R5	v6.0	CB6R5_AE7	BASEv60_HEMI_CB6R5M
BASEv60_12US1_CRACMM3	V6.0	CRACMM3	BASEv60_HEMI_CRACMM3M
BASEv60_12US1_BC_v55_CRACMM2	v6.0	CRACMM3	BASEv55_HEMI CRACMM2

4.1 Ozone Evaluation

4.1.1 Hemispheric Scale

Hemispheric ozone performance is assessed by comparing the modeled ozone to routine ozonesonde and airborne observations. Figure 4-1 shows the monthly average of ozonesonde observations and paired model monthly averages in the northern hemisphere in different latitude and vertical layer ranges. Results for CB6R5M both with and without aerosol nitrate photolysis are shown. Results for CRACMM3M which includes aerosol nitrate photolysis are also shown.

South of 45°N latitude, both the updated CRACMM3 (green) and CB6R5 (red) versions of CMAQv6.0 simulate ozone that compares exceptionally well with paired ozone soundings (black) at all altitude bins. Despite the strong performance at these scales, there are two seasons with some noted disagreements. The model tends to underestimate the soundings at all three altitude bins in the winter months. The model overpredicts ozone values during the later summer months in the top-most model altitude bin shown here (Layers 27 – 33). In comparison, an incremental model test removing only the aerosol photolysis nitrate updates simulates ozone mixing ratios that are much lower (blue) than those observed by the soundings in all months and altitude bins (black line), with one exception. At high altitudes south of 45°N latitude (top-right panel), the model tendency, irrespective of mechanism or updates, is to simulate more ozone in the late summer than in other seasons. The modeled summer peak at high altitudes is not reflected by observations, resulting in the aforementioned high bias during summer at higher altitudes for CMAQv6.0. In other seasons, the addition of aerosol nitrate photolysis resulted in better performance and closing of the large overall low bias seen in the model sensitivity simulation where aerosol nitrate photolysis was removed from the CB6R5M mechanism in CMAQv6.0 (blue line).

North of 45°N latitude (left panels), irrespective of mechanism or inclusion of updates to aerosol nitrate photochemistry, the model underestimates ozone soundings during winter in all altitude bins.

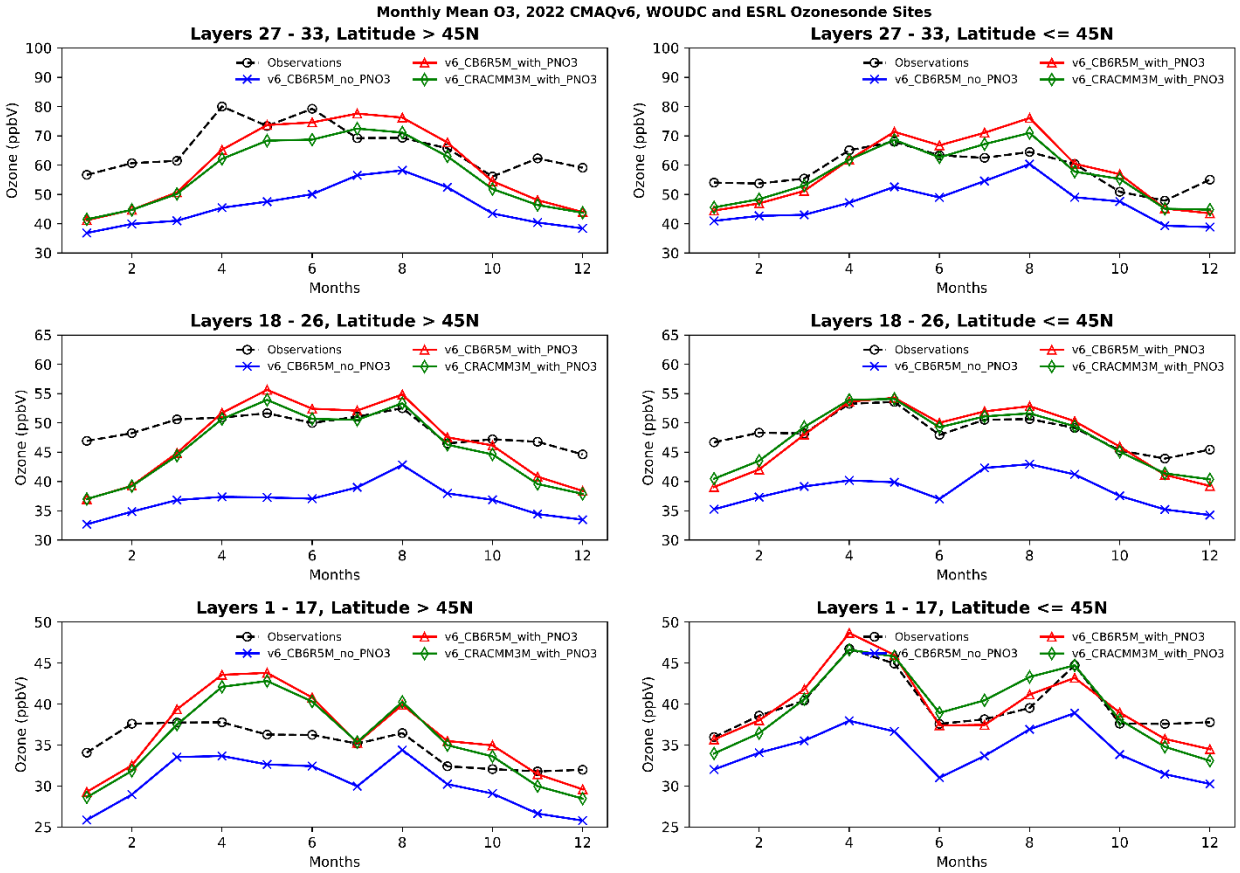

Figure 4-1 Monthly average ozone from 2022 northern hemisphere simulations for CB6R5M with and without aerosol nitrate photolysis and for CRACMM3M (also includes aerosol nitrate photolysis) compared to ozonesonde observations averaged by latitude bands and separated by model layers.

Figure 4-2 shows hemispheric-scale CMAQv6.0 and CMAQv5.5 performance versus time- and space-paired measurements collected by the program for an In-service Aircraft for a Global Observing System (IAGOS), which sample vertical profiles of ozone and other parameters onboard commercial aircraft. The locations sampled are determined by standard operations of the airline participating. For the hemispheric evaluation presented here, there were more than 300 profiles sampling each altitude and season with valid data. As many ascents and descents occur in stable night or morning hours in regions that typically have fresh NO_x emissions, the ozone profile tends to decrease near the surface, a pattern relatively well captured by the model on average. Aloft, the performance of CMAQv6.0 is reasonable, and much improved in comparison to CMAQv5.5. Updates to CMAQv6.0 mitigate large ozone biases in all seasons. In winter (DJF) and spring (MAM), CMAQv6.0 slightly underestimates ozone above 1 km altitude. In summer (JJA) and fall (SON), CMAQv6.0 closely matches ozone observations up to ~4.5 km altitude,

above which it tends to be biased high relative to measurements. This shift from low-bias to high-bias between seasons at high altitudes is broadly consistent with the ozonesonde analysis presented above for model layers between 27 and 33.

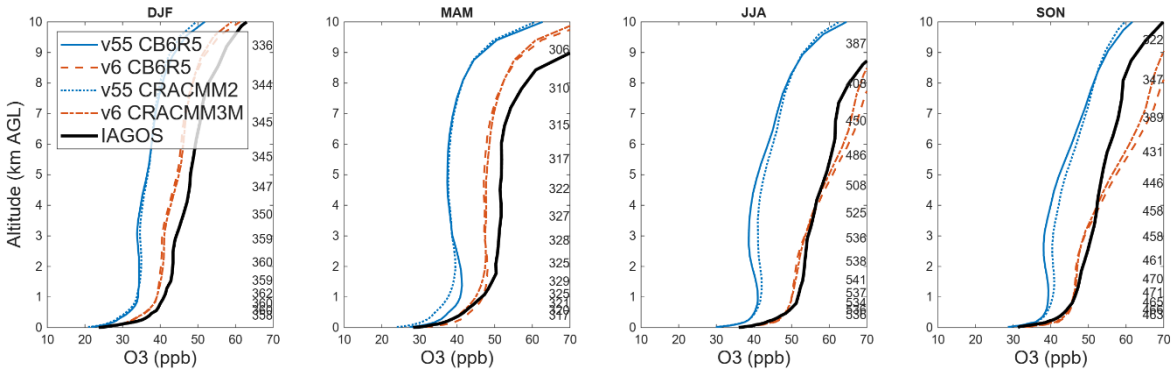

Figure 4-2. Seasonally averaged vertical profiles of pairwise model-measurement matches for CMAQv5.5 and CMAQv6.0 northern hemisphere simulations for CRACMM3M and CB6R5M and In-service Aircraft for a Global Observing System (IAGOS). The number of vertical profiles with valid ozone data in each altitude bin is listed on the right axis. There are more than 300 soundings with valid data in each season.

4.1.2 CONUS – Regional and Seasonal Evaluation

Figure 4-3 shows the monthly averaged time series of maximum daily 8-hour average ozone (MDA8 O3) for five sets of 12US1 simulations. Figure 4-4 summarizes the ozone season (May – September) MDA8 ozone performance statistics (MB, NMB, RMSE and the correlation coefficient) between five simulations on a 12US1 grid across the NOAA Climate Regions (https://www.ncdc.noaa.gov/monitoring-references/maps/us-climate-regions.php, last access: 12 June 2026). The five simulations are summarized in Table 4-2. Figures in Section 5 explicitly show spatial plots of model-model differences to highlight spatial patterns.

At a regional-scale and monthly-averaged, CMAQv6.0 simulates MDA8 ozone in satisfactory agreement with measurements at Air Quality System (AQS) sites (black line, Figure 4-3), using both the CRACMM3 and CB6R5 mechanisms (red and purple lines, respectively Figure 4-3). Agreement with measurements in CMAQv6.0 (red and purple line) is dramatically improved relative to the performance of simulations using CMAQv5.5 (blue and yellow lines, Figure 4-3), particularly in the Northwest, West, Southwest and the Northern Rockies and Plains regions of the US. The differences in model simulations using CB6R5 or CRACMM chemical mechanisms are much smaller than the differences driven by common updates included in both mechanisms from CMAQv5.5 (gray and yellow) to CMAQv6.0 (purple and red) (Figure 4-3). In the same western regions, a much larger fraction of the improvement in model performance is due to

updates included in CMAQv6.0 boundary condition simulation (compare gray and red line, Figure 4-3) than in the 12US1 simulation (compare gray and yellow line, Figure 4-3). In the South, Upper Midwest, Ohio Valley, and eastern regions, the performance of CMAQv6.0 with respect to measurements is more mixed (Figure 4-3 purple and red lines versus black line). The model performs well for the early part of the year through mid-to-late spring, depending on region. Performance is slightly worse in the middle of the year, with the timing of the model-measurement divergence depending on the specific region, followed by better performances again in the later part of the year. Summertime model high biases have been reported previously (e.g., US EPA (2026)), most notably in the southeast regions. The updates included in CMAQv6.0 increased this bias. Future efforts will seek to better understand the causes of the summertime high bias.

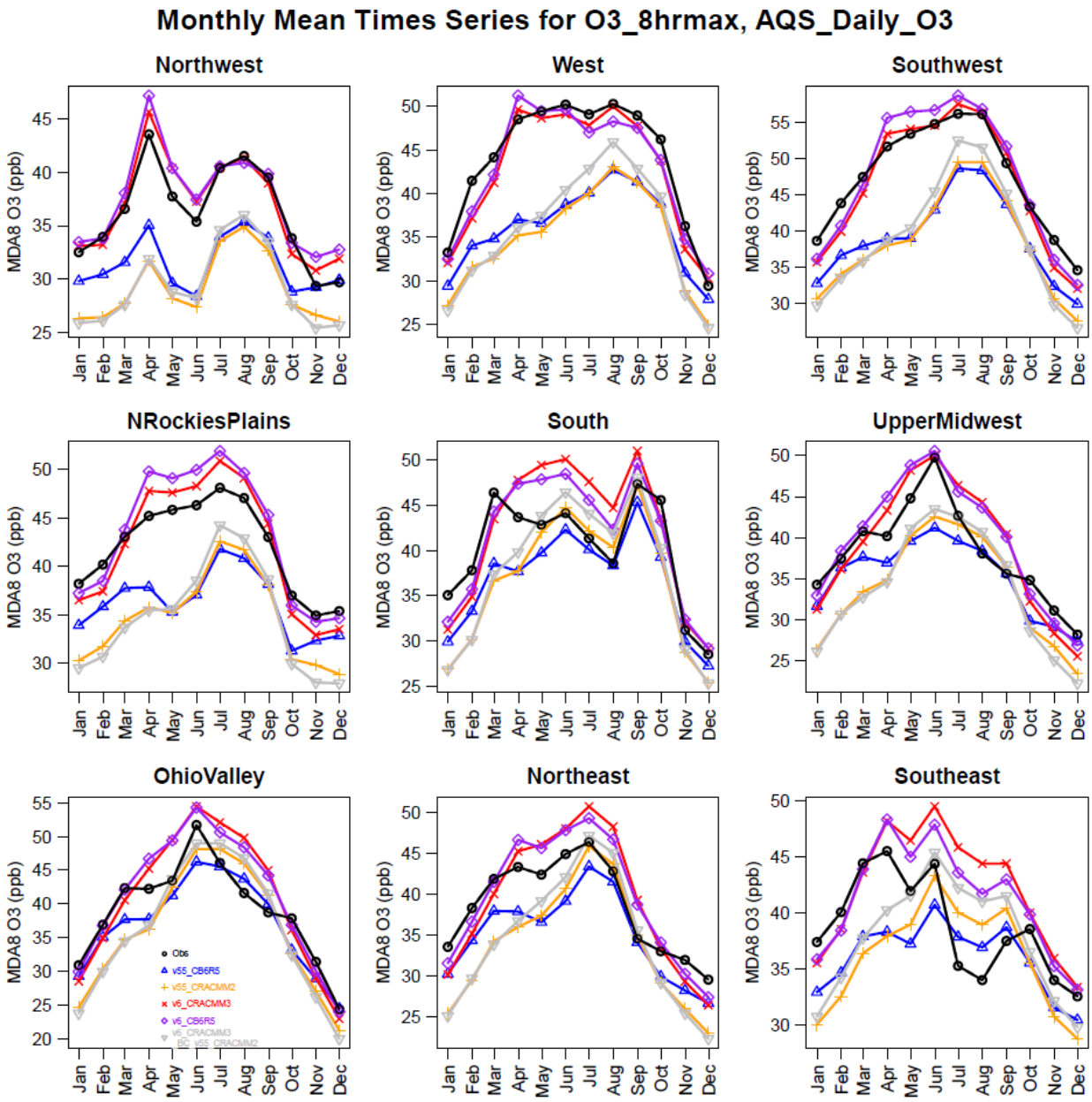

Figure 4-3 Monthly mean MDA8 ozone AQS observations and paired monthly mean model values at observation sites, separated by region. Table 4-2 provides more details on these simulations.

Figure 4-4 highlights details of model performance for the 2022 model year ozone season (May – September) for the same set of five model simulations (Table 4-2) as described above. The pattern of mean bias and normalized mean bias provides quantitative detail to the assessment presented qualitatively above: updates included in CMAQv6.0 increase simulated ozone across all regions in the ozone season. This mitigates CMAQv5.5 negative biases in the western regions

of the US and dramatically improves model performance in those areas. For the CMAQv6.0 CONUS simulation using boundary conditions generated with the CMAQv5.5 hemispheric scale model (right column), bias improvement is modest in comparison to the same CONUS simulation with hemispheric v6.0 boundary conditions, highlighting again that the updates in CMAQv6.0 tend to produce a larger fraction of their impacts at global scales than at continental scales. In the regions east of the Rocky Mountains (Figure 4-4), the large-scale increase of ozone generated by updates included in CMAQv6.0 tends to worsen average bias, shifting from relatively unbiased CMAQv5.5 to moderate to large positive biases in CMAQv6.0. For the eastern regions, the performance of the mixed simulation, using CMAQv6.0 for CONUS and hemispheric CMAQv5.5 for boundary conditions, leads to performance that is closer to halfway between the fully CMAQv5.5 or fully CMAQv6.0 simulations.

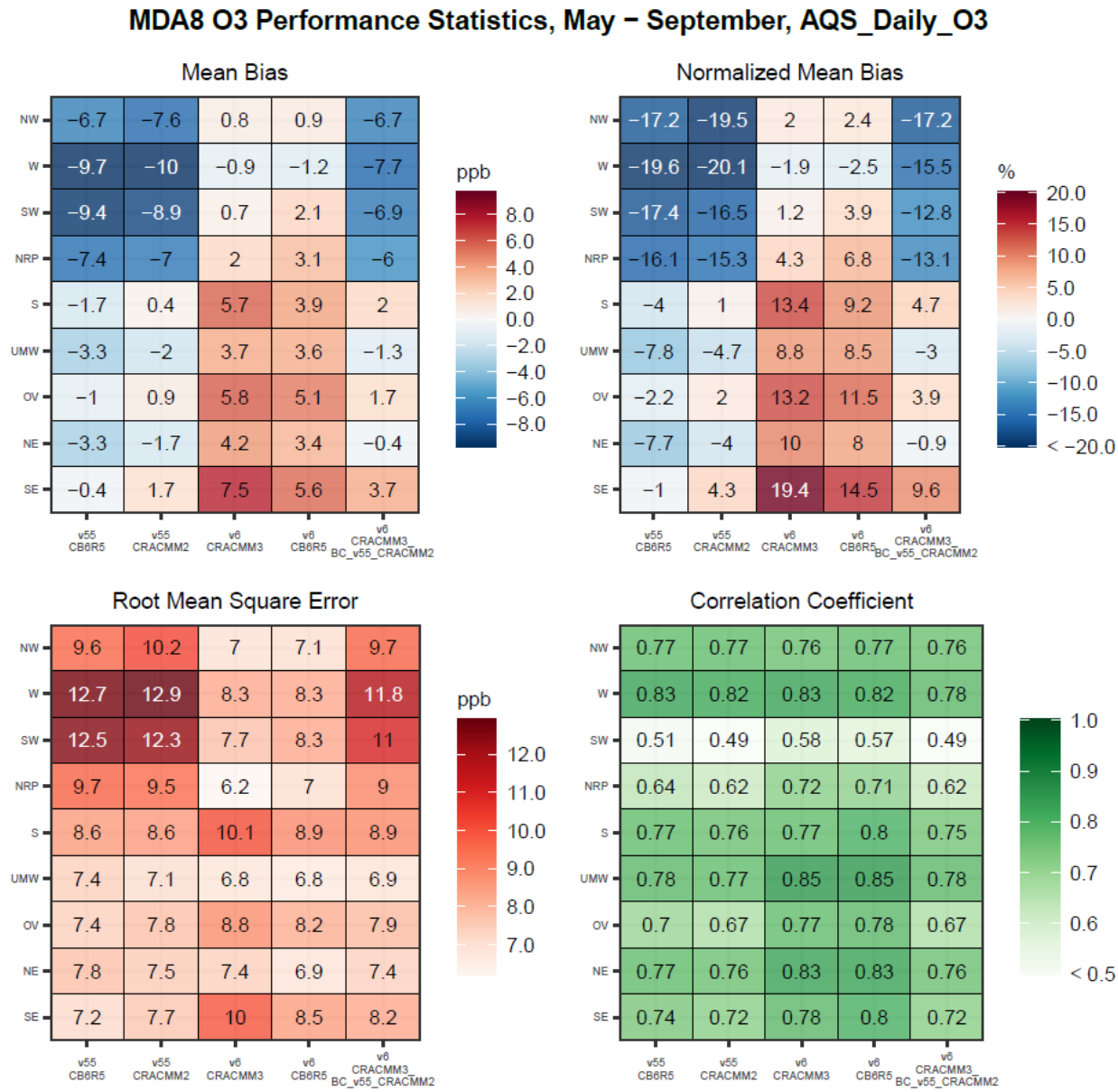

Figure 4-4 Performance statistics by simulation (along x-axis) and region (along y-axis) for MDA8 ozone from May – September at AQS monitoring sites. Region abbreviations refer to the following NOAA climate regions: NW=Northwest, W=West, SW=Southwest, NRP=Northern Rockies and Plains, S=South, UMW=Upper Midwest; OV=Ohio Vally, NE=Northeast, SE=Southeast. Table 4-2 provides more details on these simulations.

Figure 4-5, Figure 4-6, Figure 4-7, and Figure 4-8 show the observed seasonal average MDA8 ozone concentrations at AQS sites along with the seasonal average model bias for CMAQv5.5 using CRACMM2 and CB6R5 and for CMAQv6.0 using CRACMM3 and CB6R5 for the 12US1 domain. In much of the western US, MDA8 ozone in CMAQv5.5 is biased low across all

seasons, with the largest negative bias occurring in spring. In the eastern US, MDA8 ozone in CMAQv5.5 is biased low in winter and spring. Biases are mixed in the eastern US during summer, with high biases more prominent in the southeastern US. Fall performance ranges from low to neutral biases.

The updates in CMAQv6.0 increase ozone across all seasons, mostly due to the addition of aerosol nitrate photolysis in the hemispheric domain that provides the boundary conditions for the CONUS simulations. The increase in ozone has mixed effects on performance. Biases during winter shifted from low biased to a mix of mostly low to neutral biases. Springtime biases went from very low to mostly a mix of neutral and high biases. During summer, high biases in the eastern US were exacerbated while low biases in the western US shifted to being slightly high biased with notable exceptions in the Central Valley and Los Angeles areas of California and in the Phoenix, Arizona, area remaining low biased. Fall biases shifted from neutral to high biased in the eastern US while in the western US the biases shifted from being mostly low biases to a mix of low, neutral, and high biases depending on the specific region.

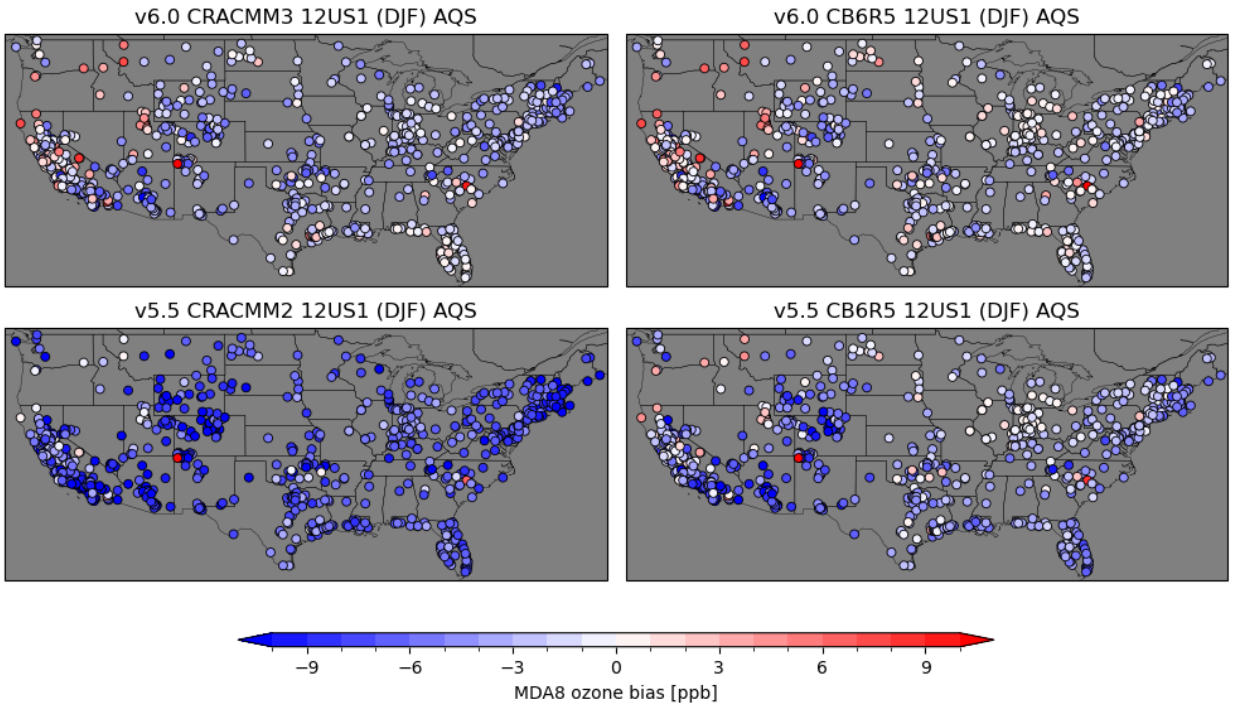

Figure 4-5 Winter (DJF) average MDA8 ozone bias at AQS sites for 12US1 simulations with CMAQv6.0 with CRACMM3 (top left), CMAQv5.5 with CRACMM2 (bottom left), CMAQv6.0 with CB6R5 (top right), and CMAQv5.5 with CB6R5 (bottom right).

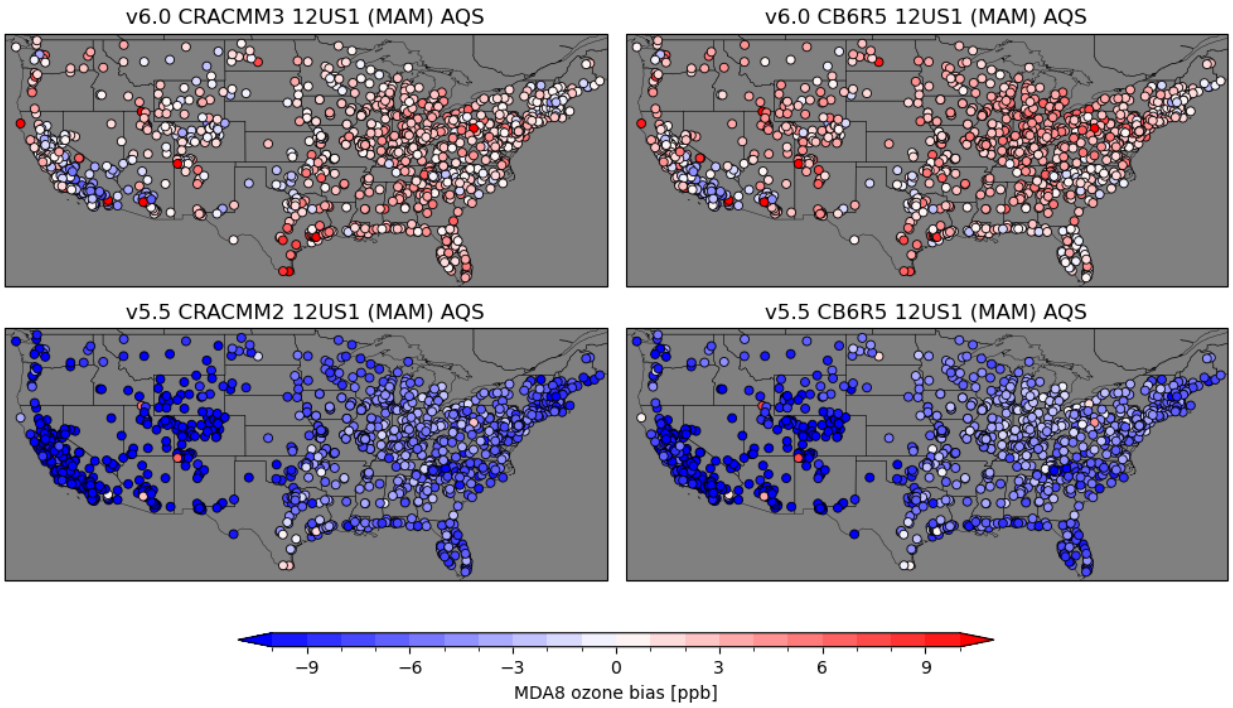

Figure 4-6 Spring (MAM) average MDA8 ozone bias at AQS sites for 12US1 simulations with CMAQv6.0 with CRACMM3 (top left), CMAQv5.5 with CRACMM2 (bottom left), CMAQv6.0 with CB6R5 (top right), and CMAQv5.5 with CB6R5 (bottom right).

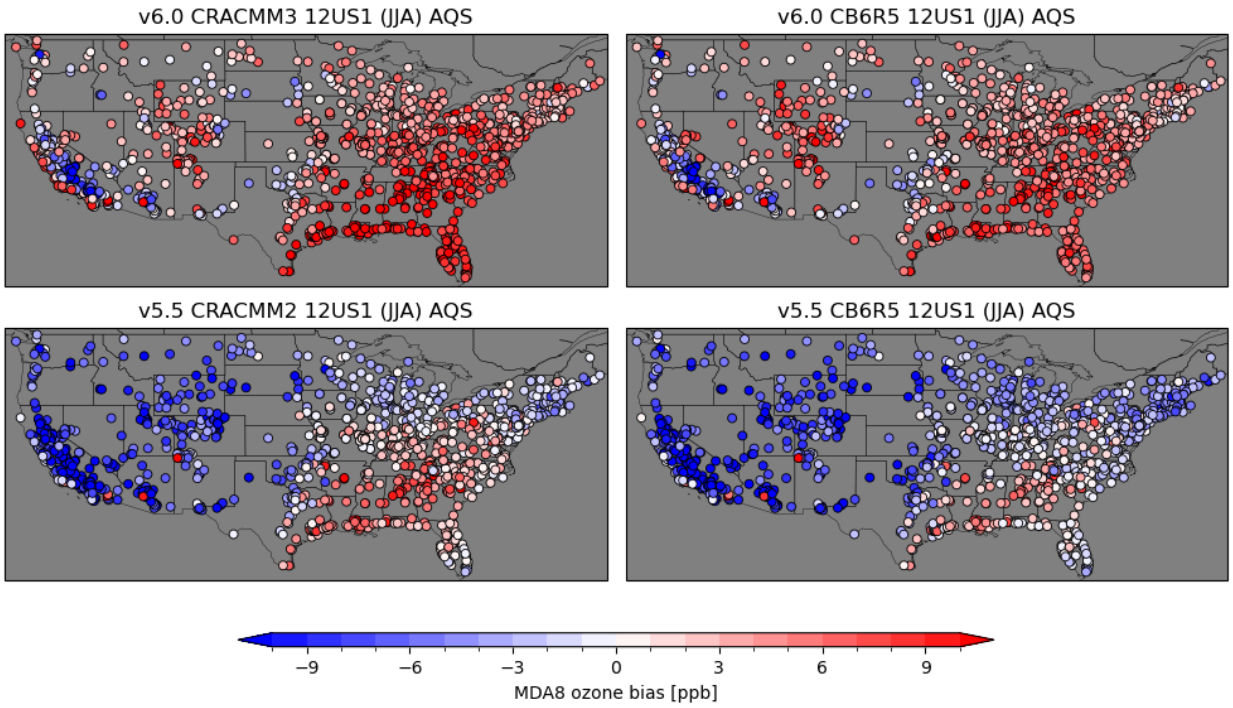

Figure 4-7 Summer (JJA) average MDA8 ozone bias at AQS sites for 12US1 simulations with CMAQv6.0 with CRACMM3 (top left), CMAQv5.5 with CRACMM2 (bottom left), CMAQv6.0 with CB6R5 (top right), and CMAQv5.5 with CB6R5 (bottom right).

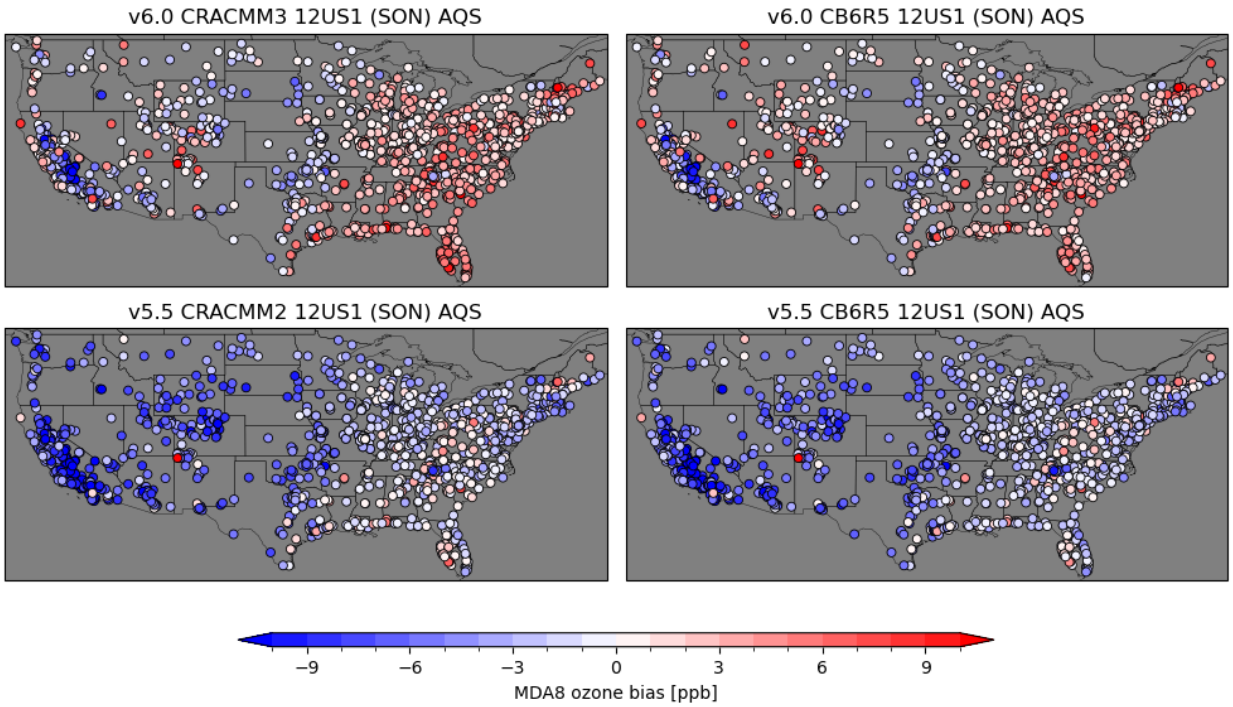

Figure 4-8 Fall (SON) average MDA8 ozone bias at AQS sites for 12US1 simulations with CMAQv6.0 with CRACMM3 (top left), CMAQv5.5 with CRACMM2 (bottom left), CMAQv6.0 with CB6R5 (top right), and CMAQv5.5 with CB6R5 (bottom right).

4.2 $PM_{2.5}$ Evaluation

Changes in $PM_{2.5}$ come primarily from changes in the online calculation of windblown dust in CMAQv6.0 as compared to CMAQv5.5. In CMAQv6.0, the consideration of non-photosynthetic vegetation (aka "brown vegetation") greatly reduces the windblown dust emissions over arid regions. See Section 6.2.1 for detailed results on the effects of changes to windblown dust emissions. While the update to dust emissions is the dominant feature of the evaluation at the hemispheric and CONUS spatial scales, model updates to CRACMM3 (see Section 6.1), STAGE dry deposition (see Section 6.3), and vertical mixing options (see Section 6.4) also contribute more modest changes important to specific regions, seasons, and $PM_{2.5}$ constituents.

For a number of previous air quality modeling applications, windblown dust is not included as a source of $PM_{2.5}$ emissions in the CONUS domain (US EPA, 2026) because of known large biases (e.g., Huang and Foroutan (2022)). In the evaluations that follow, windblown dust is included in both CMAQv5.5 and CMAQv6.0 simulations for both the hemispheric simulations providing boundary conditions to the CONUS simulations and in the CONUS simulations themselves. The CMAQv6.0 simulations include the updates described in Section 2.2.1. The CMAQv5.5 simulations have known issues with high windblown dust, but windblown dust is included in

both the hemispheric and CONUS CMAQv5.5 simulations for scientific consistency across scales in both sets.

At the hemispheric-scale, PM performance is evaluated by comparing modeled aerosol optical depth (AOD) to observed AOD. The use of AOD for the hemispheric model is intended to assess the large-scale transport of PM within the hemisphere. At the CONUS-scale, PM performance is evaluated by comparing modeled and observed total $PM_{2.5}$ and $PM_{2.5}$ components at regulatory surface monitoring stations. Comparisons against surface $PM_{2.5}$ monitors are less useful at the hemispheric scale since the 108 km grid scale is not expected to be representative of conditions at a monitoring site. Evaluation against $PM_{2.5}$ at surface monitoring sites is more appropriate for the 12 km CONUS-scale simulations.

4.2.1 Hemispheric-Scale Aerosol Optical Depth

Model predictions of AOD were compared to surface-based retrievals made at all Aerosol Robotic Network (AERONET) sites for both sets of CMAQv5.5 and CMAQv6.0 CRACMM and CB6R5 simulations (Figure 4-9). Weekly integrated comparison of modeled and measured AOD shows that CMAQv6.0 predictions tend to be closer to measurements during periods of large-scale windblown dust events common during the spring season. This improvement in model performance is evident in both the eastern U.S., typically thought of as a dust receptor region, and in source regions, like the western U.S. and the Sahara Desert. The differences driven by simulation mechanisms (darker vs. lighter color) are much smaller than the difference between CMAQ versions (blue vs. red), which contain updates to inline emissions, most notably reductions to windblown dust. The CMAQv6.0 model simulations perform much better versus the observations in the springtime weeks 12 – 20 in all three regions shown. In the Sahara Desert region, CMAQv6.0 tends to slightly underestimate AERONET observations in the summer through early fall while the CMAQv5.5 simulation tends to overestimate observations. The spatial coverage of AERONET sites in the Sahara region is limited, and there is spatial heterogeneity in model biases across the sites in this region, so findings based on comparison to AERONET sites in the region may differ from findings based on a comparison to satellite-based AOD products which provide broader coverage.

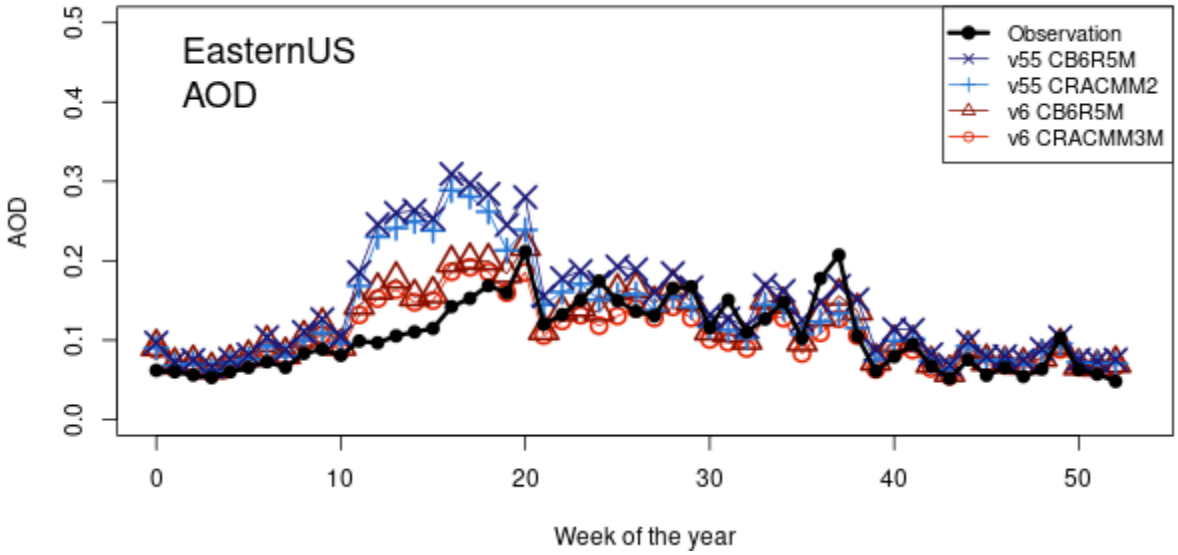
EasternUS
AOD
Observation
v55 CB6R5M
v55 CRACMM2
v6 CB6R5M
v6 CRACMM3M
AOD
0.0
0.1
0.2
0.3
0.4
0.5
0
10
20
30
40
50
Week of the year

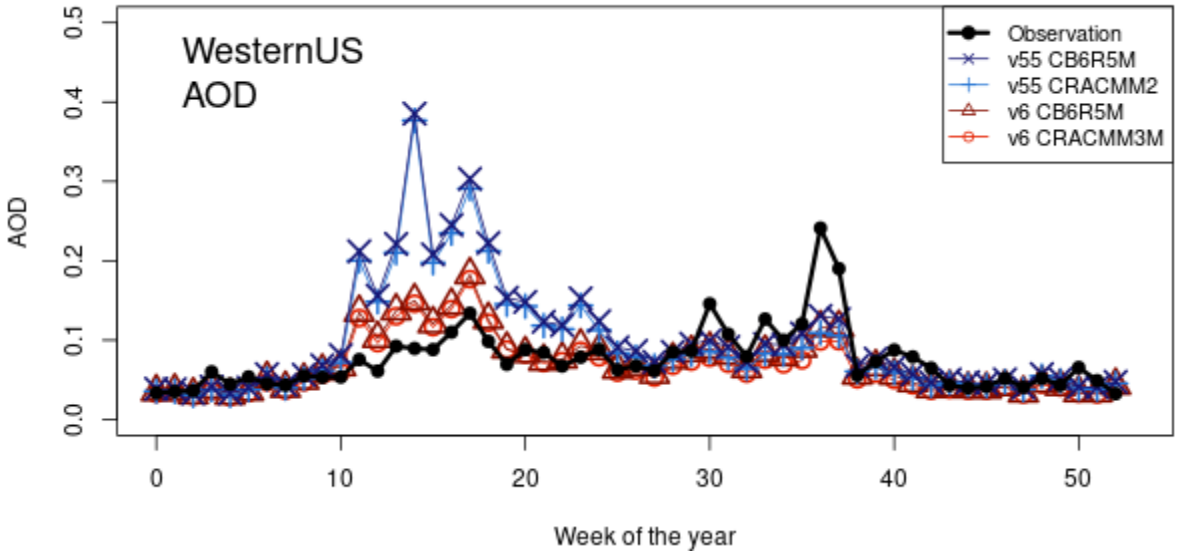
WesternUS
AOD
Observation
v55 CB6R5M
v55 CRACMM2
v6 CB6R5M
v6 CRACMM3M
AOD
0.0
0.1
0.2
0.3
0.4
0.5
0
10
20
30
40
50
Week of the year

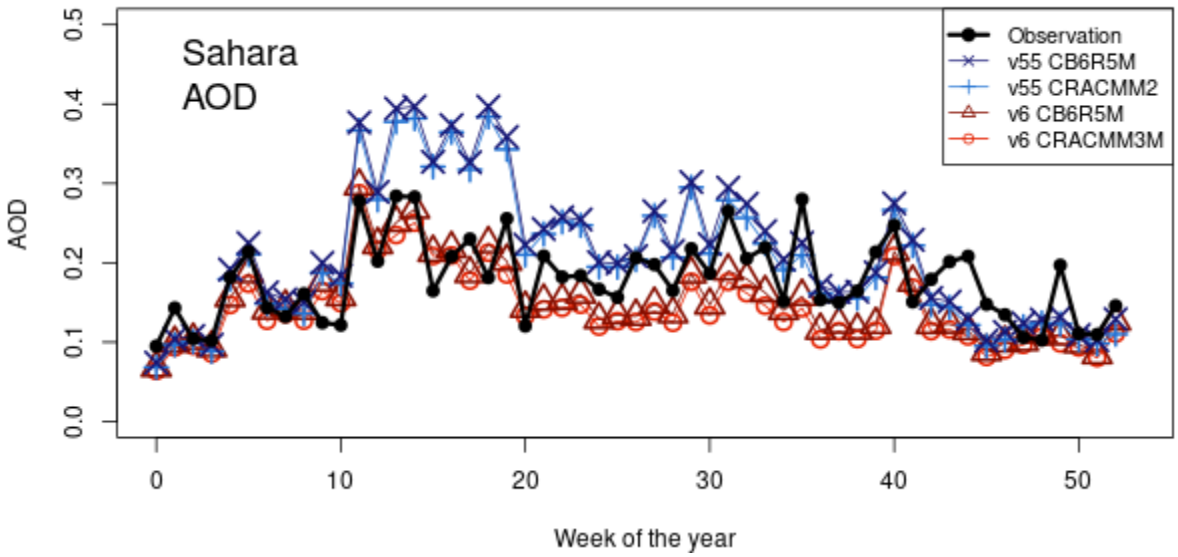

Figure 4-9 Weekly averaged CMAQ predicted AOD for CMAQ version 5.5 and version 6.0 for the year 2022. Modeled predictions were compared to measurements at ground-based AERONET monitoring sites.

4.2.2 CONUS-scale Total $PM_{2.5}$

Total $PM_{2.5}$ concentrations were compared to measurements from the AQS network, which is comprised of both filter measurements and sensor measurements. For $PM_{2.5}$ and $PM_{2.5}$ components evaluated here, $PM_{2.5}$ was calculated from the fraction of the Aitken, accumulation, and coarse mode mass below 2.5 µm in diameter. In comparing CMAQv5.5 (run with both CB6R5 and CRACMM2) with CMAQv6.0 (run with both CB6R5 and CRACMM3), $PM_{2.5}$ concentrations in most of the CONUS domain decreased (particularly in the Southwest) and were largely driven by non-chemistry updates (Section 6.1). These differences generally resulted in improved $PM_{2.5}$ performance in regions where CMAQv5.5 overpredicted $PM_{2.5}$ concentrations and some greater underestimations in parts of the Southeast and Northwest (Figure 4-10).

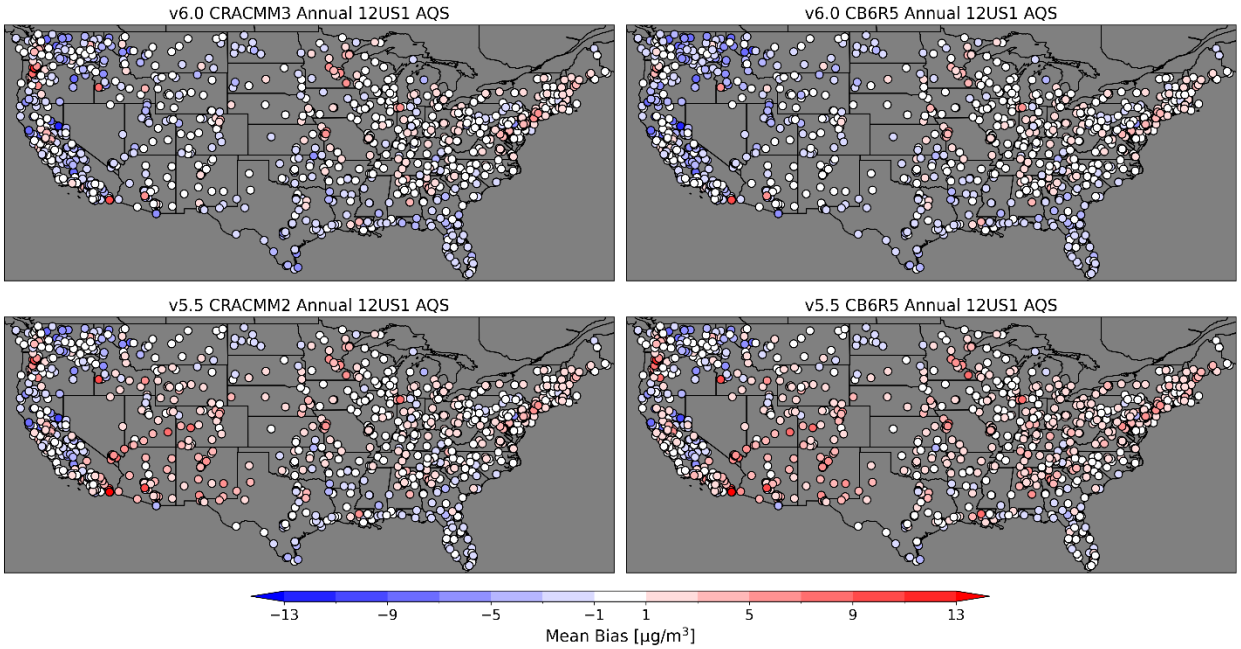

Figure 4-10 Annual mean bias in CMAQ predicted $PM_{2.5}$ for versions 5.5 and version 6.0 for the year 2022. Modeled $PM_{2.5}$ was compared to $PM_{2.5}$ measured at AQS monitoring sites.

CMAQv5.5 overpredictions of $PM_{2.5}$ were the most pronounced during the Spring (Figure 4-11) – with the largest regional/seasonal mean bias (+8.9 μg/m^3; Southwest) reduced to -0.24 μg/m^3 in CMAQv6.0 with CB6R5 (a similar pattern occurs for the CRACMM simulations). $PM_{2.5}$ is generally underpredicted in the Summer in CMAQv6.0 and in the West for all seasons, except for slight overpredictions in the Ohio Valley and Northeast (with CB6R5) and in the Northwest (with CRACMM3) (Figure 4-11).

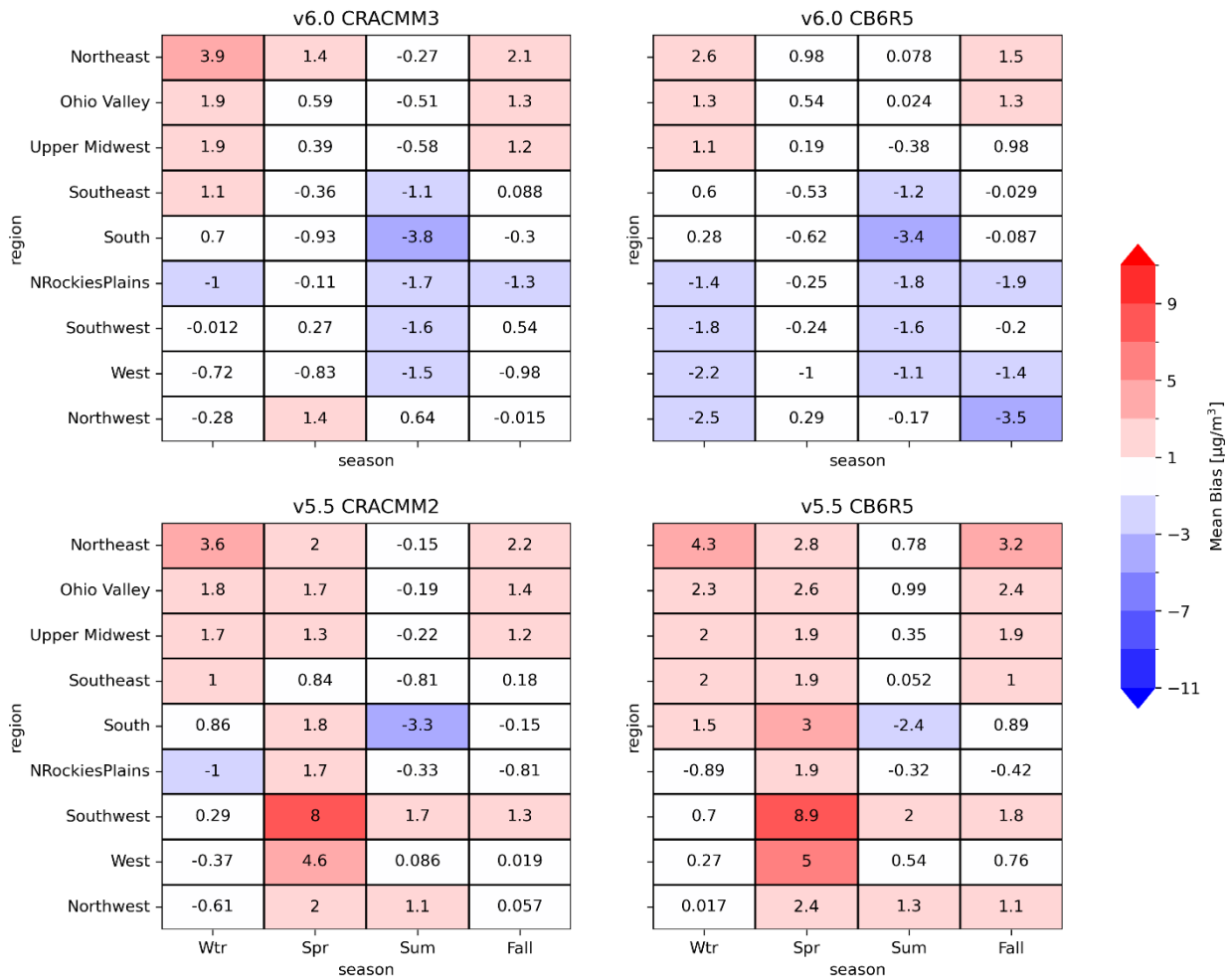

Figure 4-11 Seasonal mean bias in $PM_{2.5}$ by NOAA Climate Region for a yearly simulation of 2022 on the 12US1 CONUS Domain. Modeled $PM_{2.5}$ was compared with measurements from AQS monitoring network.

4.2.3 CONUS-scale Speciated $PM_{2.5}$

Filter-based methods are required to measure $PM_{2.5}$ component species such as sulfate (SO_4), nitrate (NO_3), elemental carbon (EC), organic carbon (OC), and soil $PM_{2.5}$. Soil $PM_{2.5}$ is calculated as 2.2*Al+2.49*Si+1.63*Ca+2.42*Fe+1.94*Ti following equation 5 of Malm et al. (1994). Filter measurements are available via CSN, IMPROVE and CASTNET monitoring sites, and model performance for these species is described in this section. It is important to note the geographical and source differences in these monitors. Most CSN monitors are located in largely urban regions and more densely located in the Eastern U.S., and both IMPROVE and CASTNET monitors are located in rural areas largely in the Western U.S.

Similar to the findings described in Section 4.2.2, aggregated total annual $PM_{2.5}$ mass across monitors at all filter measurement sites decreased between CMAQv5.5 and CMAQv6.0 (Figure 4-12). Soil $PM_{2.5}$ fractions decreased the most between CMAQv5.5 and CMAQv6.0, with a

larger decrease at IMPROVE monitors due to relatively large reductions in soil $PM_{2.5}$ in Western rural areas than Eastern urban areas. The reductions in soil $PM_{2.5}$ contributed to increases in the $PM_{2.5}$ fractions of SO_4, EC, and OC.

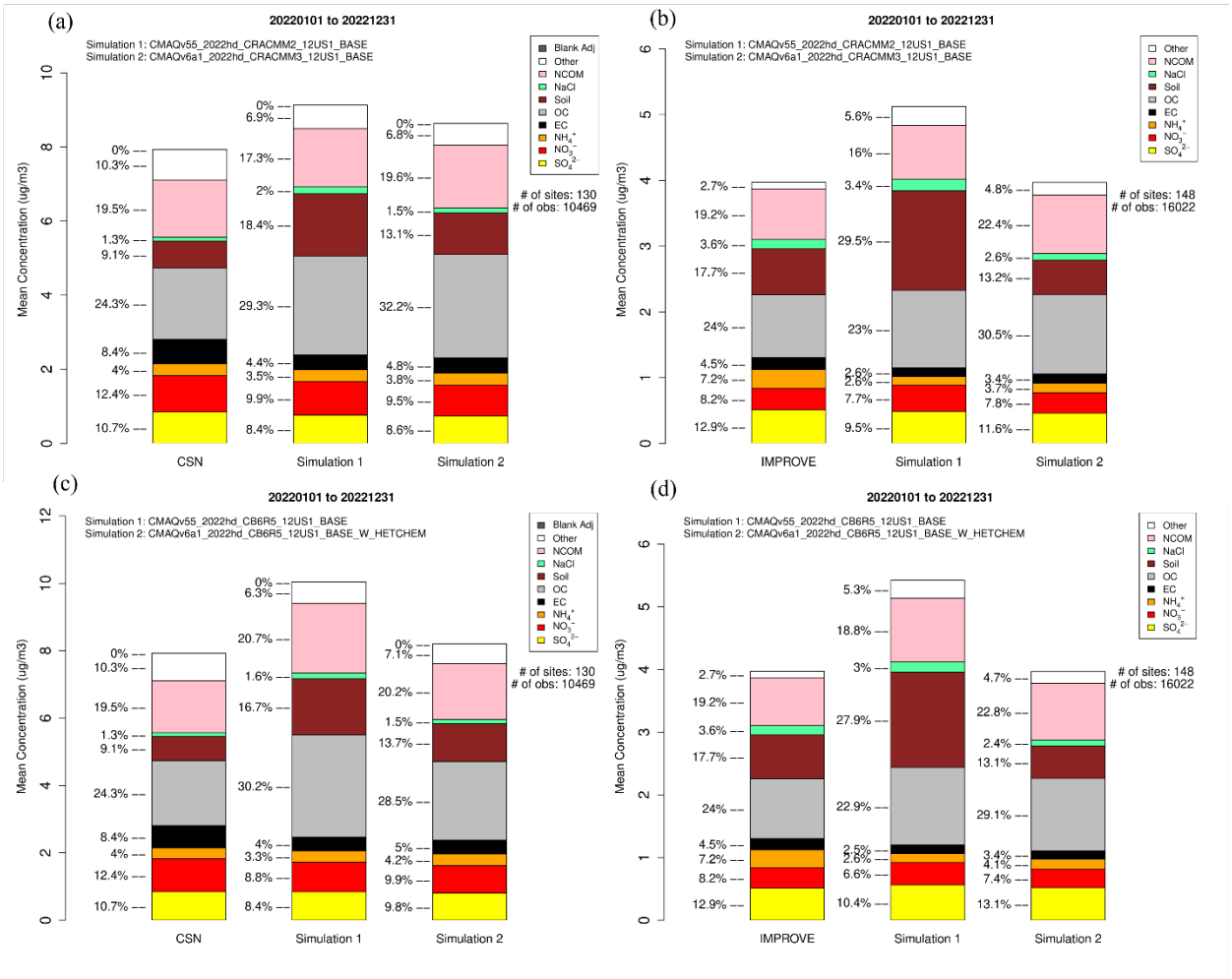

Figure 4-12 Annual mean speciated $PM_{2.5}$ concentrations across all monitors for the CSN network (a, c) and the IMPROVE network (b, d) compared with CMAQv5.5 and CMAQv6.0 predicted speciated $PM_{2.5}$ from CRACMM (a, b) and CB6 (c, d) model runs.

4.2.3.1 SO_4

Concentrations of SO_4 do not change significantly in CMAQv6.0 compared to CMAQv5.5, except for in areas such as Fairbanks, Alaska, and the North China Plain during winter where the addition of heterogeneous sulfur chemistry is particularly important (Section 2.1.2). Over the 12US1 CONUS domain, performance for SO4 is broadly similar in CMAQv5.5 vs. CMAQv6.0 (Figure 4-13 and Figure 4-14).

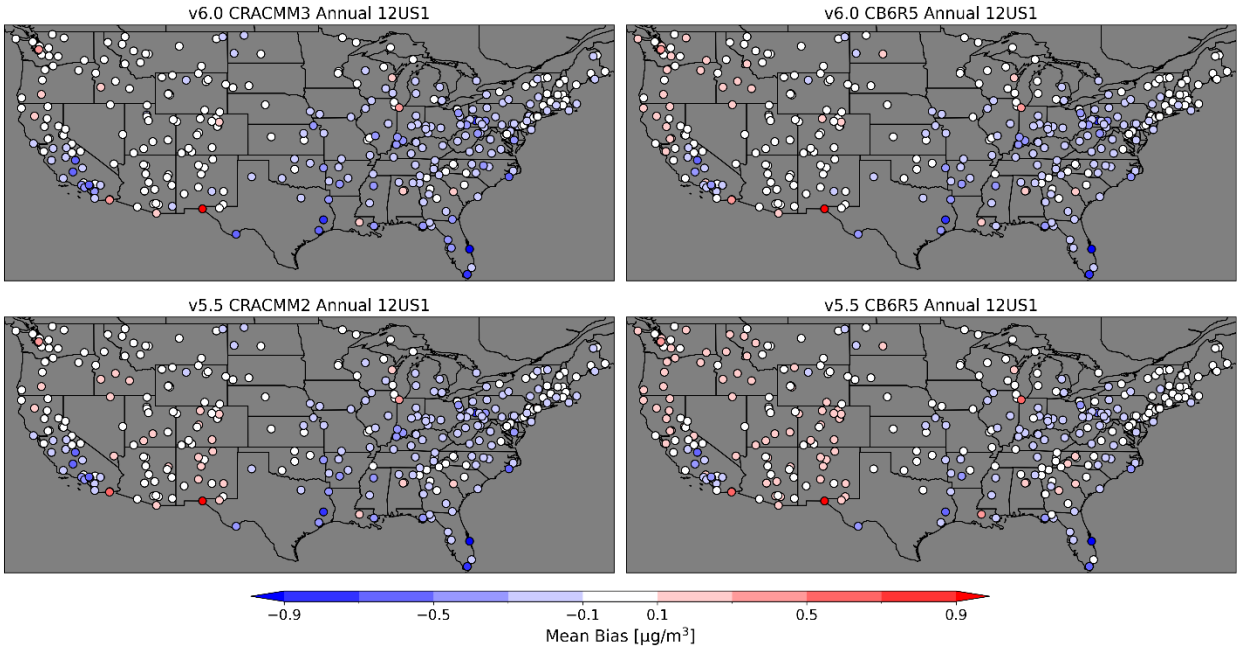

Figure 4-13 Annual mean bias in CMAQ predicted SO_4 for version 5.5 and version 6.0 for the year 2022. Modeled SO_4 was compared to SO_4 measured at IMPROVE, CSN, and CASTNET monitoring sites.

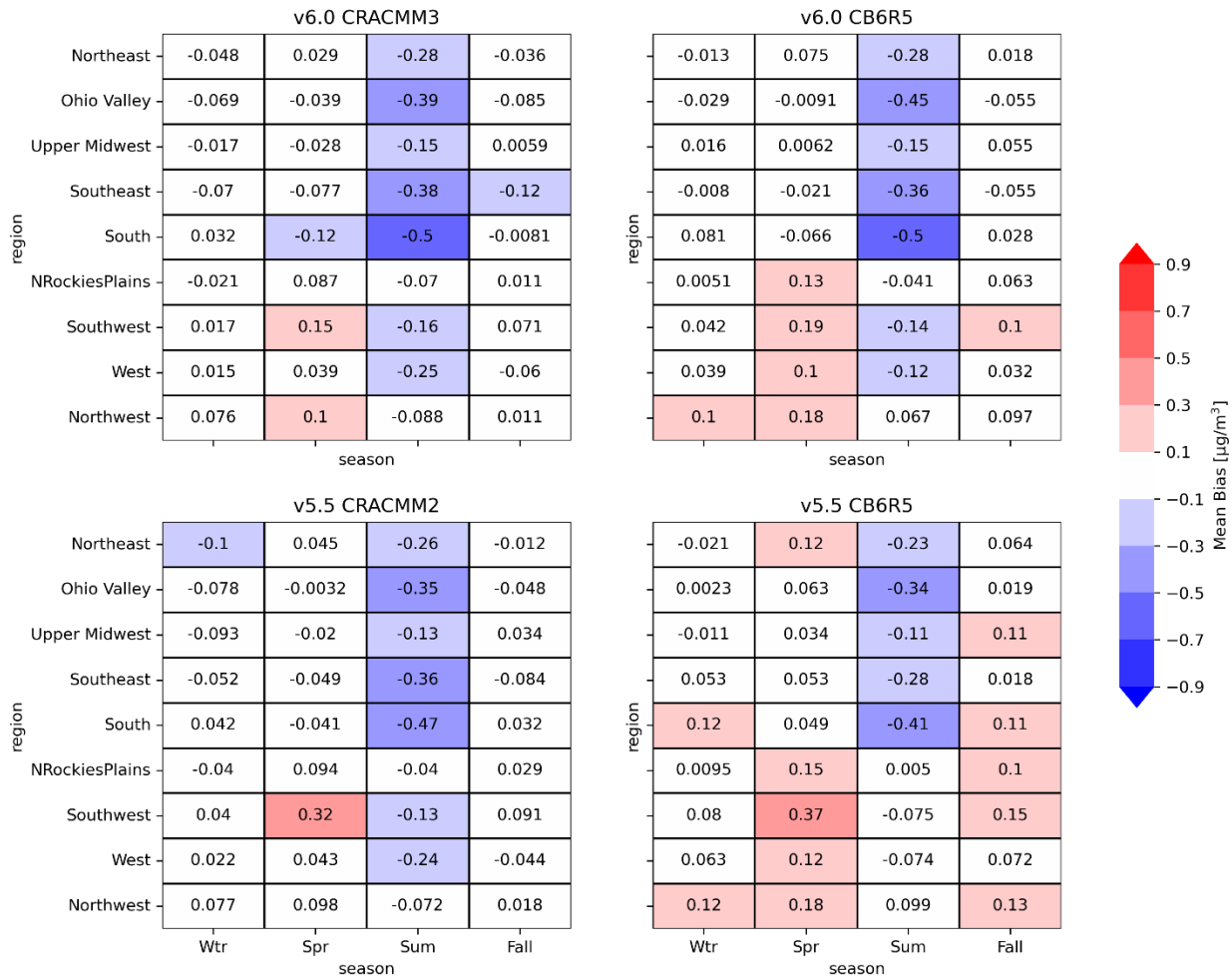

Figure 4-14 Seasonal mean bias in SO_4 by NOAA Climate Region for a yearly simulation of 2022 on the 12US1 CONUS Domain. Modeled SO_4 was compared with filter measurements from the IMPROVE, CSN, and CASTNET monitoring network.

While impacts of version 6.0 updates over CONUS are relatively small, fine-scale modeling over Fairbanks, Alaska, showed a significant increase in modeled particulate sulfur in winter with the addition of heterogeneous sulfur chemistry in CMAQv6.0 (see Section 2.1.2). Fairbanks is located in a $PM_{2.5}$ nonattainment area that experiences severe PM pollution episodes in the cold and dark winters characteristic of the area. During these periods of high $PM_{2.5}$, up to 20% of the observed $PM_{2.5}$ is sulfate. While previous CMAQ modeling showed large underpredictions of sulfate during a set of wintertime PM episodes (ADEC, 2014), the additional sulfur chemistry in CMAQv6.0 improves model performance for particulate sulfur for simulations coinciding with the 2022 ALPACA winter air quality study (Figure 4-15, solid blue vs. dashed red line).

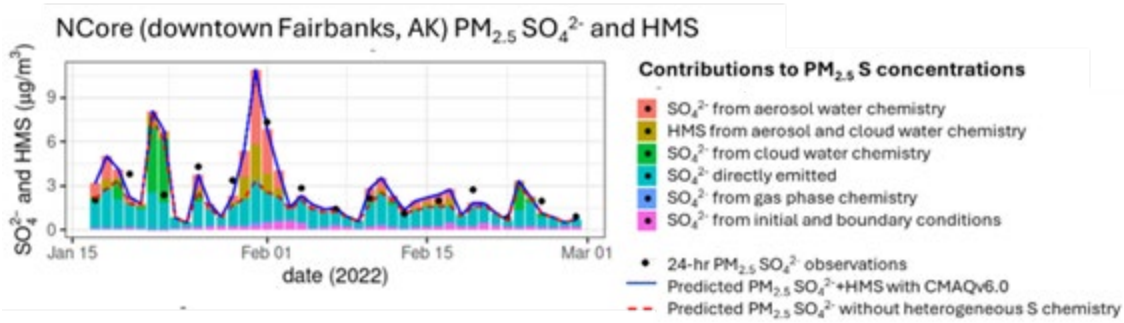

Figure 4-15 Predicted and observed $PM_{2.5}$ sulfur species concentrations in downtown Fairbanks, Alaska, during ALPACA 2022. 24-hr $PM_{2.5}$ SO_4 observations (every third day) are represented by black dots. The blue line represents predictions of $PM_{2.5}$ SO_4 and HMS with heterogeneous sulfur chemistry, while the red dashed-line is predicted $PM_{2.5}$ SO_4 without heterogeneous sulfur chemistry.

4.2.3.2 NO_3

Annual mean bias in modeled NO_3 at CSN, IMPROVE, and CASTNET monitoring sites are shown in Figure 4-16 for the CMAQv5.5 and CMAQv6.0 cases. Concentrations of NO_3 are slightly reduced on average in CMAQv6.0 compared to CMAQv5.5, but the magnitude of the changes are small and do not significantly affect the overall interpretation of NO_3 performance in CMAQ. On an annual basis, positive mean biases in the Southeast in CMAQv5.5 were reduced by ~ 0.01-0.12 µg/m^3 in CMAQv6.0 and positive mean biases in the Southwest were reduced by ~ 0.02-0.4 µg/m^3 on average across sites for the year 2022. Negative mean biases in predicting NO_3 in CMAQv5.5, however, become more negative in CMAQv6.0.

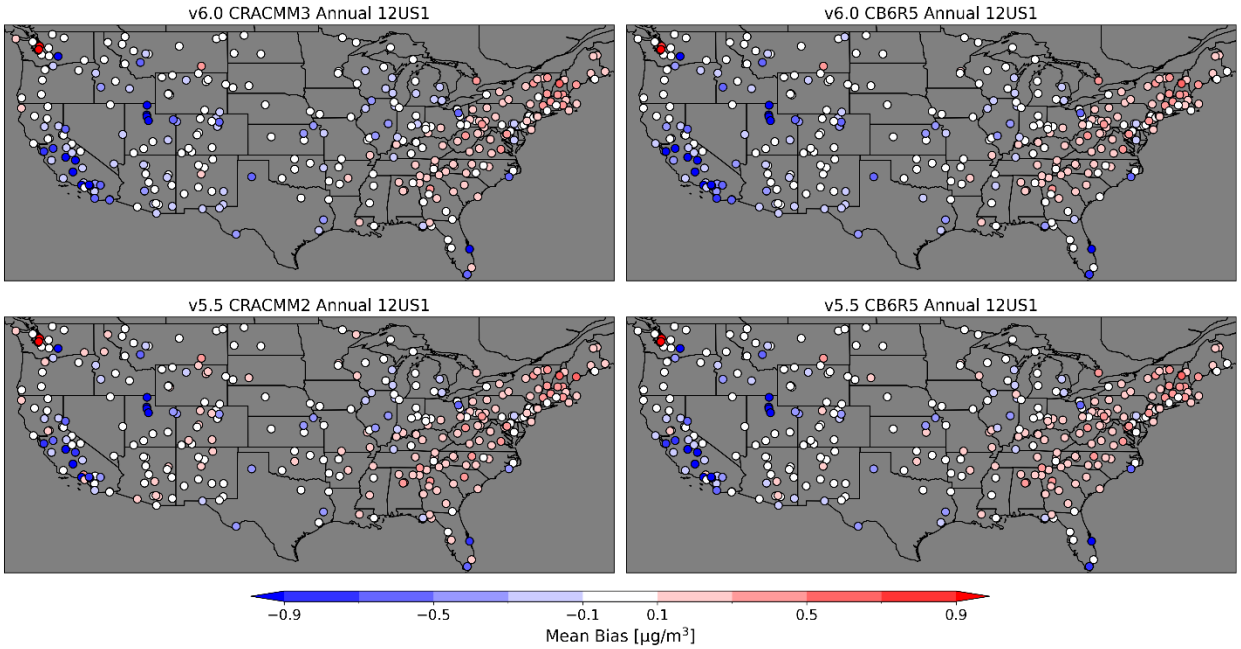

Figure 4-16 Annual mean bias in CMAQ predicted NO_3 for versions 5.5 and version 6.0 for the year 2022. Modeled NO_3 was compared to NO_3 measured at IMPROVE, CSN, and CASTNET monitoring sites.

Wintertime NO_3 is overestimated in the East (with regional/seasonal average mean biases of 0.22-0.75 μg/m^3) in CMAQv5.5, and this positive bias remains in CMAQv6.0 (Figure 4-17). Underpredictions of NO_3 in the West in CMAQv5.5 were furthered in CMAQv6.0. In the Southeast, NO_3 overestimates were reduced in CMAQv6.0 during the Spring and Fall but furthered or not affected in the Winter. Similarly, in the Southwest, NO_3 overestimates in Spring were reduced in CMAQv6.0, but the NO_3 reductions led to underestimates during other seasons.

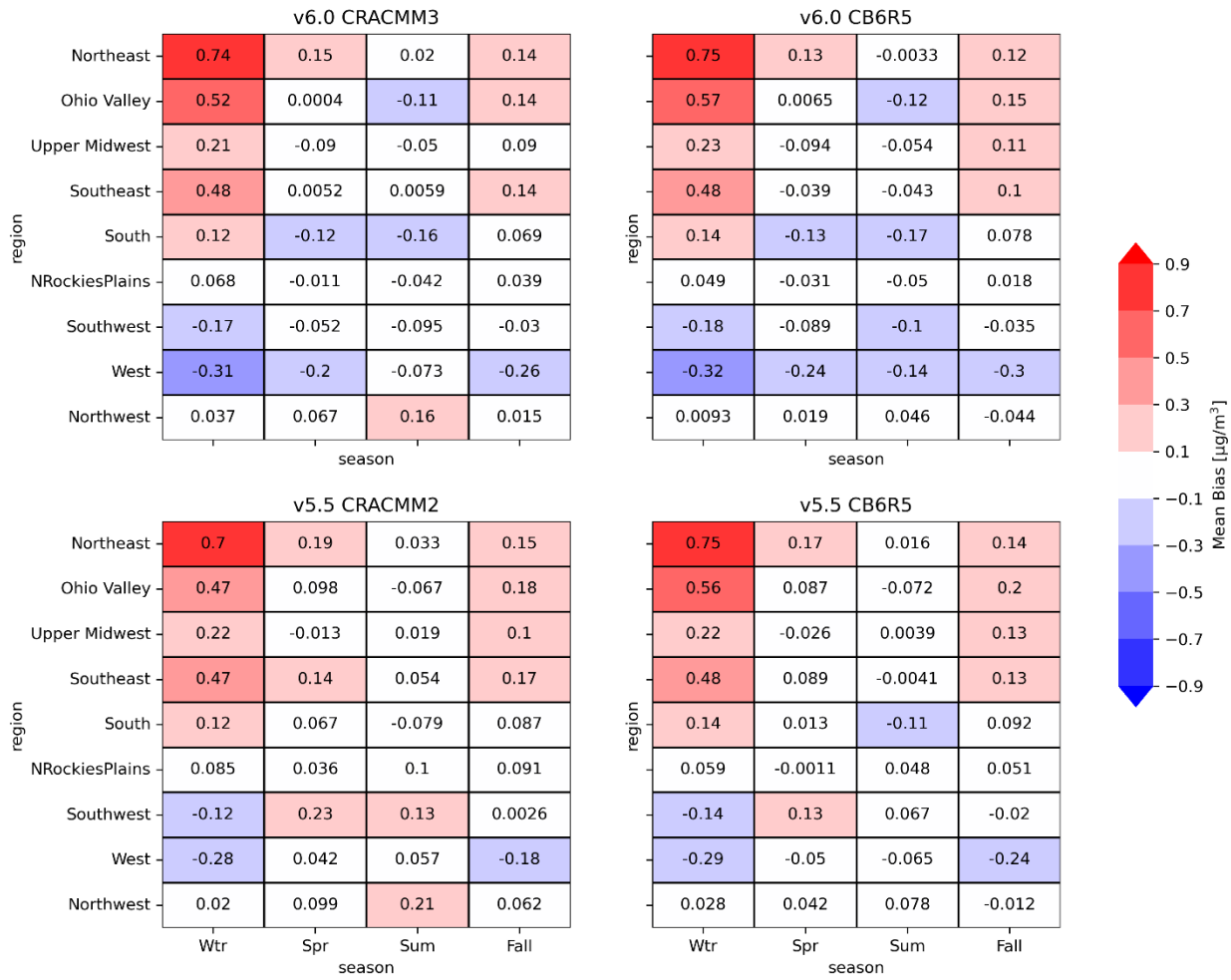

Figure 4-17 Seasonal mean bias in NO_3 by NOAA Climate Region for a yearly simulation of 2022 on the 12US1 CONUS Domain. Modeled NO_3 was compared with filter measurements from the IMPROVE, CSN, and CASTNET monitoring network.

4.2.3.3 EC

Model updates from v5.5 to v6.0 did not change model performance for EC substantially. EC is underpredicted in both the CMAQv5.5 and CMAQv6.0 simulations for annual (Figure 4-18) and seasonal (Figure 4-19) evaluation cases.

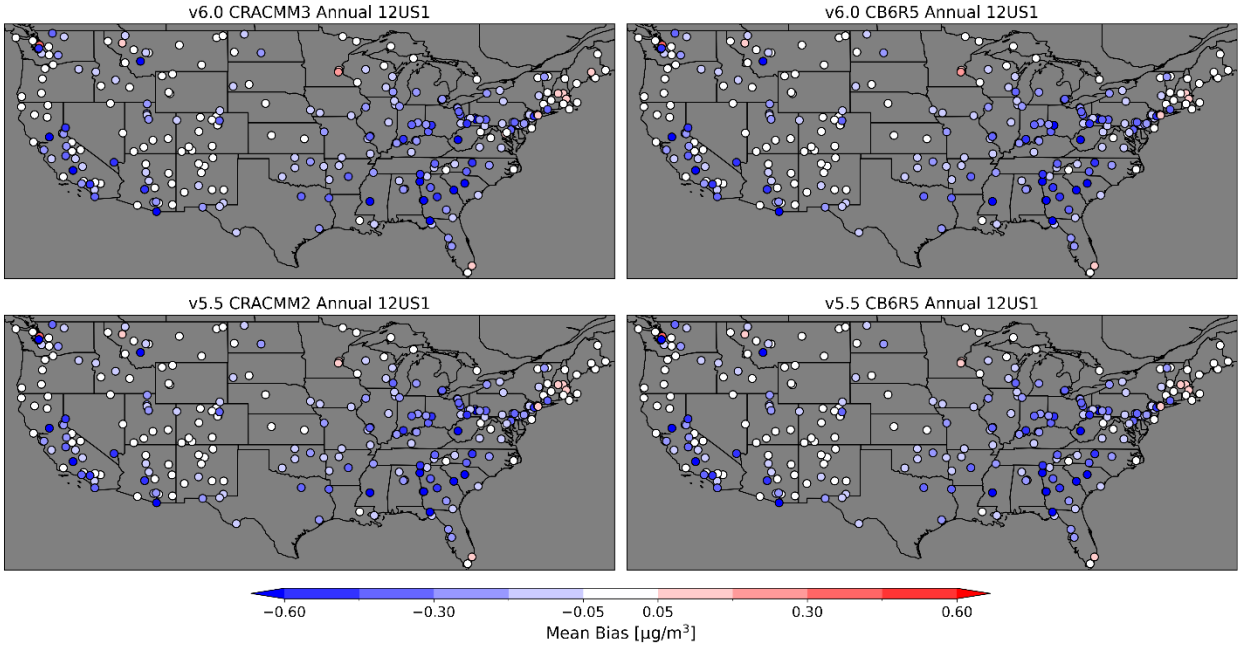

Figure 4-18 Annual mean bias in CMAQ predicted EC for versions 5.5 and version 6.0 for the year 2022. Modeled EC was compared to EC measured at IMPROVE and CSN monitoring sites.

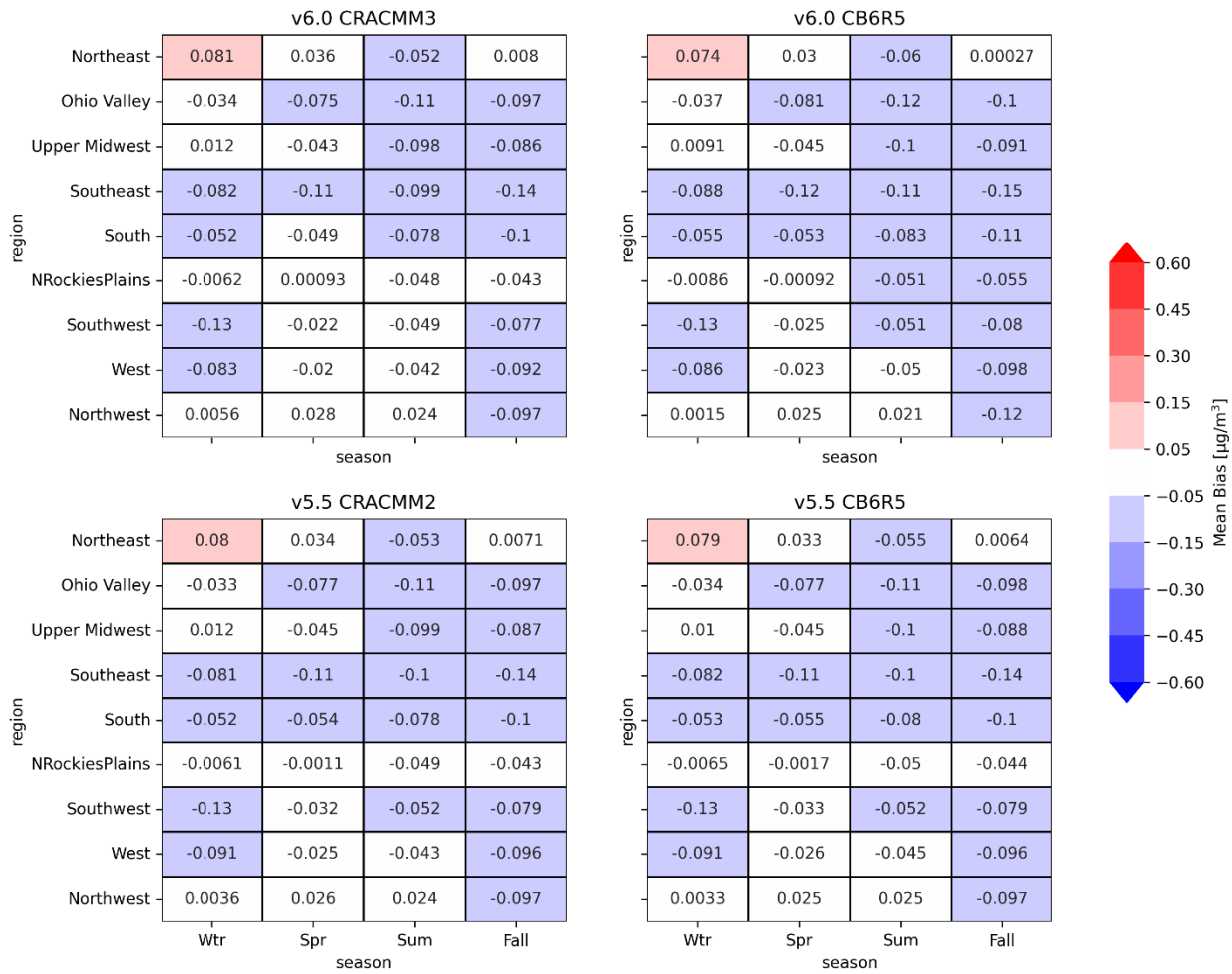

Figure 4-19 Seasonal mean bias in EC by NOAA Climate Region for a yearly simulation of 2022 on the 12US1 CONUS Domain. Modeled EC was compared with filter measurements from the IMPROVE and CSN monitoring network.

4.2.3.4 OC

OC concentrations simulated with CMAQv5.5 are generally overestimated across the U.S., particularly in the east. Overpredictions of OC concentrations were similar or greater in CMAQv6.0 compared with CMAQv5.5 (Figure 4-20).

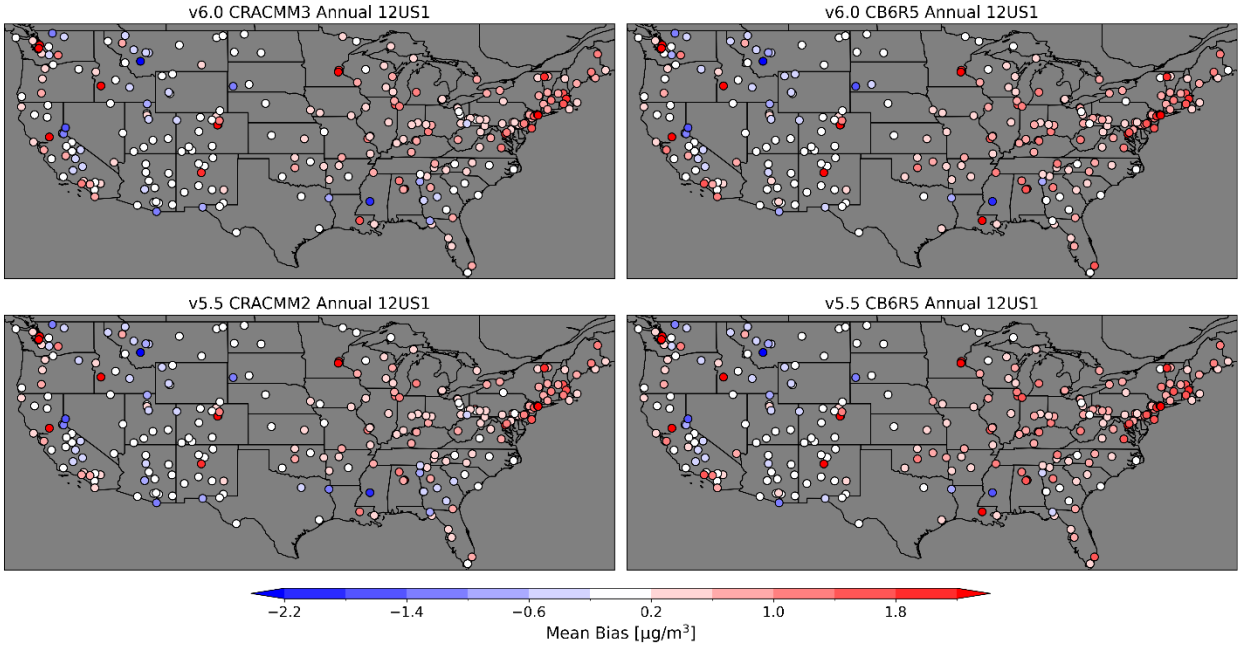

Figure 4-20 Annual mean bias in CMAQ predicted OC for versions 5.5 and version 6.0 for the year 2022. Modeled OC was compared to OC measured at IMPROVE and CSN monitoring sites.

OC performance was similar for CMAQv5.5 and CMAQv6.0 across regions and seasons for both chemical mechanisms (Figure 4-21).

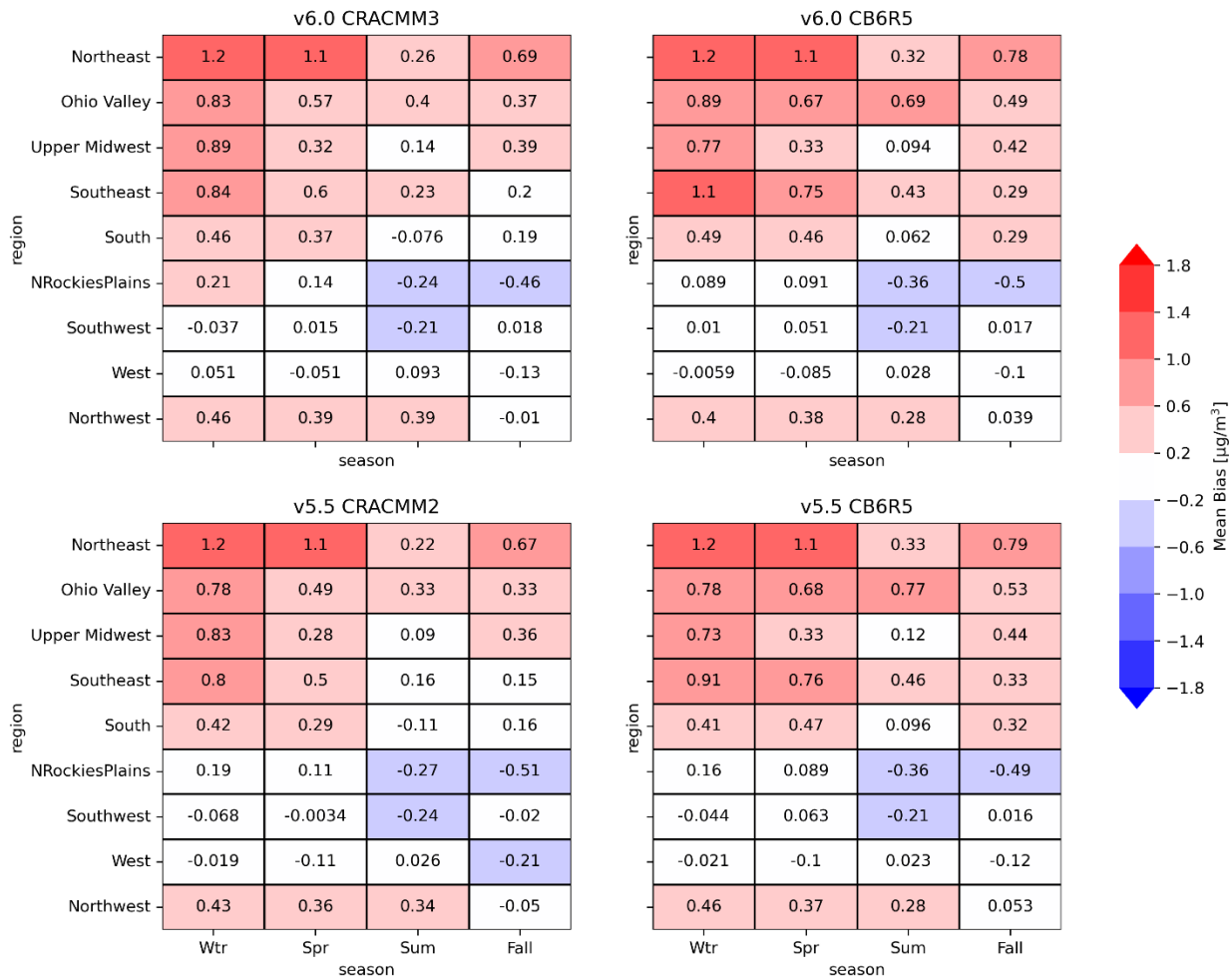

Figure 4-21 Seasonal mean bias in OC by NOAA Climate Region for a yearly simulation of 2022 on the 12US1 CONUS Domain. Modeled OC was compared with filter measurements from the IMPROVE and CSN monitoring network.

4.2.3.5 Soil

The model updates from CMAQv5.5 to CMAQv6.0 influenced predictions of $PM_{2.5}$ soil more than the other $PM_{2.5}$ components (Figure 4-12) and led to differences in the mean bias for $PM_{2.5}$ soil predictions between the two model versions (Figure 4-22). CMAQ-predicted $PM_{2.5}$ soil was largely improved between version 5.5 and 6.0 due to the introduction of non-photosynthetically active vegetation (which prevents erosion and updrafting of soil $PM_{2.5}$ outside of Summer) and a correction to NLCD landuse categorization that changes some barren grid cells to shrubland. The decrease in $PM_{2.5}$ soil did, however, lead to negative bias in predicting this component in CMAQv6.0, particularly in the West (Figure 4-23).

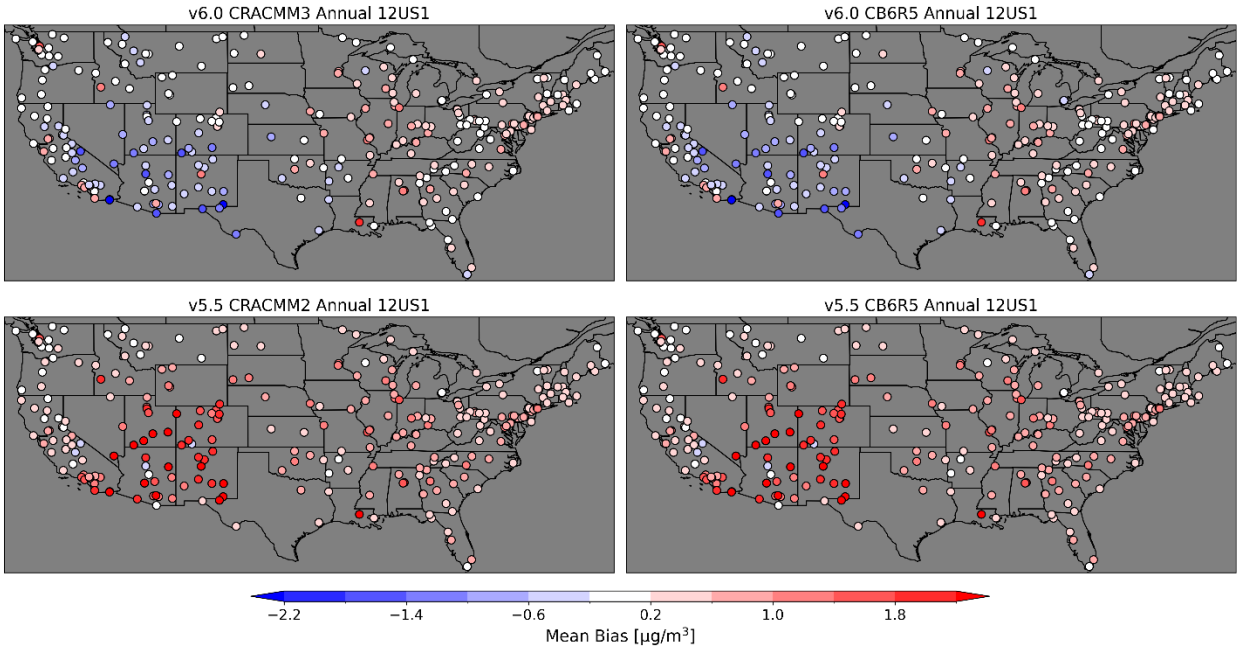

Figure 4-22 Annual mean bias in CMAQ predicted soil for versions 5.5 and version 6.0 for the year 2022. Modeled soil $PM_{2.5}$ was compared to soil $PM_{2.5}$ measured at IMPROVE and CSN monitoring sites.

The largest improvements in model performance for CMAQv6.0 compared with CMAQv5.5 in predicting soil $PM_{2.5}$ occurred during Spring (Figure 4-23). For Summer, overpredictions in soil $PM_{2.5}$ in the CMAQv5.5 simulation corresponded to underpredictions in the CMAQv6.0 simulation for some cases in the western U.S.

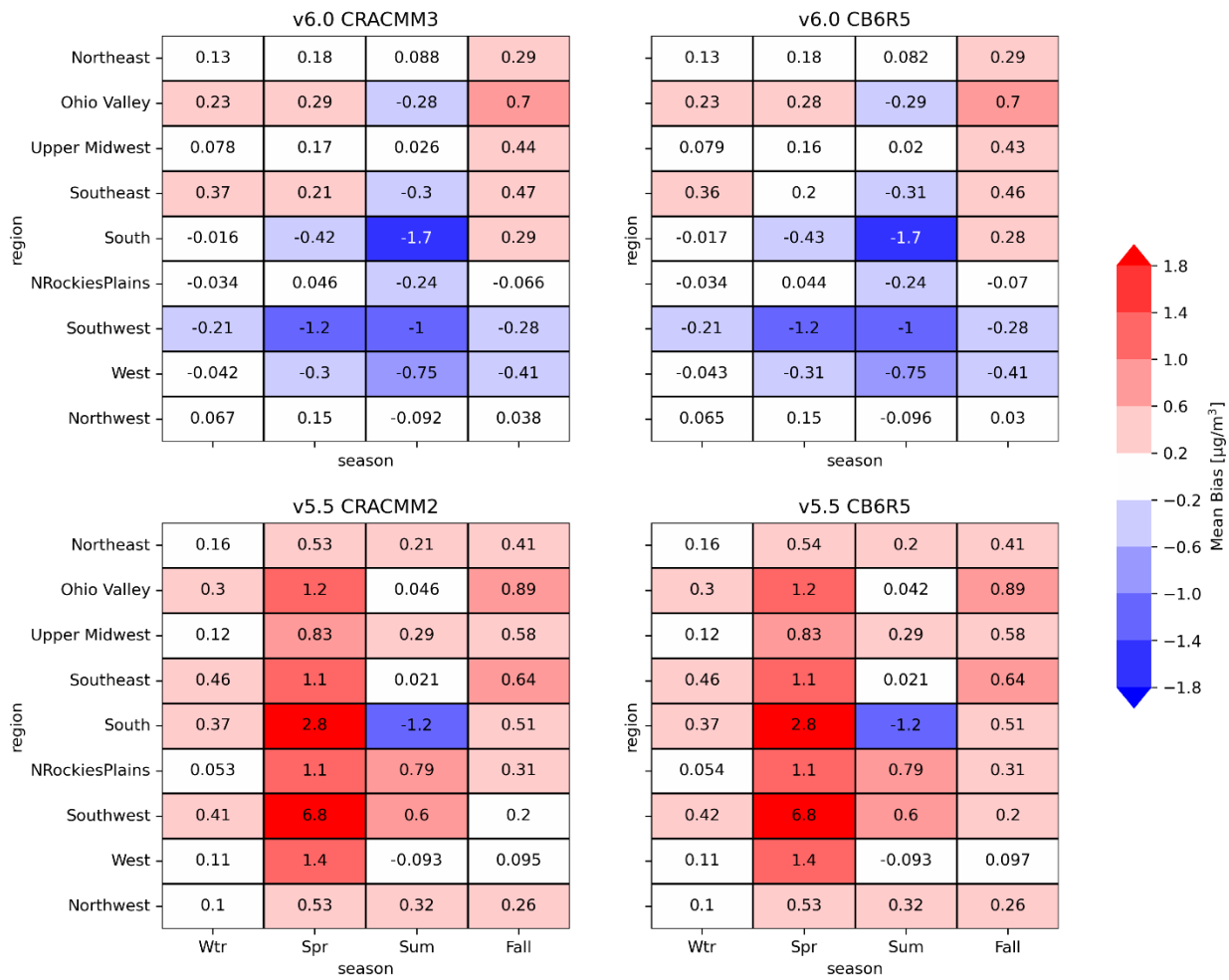

Figure 4-23 Seasonal mean bias in soil by NOAA Climate Region for a yearly simulation of 2022 on the 12US1 CONUS Domain. Modeled soil was compared with filter measurements from the IMPROVE and CSN monitoring network.

5. Model Version Intercomparison

Below, we show the differences of model results between base configurations of CMAQv5.5 and CMAQv6.0 for each mechanism, separately. We used the CRACMM platform for most of the sensitivity simulations that isolate individual or a subset of updates. The meteorological mixing sensitivity was conducted with the CB6R5 mechanism. Since these updates from CMAQv5.5 to CMAQv6.0 affect key performance metrics similarly across CB6R5 and CRACMM mechanisms, we do not foresee meaningfully different interpretations of the sensitivity simulations using either of the mechanisms.

5.1 Seasonal Ozone Comparison for CMAQv5.5 and CMAQv6.0

Figure 5-1 and Figure 5-2 show seasonal surface-level ozone concentrations for CMAQv5.5 and CMAQv6.0 for CRACMM and CB6R5 for the base hemispheric model. Ozone concentration increases are large across the entire domain, due principally to increased ozone formation from the "renoxification" of nitrate due to photolysis of nitrate in the aerosol phase. Impacts of nearly all other updates are much smaller than those driven by particulate nitrate photolysis but are explored in more detail in Section 6. The one exception is that in regions with snow and ice coverage, a bugfix to the STAGE deposition module in CMAQv6.0 decreases seasonal-averaged ozone relative to CMAQv5.5, more than offsetting the broad-scale increases in ozone that otherwise broadly affect the domain.

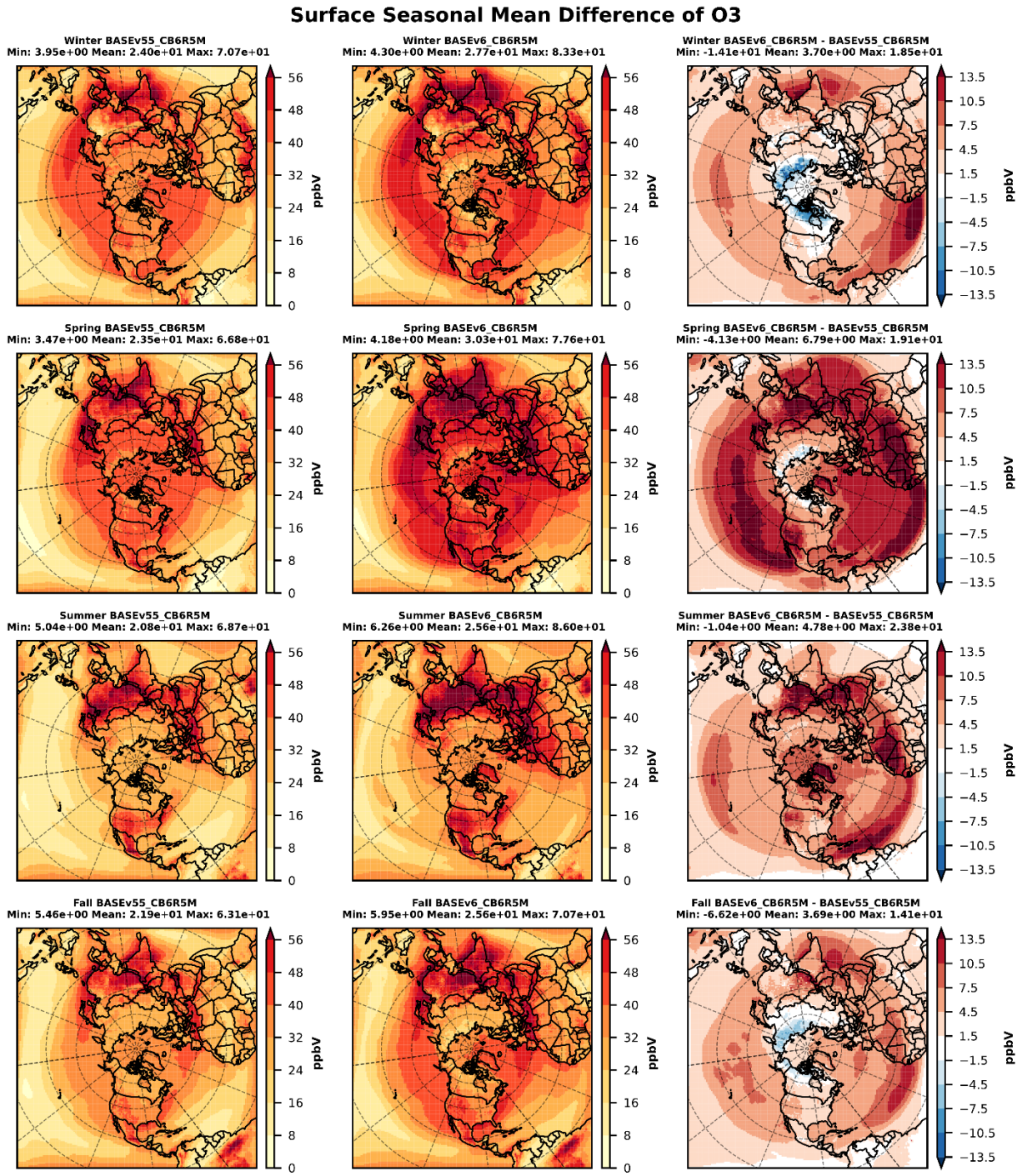

Figure 5-1 Seasonal mean ozone concentrations with BASEv55_HEMI_CB6R5M (left column), BASEv60_HEMI_CB6R5M (middle column), and the difference BASEv60_HEMI_CB6R5M – BASEv55_HEMI_CB6R5M (right column).

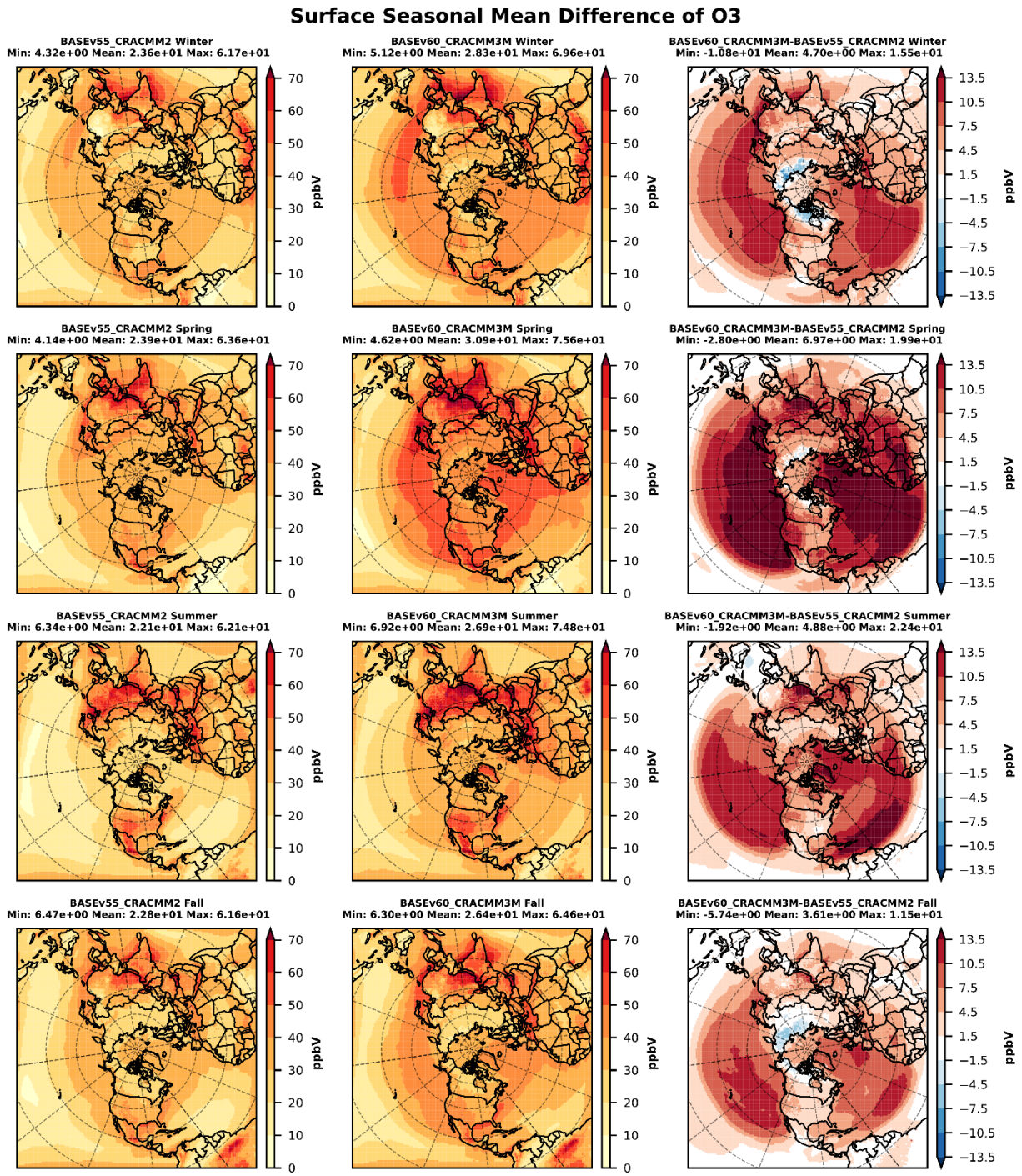

Figure 5-2 Seasonal mean ozone concentrations with BASEv55_HEMI_CRACMM2 (left column), BASEv60_HEMI_CRACMM3M (middle column), and the difference BASEv60_HEMI_CRACMM3M – BASEv55_HEMI_CRACMM2 (right column).

CMAQv6.0 model updates generally increase ozone throughout the CONUS domain in each season (Figure 5-3 and Figure 5-4) principally driven by changes in the hemispheric scale model and long-range transport. The inclusion of aerosol nitrate photolysis in the hemispheric simulation providing the boundary conditions accounts for vast majority of the change in ozone. Over CONUS, the largest increases are during spring and in the western US.

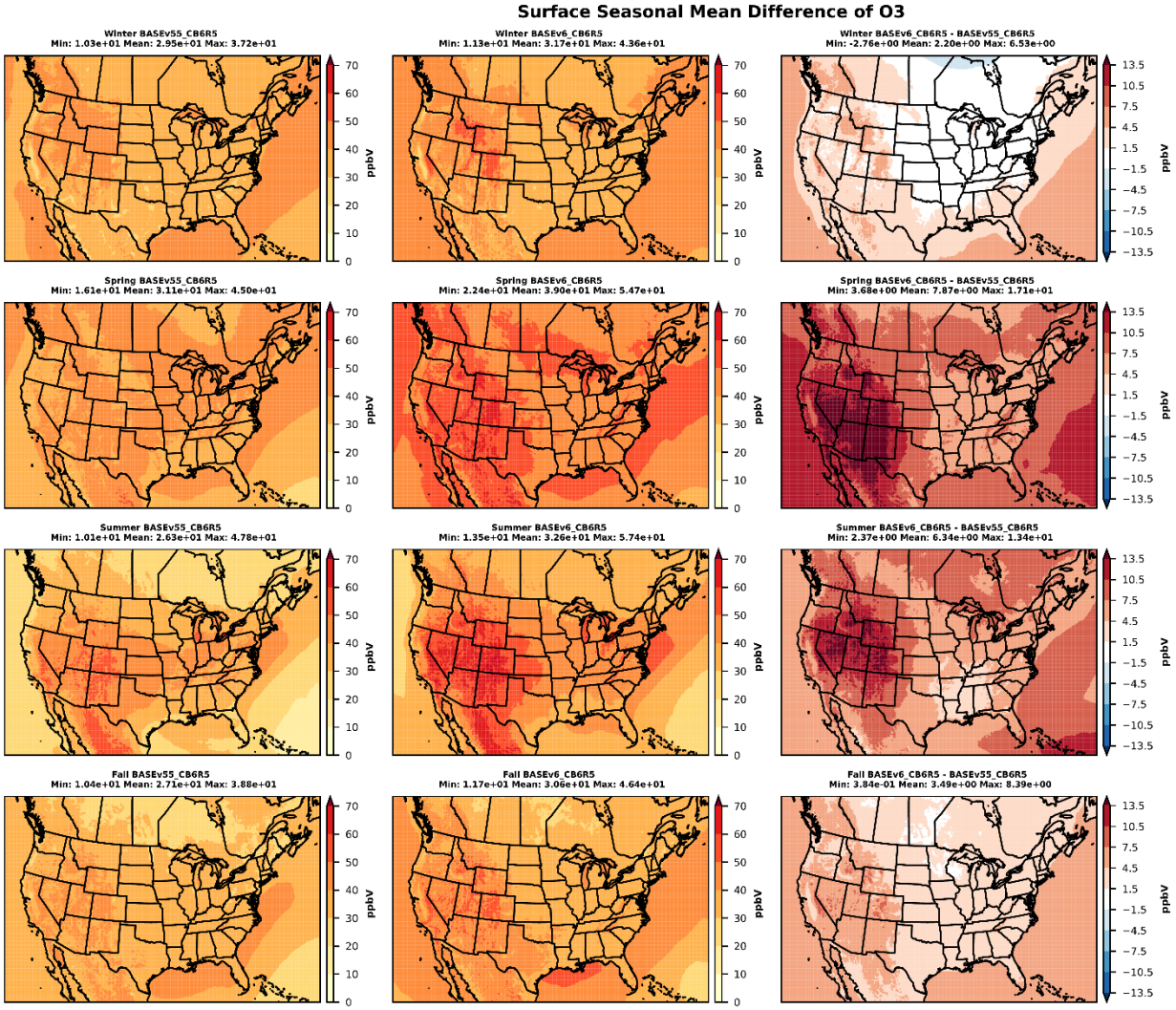

Figure 5-3 Seasonal average changes in ozone in CMAQv6.0 compared to CMAQv5.5 using CB6R5 for 12US1 domain.

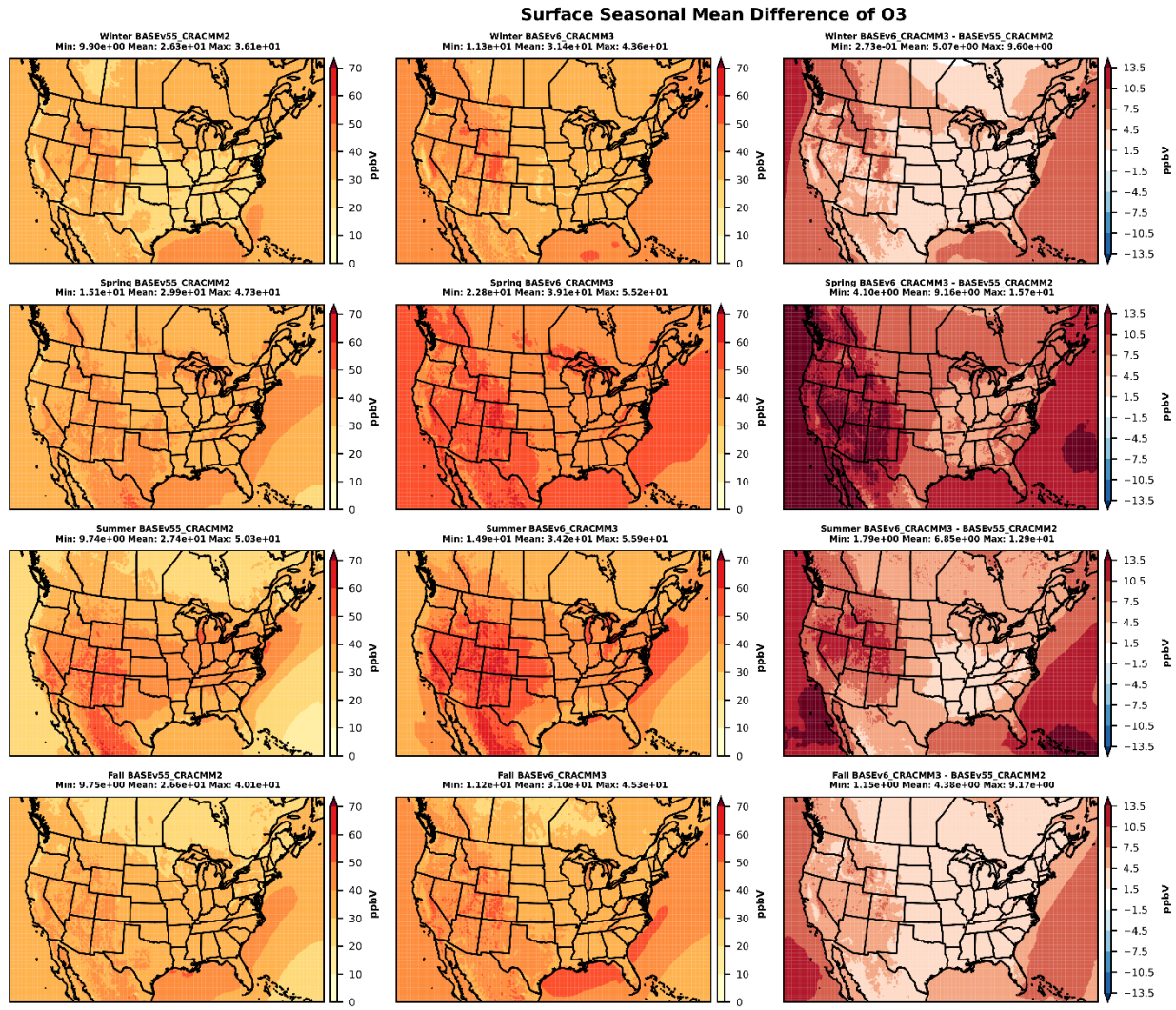

Figure 5-4 Seasonal average changes in ozone in CMAQv6.0 compared to CMAQv5.5 using CRACMM for 12US1 domain.

5.2 Seasonal $PM_{2.5}$ Comparison for CMAQv5.5 and CMAQv6.0

Updates in CMAQv6.0 greatly reduce the windblown dust in the CONUS domain relative to CMAQv5.5 leading to improved performance. Results shown here include emissions of windblown dust in both the CMAQv5.5 and CMAQv6.0 simulations to demonstrate the large changes in $PM_{2.5}$ resulting from these updates. There are large reductions in seasonal average $PM_{2.5}$ in areas where dust emissions are more prevalent (Figure 5-6 (CB6R5) and Figure 5-7 (CRACMM3)).

There was also a notable increase in $PM_{2.5}$ over eastern China during the winter season (Figure 5-5) between model versions 5.5 and 6.0. This is partially due to the addition of heterogeneous sulfur chemistry in CMAQv6.0. While seasonal average impacts of the added chemistry on

$PM_{2.5}$ over CONUS are not very large (Figure 5-5), the additional chemical reactions can lead to significantly increased particulate sulfur concentrations and improve model performance in locations like Fairbanks, AK, and China during the winter season (Figure 4-15).

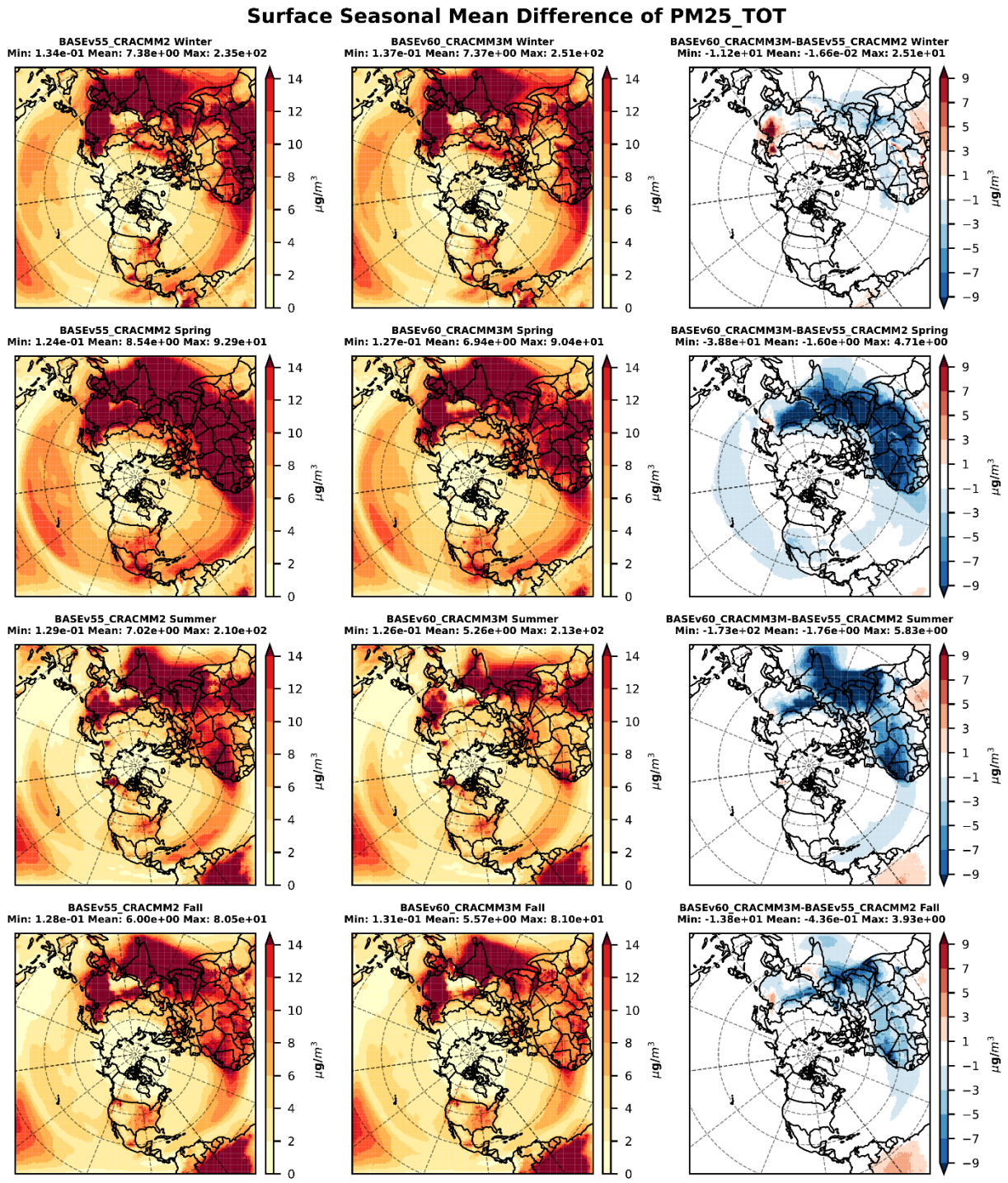

Figure 5-5 Seasonal mean $PM_{2.5}$ concentrations with BASEv55_HEMI_CRACMM2 (left column), BASEv60_HEMI_CRACMM3M (middle column), and the difference BASEv60_HEMI_CRACMM3M – BASEv55_HEMI_CRACMM2 (right column).

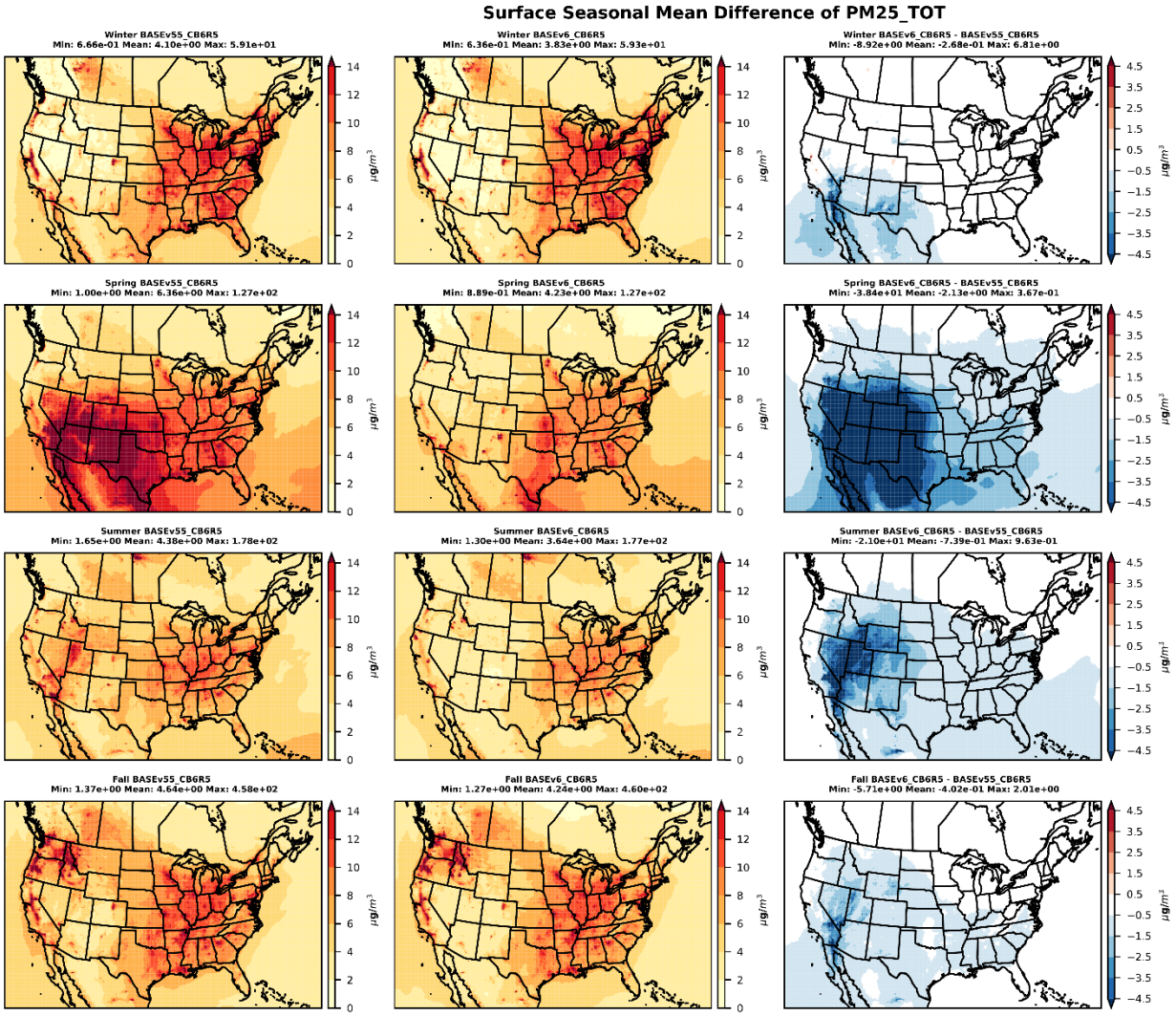

Figure 5-6 Seasonal average changes in $PM_{2.5}$ in CMAQv6.0 compared to CMAQv5.5 using CB6R5 for 12US1 domain.

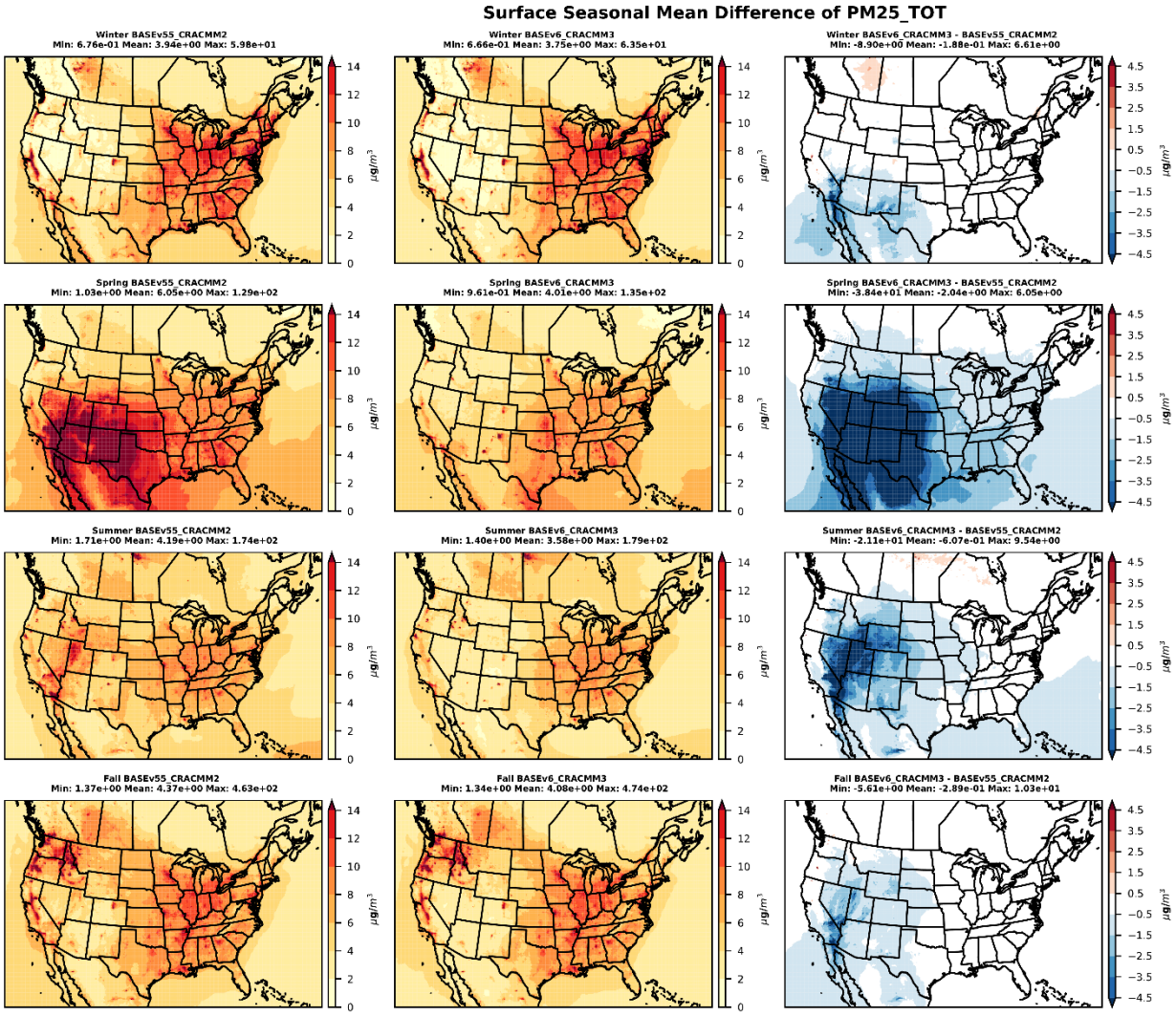

Figure 5-7 Seasonal average changes in $PM_{2.5}$ in CMAQv6.0 compared to CMAQv5.5 using CRACMM for 12US1 domain.

6. Incremental Testing of Significant Model Updates

In general, the model and mechanism updates are insensitive to the base chemical mechanism, whether CB6R5 or CRACMM (see Sections 4 and 5). Given the similarity of responsiveness, incremental tests of individual updates are only analyzed for CRACMM. Section 6.1 describes the impacts of chemistry and non-chemistry updates holistically. Sections 6.2 – 6.4 describe the impacts of non-chemistry science updates to emissions (Section 6.2), dry deposition (Section 6.3) and meteorology or vertical mixing modules (Section 6.4).

6.1 Chemistry vs. Non-chemistry Increments

Figure 6-1 and Figure 6-2 disaggregate the impacts due to chemistry and non-chemistry updates in CMAQv6.0 on simulated seasonal average ozone and $PM_{2.5}$, respectively. For each of four seasons (four rows), both figures show the following:

- base model CMAQv5.5 CRACMM2 results (left column),
- difference between CMAQv5.5 CRACMM2 and CMAQv6.0 CRACMM3 base models (second column),
- difference between the CMAQv5.5 CRACMM2 base model and CMAQv6.0 using CRACMM2 to highlight updates not involving chemistry (third column), and
- difference between the CMAQv6.0 CRACMM2 model and the base CMAQv6.0 CRACMM3 model to highlight the impacts of chemistry updates.

Chemistry updates are responsible for most impacts on the ozone simulation (Figure 6-1, right column). Non-chemistry updates are responsible for most impacts on $PM_{2.5}$ simulation (Figure 6-2, third column from left).

Updates to aerosol nitrate photolysis chemistry included in CMAQv6.0 drive most of the changes in ozone simulations, across seasons and regions (Figure 6-1). The large increases in simulated ozone driven by updates to chemistry (fourth column) are partly offset by non-chemistry updates in colder regions and seasons (third column). Updates to deposition processes for snow and ice surfaces drive these reductions. At the hemispheric scale (Section 5.1, Figure 5-1 and Figure 5-2, right column), these same non-chemistry updates result in the CMAQv6.0 ozone simulation decreases over snow and ice in the Arctic relative to CMAQv5.5, negating the increases occuring at the broader scale.

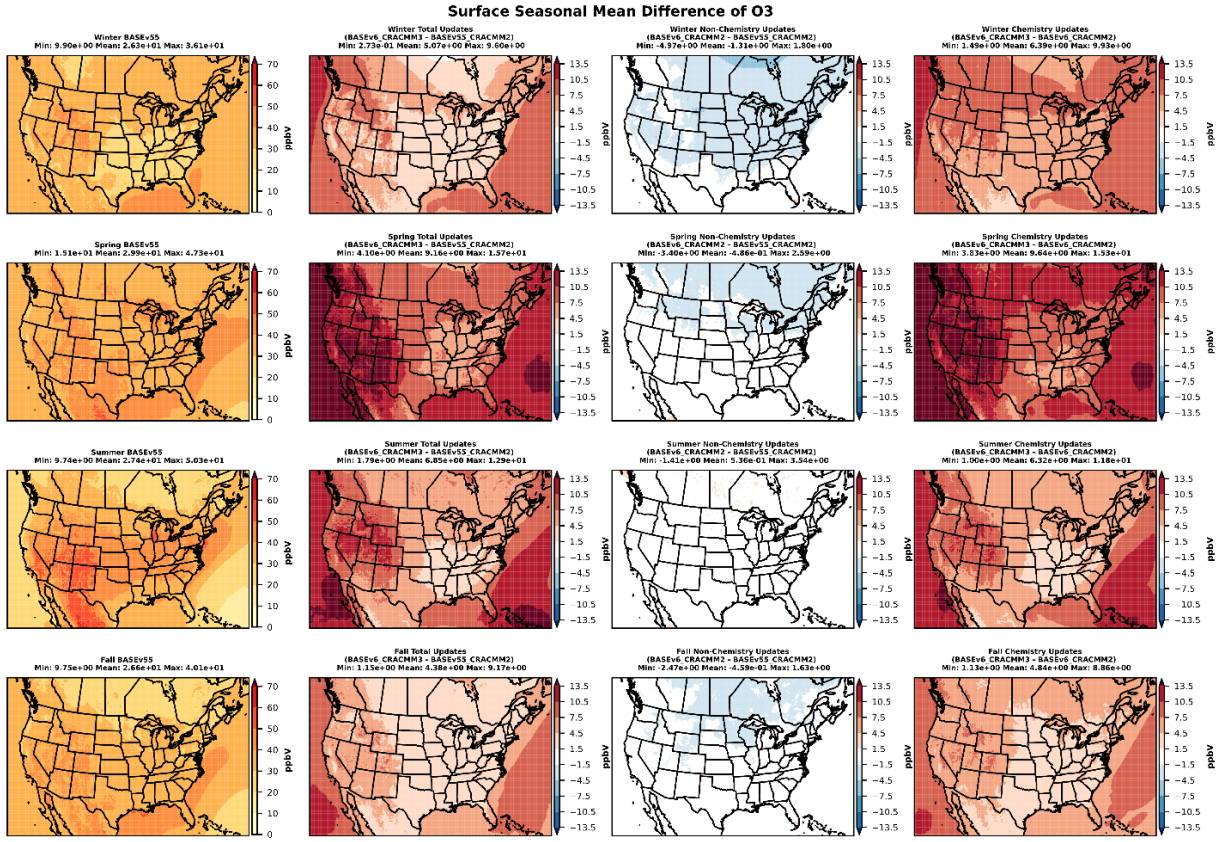

Figure 6-1 Seasonal average ozone in CMAQv5.5 base simulation (left column), changes in ozone using CRACMM3 for CMAQv6.0 compared to CRACMM2 for CMAQv5.5 (second from left column), changes from non-chemistry updates when using CRACMM2 with CMAQv5.5 and CMAQv6.0 (second from right column), and changes from updating the chemistry to CRACMM3 from CRACMM2 with CMAQv6.0 (right column). Changes shown here include changes both from boundary conditions generated from hemispheric CMAQ simulations using different versions (CMAQv5.5 and CMAQv6.0) and differences in the version of CMAQ used for the CONUS simulations (CMAQv5.5 and CMAQv6.0).

Model updates between CMAQv5.5 and CMAQv6.0 generally decrease simulated $PM_{2.5}$ or result in no net change across seasons and regions of CONUS (Figure 6-2, second column). Model updates decrease simulated $PM_{2.5}$ in seasons and regions where dust events are common. The largest impacts of model updates are almost entirely due to non-chemistry updates, as shown in incremental model testing (Figure 6-2, third column). Model updates also affect non-soil components of $PM_{2.5}$, but the changes are generally smaller than updates affecting windblown dust emissions but can be larger for certain seasons and regions. For the CRACMM simulations, there are increases in $PM_{2.5}$ due to CMAQv6.0 updates to chemistry (Figure 6-2, right-most column). These increases primarily occur in the summer and come from increases in organic aerosol concentrations resulting from changes in the treatment of autoxidation of monoterpene

oxidation products. Monoterpene chemistry updates are not included in CB6R5. This difference between the CB6R5 and CRACMM updates to monoterpene chemistry included in CMAQv6.0, and the resulting impacts on $PM_{2.5}$, is evident in the model intercomparison (Section 5.2). The CMAQv6.0 updates to CB6R5 produce slightly larger summertime $PM_{2.5}$ decreases in the southeast US than the CMAQv6.0 updates to CRACMM, which include the monoterpene chemistry updates (Figure 5-6 vs. Figure 5-7, right column).

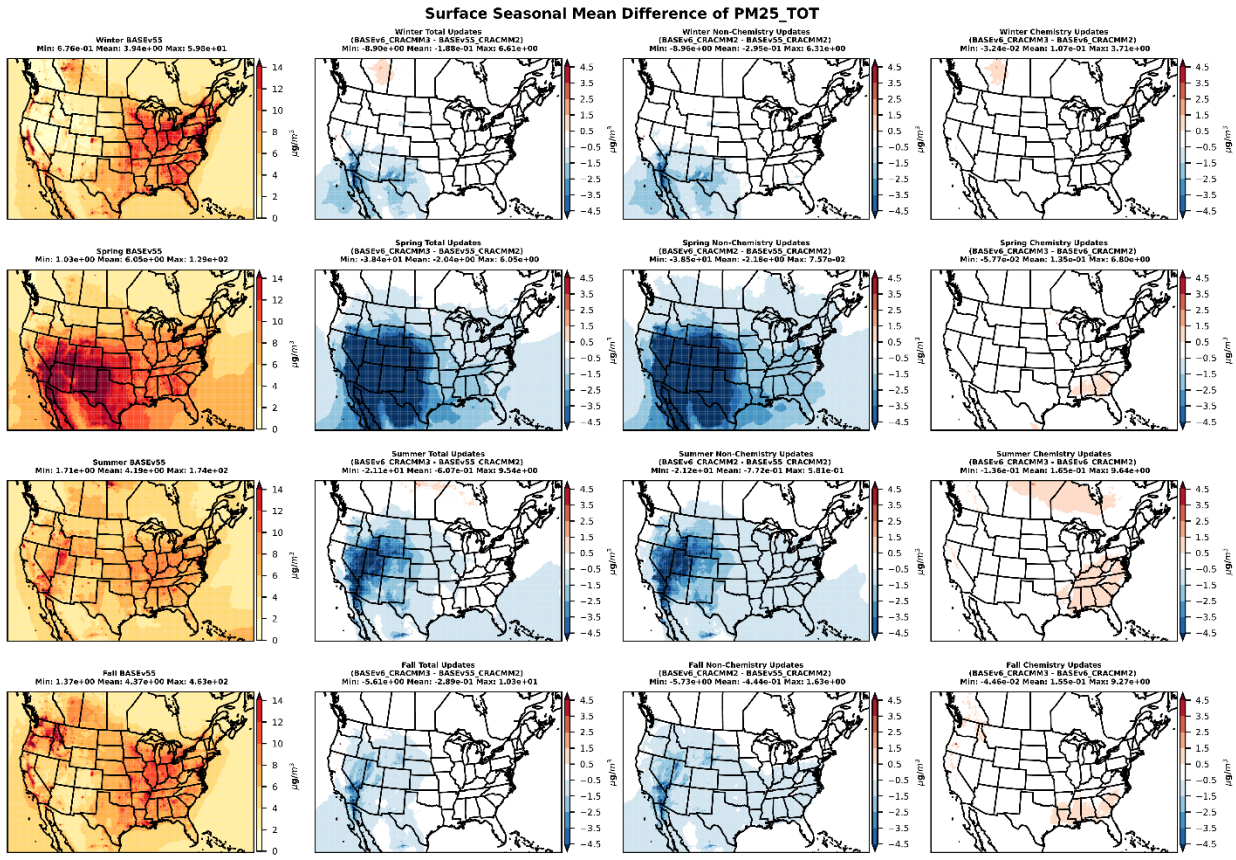

Figure 6-2. Seasonal average $PM_{2.5}$ concentrations in CMAQv5.5 base simulation (left column), total change in $PM_{2.5}$ using CRACMM3 for CMAQv6.0 compared to CRACMM2 for CMAQv5.5 (second from left column), changes from non-chemistry updates when using CRACMM2 with CMAQv5.5 and CMAQv6.0 (second from right column), and changes from updating the chemistry to CRACMM3 from CRACMM2 with CMAQv6.0 (right column). Changes shown here include changes both from boundary conditions generated from hemispheric CMAQ simulations using different versions (CMAQv5.5 and CMAQv6.0) and differences in the version of CMAQ used for the CONUS simulations (CMAQv5.5 and CMAQv6.0).

6.2 Emissions Incremental Testing

6.2.1 Windblown Dust Emissions

CMAQ's windblown dust parameterization is a physics-based approach that estimates particle emissions over erodible land types through saltation as described in Foroutan et al. (2017). As discussed in section 2.2.1, CMAQ version 6.0 includes two significant changes to this parameterization. The first change only affects North American domains and involves correcting some NLCD landuse erodibility categories from the highly erodible "barren" category to shrub/scrub and dwarf/scrub. NLCD data are not available outside of North America, and the 108HEMI domain used here used MODIS landuse data for its WRF simulation.

The second change adds an option to include sheltering from non-photosynthetically active (brown) vegetation as described by Huang and Foroutan (2022). The brown vegetation option affects all dust-producing areas on the globe when enabled. Both updates result in near-monotonic reductions of windblown dust emissions.

To enable the brown vegetation option, users must modify their run script to set the following environmental variables:

- setenv CTM_BROWN_VEG Y
- setenv PV_AVG_FILE pv_avg.dat
- setenv NPV_AVG_FILE npv_avg.dat

The required npv_avg.dat and pv_avg.dat files are currently available for download from Amazon Web Services at:

- https://cmaq-12us1-cracmm2-modeling-platform-2022.s3.amazonaws.com/2022_12US1/surface/npv_avg.dat
- https://cmaq-12us1-cracmm2-modeling-platform-2022.s3.amazonaws.com/2022_12US1/surface/pv_avg.dat

These files include satellite-based global vegetation fractions of photosynthetically active vegetation (PV) and non-photosynthetically active vegetation (NPV; brown vegetation). The files comprise a 2001-2017 climatology at 0.1° x 0.1° resolution and can be used for any domain. PV and NPV fractions affect vegetation height and roughness in the windblown dust module.

A sensitivity experiment is used to evaluate the effect of these updates on windblown dust emissions and $PM_{2.5}$ performance. This "No WBD updates" sensitivity uses the **BASEv60_HEMI** and **BASEv60_12US1** configurations with the CRACMM3M and CRACMM3 mechanisms, respectively. Consistent with Huang and Foroutan (2022), the inclusion of NPV significantly reduces the emissions of windblown dust in CMAQ.

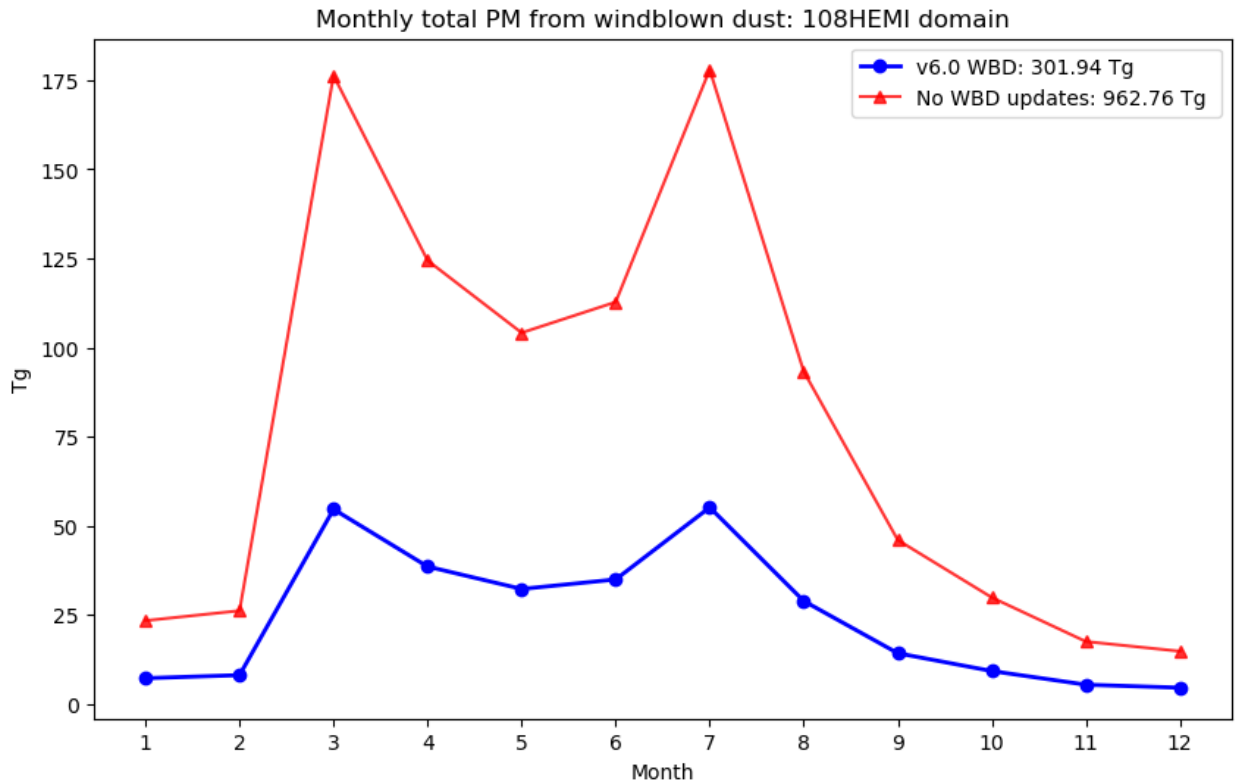

Figure 6-3 Monthly total PM emissions from windblown dust for the 108NHEMI domain.

Figure 6-3 shows the monthly total emissions for the 108HEMI domain with and without version 6.0 updates. The differences in Figure 6-3 are entirely from the inclusion of brown vegetation, since the NLCD landuse correction does not affect the 108HEMI domain. Emissions in the 108HEMI domain peak first in March, driven by the Middle East and North Africa, and peak again in July due to emissions from sub-Saharan Africa (not shown). The total effect of including brown vegetation is a ~70% reduction in annual total PM emissions from windblown dust from 962.76 Tg/yr to 301.94 Tg/yr. Figure 6-4 shows that the reductions in windblown dust are large and ubiquitous across all regions where windblown dust is typically emitted, while Figure 6-10 shows that the effects on annual average surface $PM_{2.5}$ concentrations are significant but localized to regions with high emissions. Annual average $PM_{2.5}$ decreases ~10 μg/m^3 over Africa, the Middle East, and Asia. Changes in long-range transport into the CONUS as a result of brown vegetation are not apparent in the annual mean.

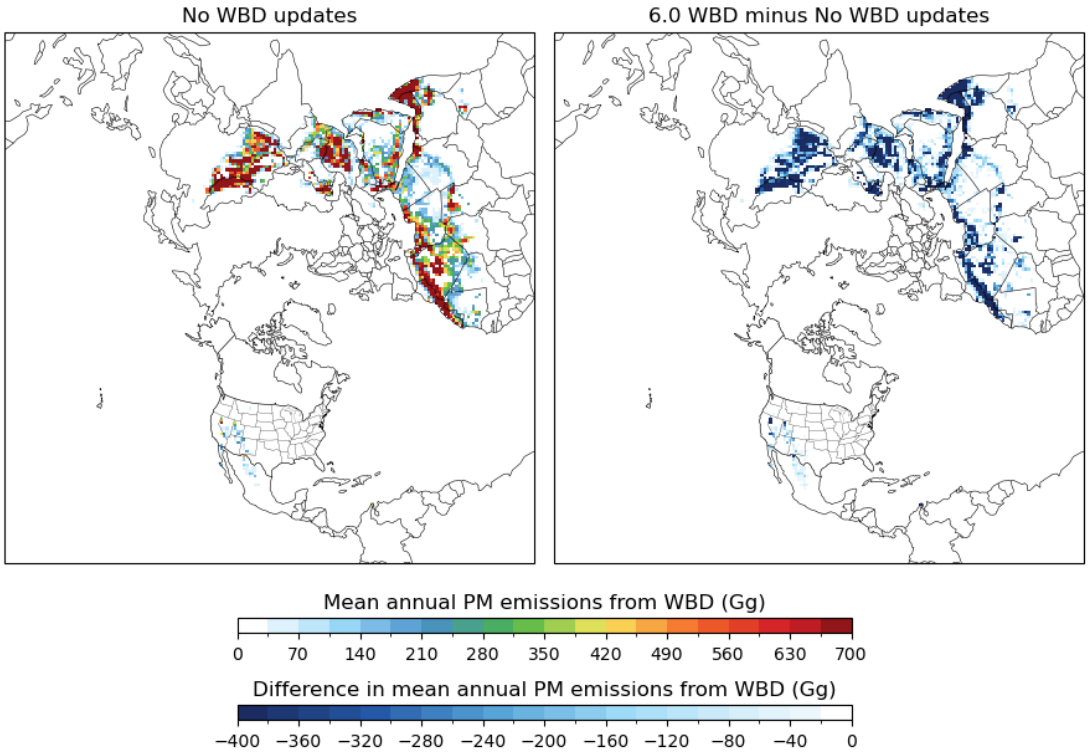

Figure 6-4 Mean annual PM emissions from windblown dust from the No WBD Updates sensitivity (left) and difference in windblown dust emissions resulting from enabling CTM_BROWN_VEG (right).

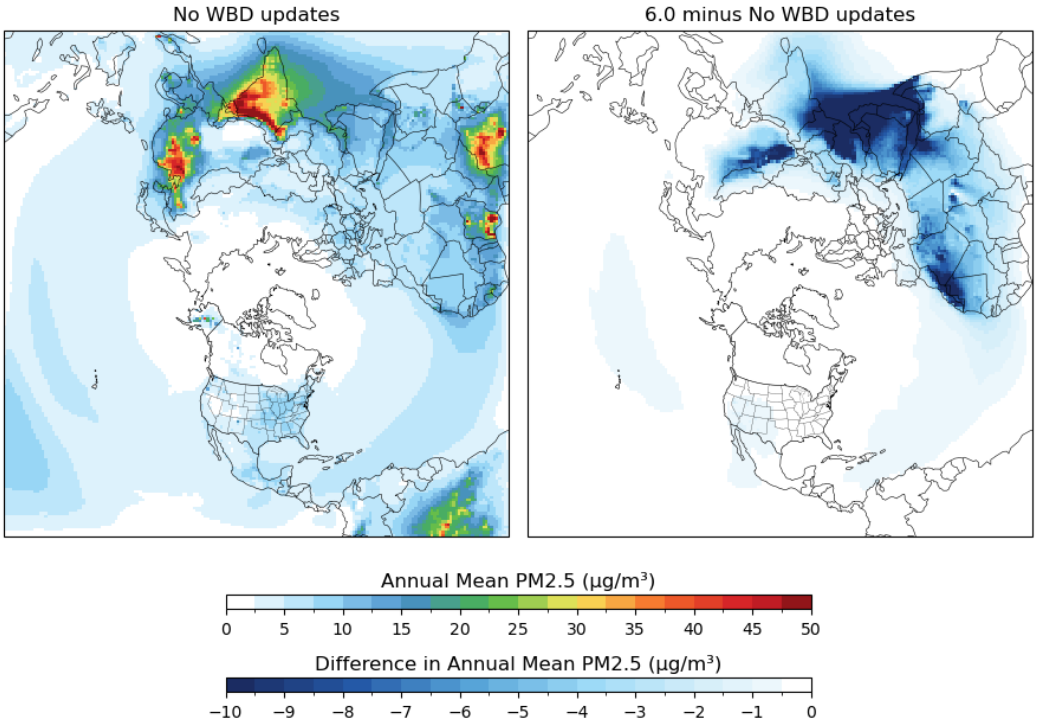

Figure 6-5 Annual mean surface $PM_{2.5}$ concentration in the No WBD Updates sensitivity simulation (left) and difference in annual mean surface $PM_{2.5}$ concentration resulting from enabling CTM_BROWN_VEG (right).

The effects of the WBD updates are more significant for the 12 km CONUS simulation (Figure 6-6), since this configuration also includes the NLCD landuse correction. For CONUS, total PM emissions decrease from 106.11 Tg/yr to 3.89 Tg/yr; with fine mode mass decreasing from 7.4 Tg/yr to 0.3 Tg/yr. The seasonal peak in domain total emissions shifts from April to May. As with the 108HEMI configuration, the CMAQ 6.0 updates result in emissions reductions across all highly emitting regions in the western US (Figure 6-7).

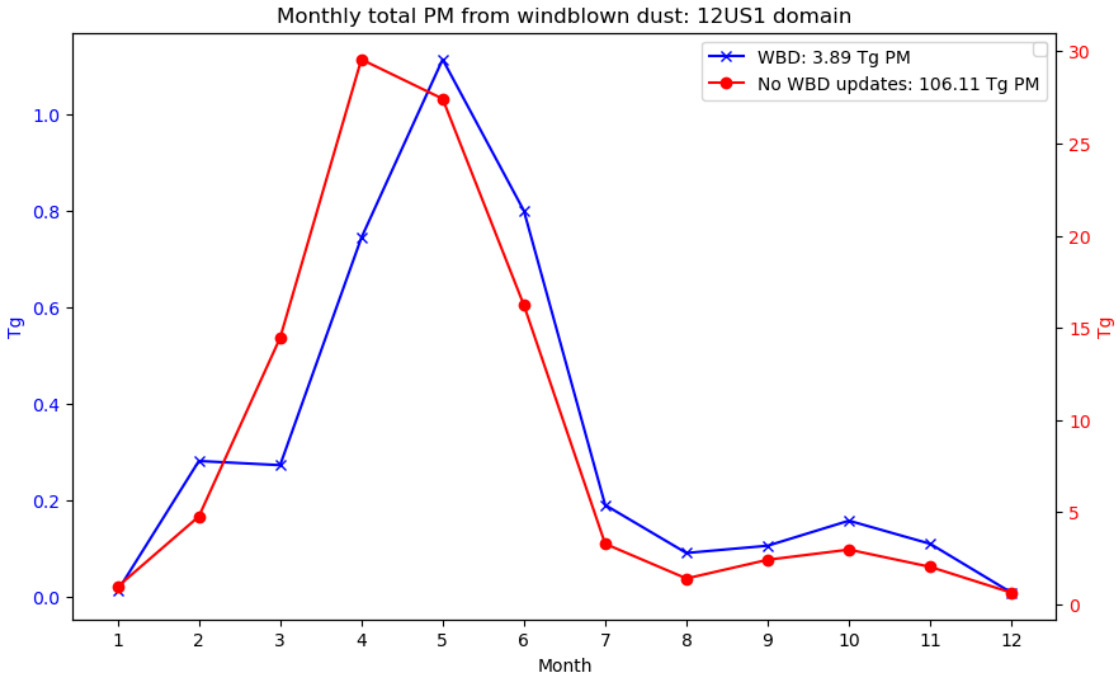

Figure 6-6 Monthly total PM emissions from windblown dust for the 12US1 domain.

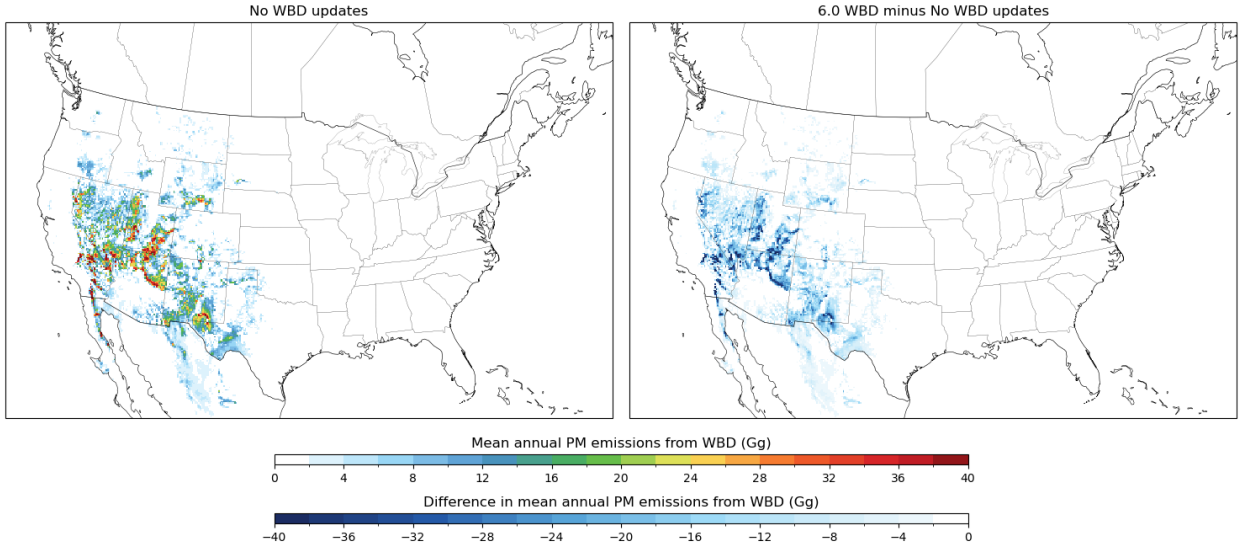

Figure 6-7 Mean annual PM emissions from windblown dust from the No WBD Updates sensitivity (left) and difference in windblown dust emissions resulting from enabling CTM_BROWN_VEG and implementing the NLCD landuse correction (right).

Improvements in western $PM_{2.5}$ bias (Figure 4-10, Figure 4-11) from CMAQ version 5.5 to version 6.0 are largely attributable to the reduction in fine mode particulate mass from

windblown dust. The sensitivity of $PM_{2.5}$ concentrations to windblown dust updates is largest in the western United States and approaches 10 µg/m^3 in the annual average (Figure 6-8).

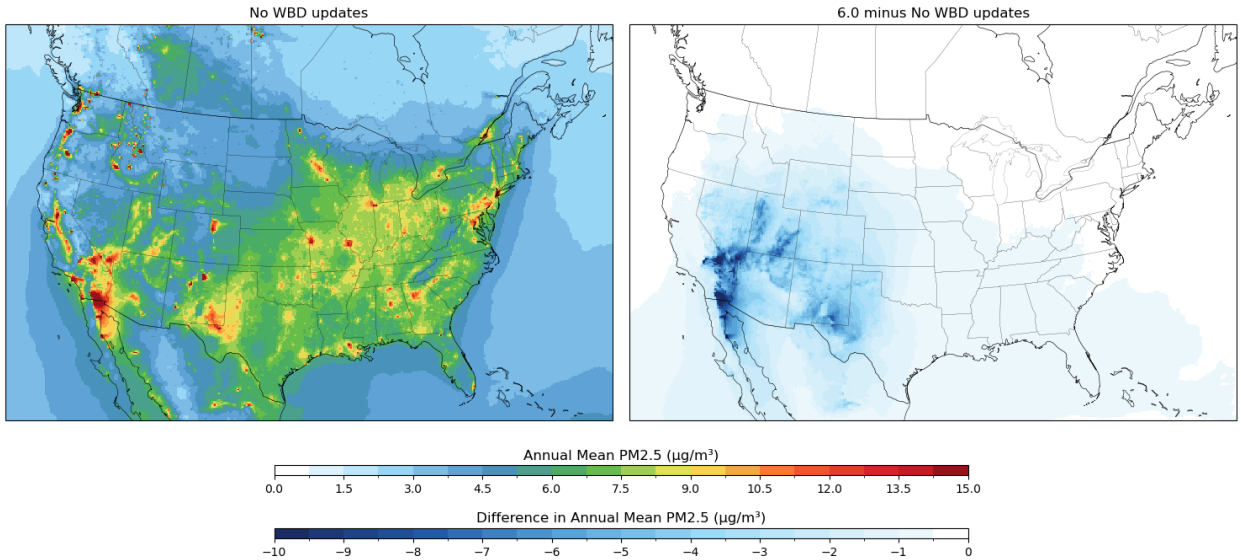

Figure 6-8 Annual mean surface $PM_{2.5}$ concentration in the No WBD Updates sensitivity simulation (left) and difference in annual mean surface $PM_{2.5}$ concentration resulting from enabling CTM_BROWN_VEG and implementing the NLCD landuse correction (right).

The large reductions in $PM_{2.5}$ bias are consistent with reductions in bias for soil concentrations (see Section 4.2.3.5). Soil concentration is calculated using the equation from Malm et al. (1994) and considers the mass of five crustal elements: Soil = 2.20Al + 2.49Si + 1.63Ca + 2.42Fe + 1.94Ti. Soil concentrations in the No WBD Updates simulation are biased high across the western United States, while soil in the version 6.0 BASE case is biased low (Figure 6-9). Despite being biased low, the new soil emissions are closer to observations and can capture temporal variability, even when averaged across the entire region (Figure 6-10).

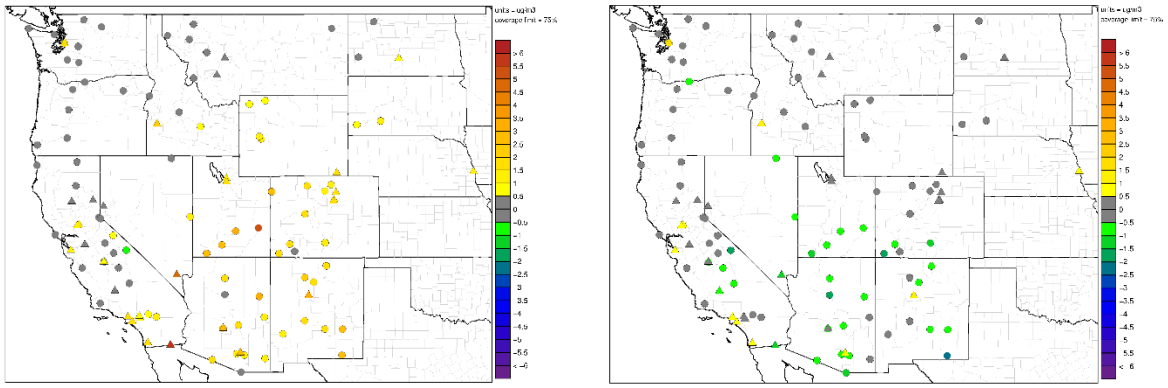

Figure 6-9 Annual mean soil bias for No WBD Updates sensitivity (left) and v6.0 BASE case (right) when compared to IMPROVE (circles) and CSN (triangles) observational networks.

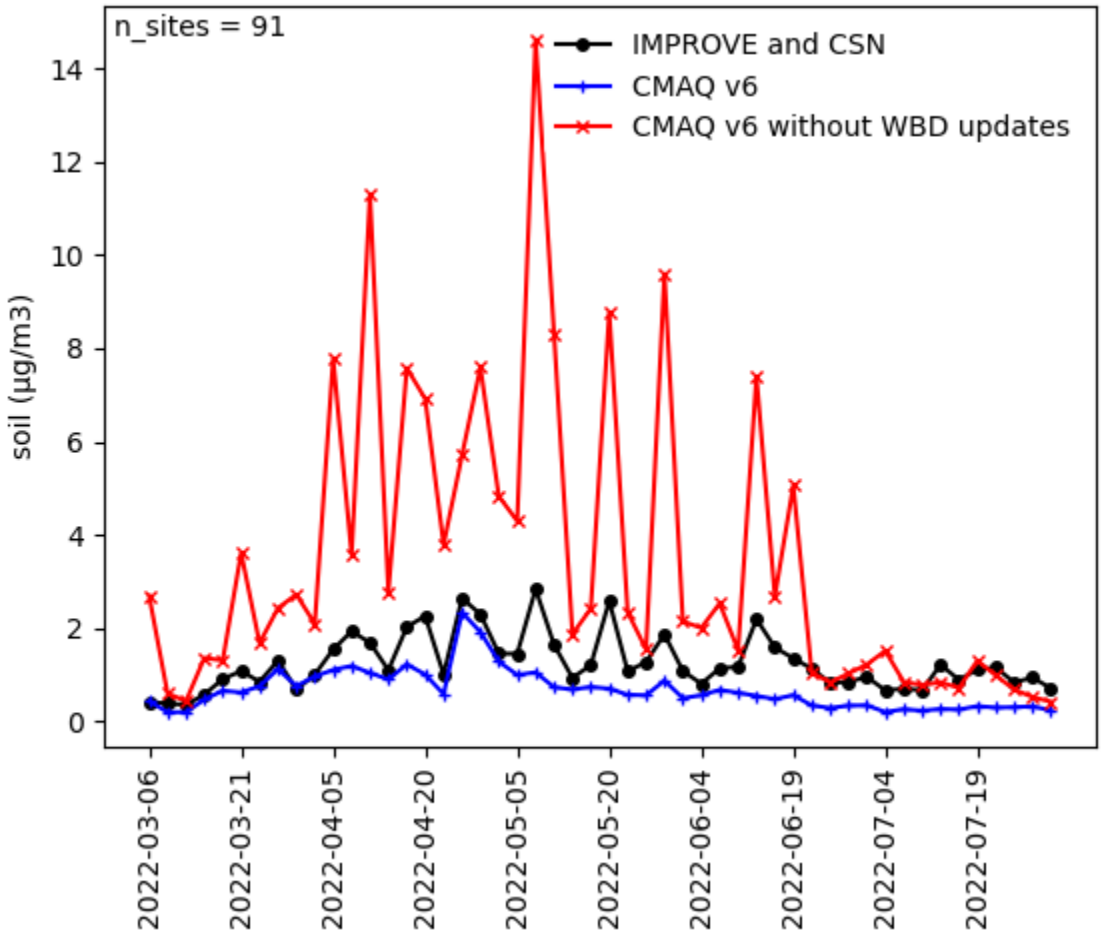

Figure 6-10 Time series of average soil concentration over the observational networks in the geographical area shown in Figure 6-9.

6.2.2 Soil Emissions of Gases to the Atmosphere (SEGA)

CMAQ simulations over North America commonly employ the Yienger and Levy (1995) parameterization to estimate emissions of oxidized nitrogen from agricultural and natural soils. This option has been available as part of CMAQ's Biogenic Emissions Inventory System (BEIS) since CMAQ version 4.7. Domains that extend beyond North America, such as the hemispheric domain described in this document, have typically used offline soil NO inventories such as those from GEIA or CAMS. The Model of Emissions of Gases and Aerosols from Nature (MEGAN; Guenther et al. (2020)) was added to CMAQ in version 5.4 as an alternative to BEIS for the representation of both biogenic VOC and soil NO emissions across all domains, with the option of calculating the latter with either a Yienger-Levy approach or the Berkeley-Dalhousie Soil NOx Parameterization (BDSNP) (Hudman et al., 2012). CMAQv6.0 introduces a new option: the Soil Emissions of Gases to the Atmosphere (SEGA) module.

SEGA is a research-grade algorithm that is based on the BDSNP approach, with modifications to most of the terms presented in equation 2 of Hudman et al. (2012). These updates are intended to allow estimation of soil emissions across scales and for any domain, without requiring input data beyond what is already required for CMAQ. The most impactful modifications are described below.

SEGA estimates a canopy reduction factor (CRF) using an asymptotic function of stomal resistance (rs) and leaf area index consistent with the measurements found in Delaria et al. (2020).

$$CRF = \frac{1}{1 + e^{0.007(127-rs)}}$$

This allows canopy reduction to vary between 0 and 60 percent. The soil temperature function (F_T) is estimated in SEGA by fitting a double Arrhenius function presented in Stark (1996) to the findings by Oikawa et al. (2015) and Stark (1996).

$$F_T = 228.3 * e^{-\frac{E_{a1}}{R}\left(\frac{1}{T}-\frac{1}{T_{ref}}\right)} - 206.5 * e^{-\frac{E_{a2}}{R}\left(\frac{1}{T}-\frac{1}{T_{ref}}\right)}$$

Where R = 8.314 J/(mol K), E_{a1} = 79.0 kJ mol^{-1}, E_{a2} = 83.2 kJ mol^{-1}, and T_{ref} = 303.15 K. SEGA estimates the soil moisture function using a modified Poisson density function from Stark (1996) with soil moisture peaks at 0.30 and 0.15 for NO and HONO, respectively.

$$F_{theta} = \frac{W}{W_{peak}} e^{\frac{1}{4}\left(1-\left(\frac{W}{W_{peak}}\right)^4\right)}$$

Where W_{peak} = 0.15 for HONO and 0.30 for NO. The emission factors for NO used in SEGA are the geometric means from Steinkamp and Lawrence (2011) for all land use types except for barren land. Barren land emissions factors are derived from Weber et al. (2015) and Chen et al. (2020). HONO emission factors are assumed to be ~60% of NO emissions based on Kim and Or (2019). The cropland emission factors are also further adjusted to be comparable to fertilizer and global totals found in Weng et al. (2020). The fertilizer adjustment factor in SEGA is estimated as a function of growing season, which is dependent on one-meter soil temperature, julian day, and latitude.

$$F_{adj} = F_{dl} * F_{Ts}$$

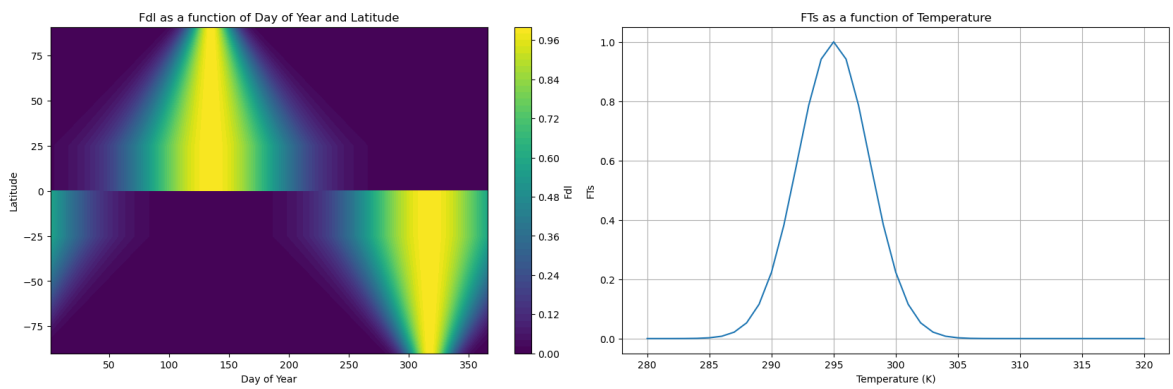

Figure 6-11 F_{dl} (left) and F_{Ts} (right). The product of these two terms is used to estimate fertilizer adjustment factor (F_{adj}).

The resulting fertilizer adjustment is maximized at lower latitudes and in warmer months of the year (Figure 6-11).

Soil NO estimates from SEGA largely resemble BDSNP at the hemispheric scale, but BDSNP includes the influence of external datasets, such as the fertilizer inputs from Potter et al. (2010). This is visible in the excessively uniform emissions over India in SEGA that results from combining the heavily fertilized and irrigated crops of the Indo-Gangetic plains with the non-irrigated cropland.

The seasonality of SEGA's emissions resembles CAMS, peaking in July. This differs from BDSNP's June peak. The magnitude of SEGA's annual soil NO emissions for the Northern Hemisphere is lower than CAMS, and both are lower than BDSNP's. However, SEGA includes

HONO that is approximately 60% of the NO emissions (3.9 Tg N from NO, 2.13 Tg N from HONO). Assuming that 2/3rds of nitrogen from soil is emitted in the Northern Hemisphere (e.g. Wang et al. (2025)), the global total for SEGA can be estimated to be 9.1 Tg N/yr. This estimate from SEGA is close to the value of 9.5 Tg N/yr estimated by Weng et al. (2020).

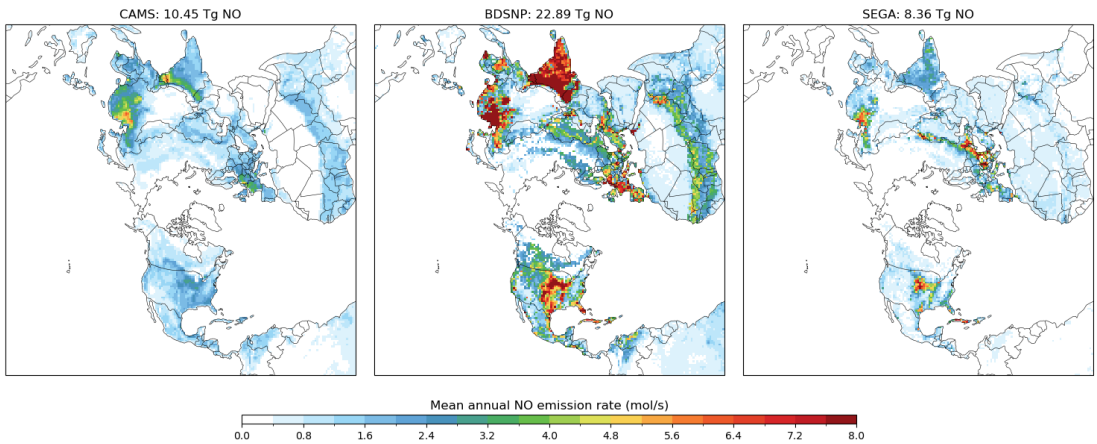

Figure 6-12 HEMI emissions of soil NO for CAMS, BDSNP, and SEGA.

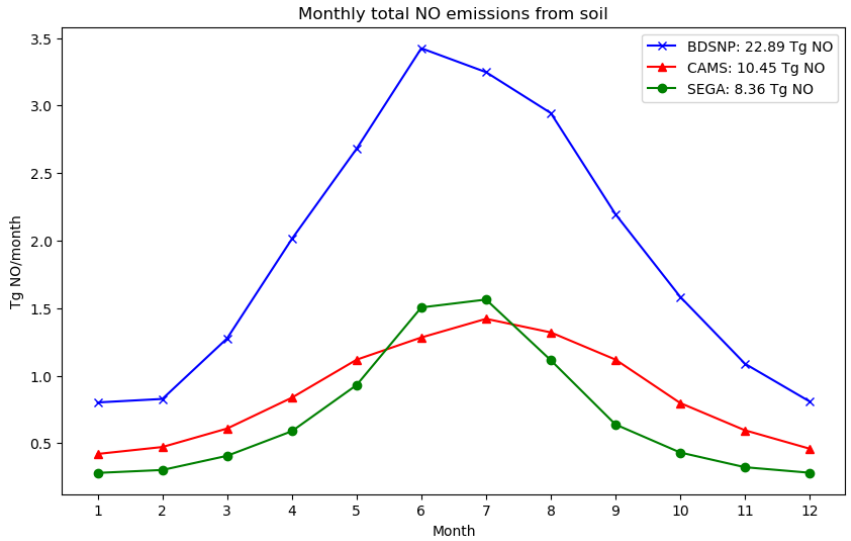

Figure 6-13 Time series of soil NO emissions with different science options used in the 108NHEMI simulations.

Over the 12US1 domain the appropriate comparison is between BEIS, BDSNP, and SEGA. We exclude the MEGAN's YL option here since its emissions are unreasonably low and the BEIS YL implementation is the standard option for applications within the CONUS domain. Figure

6-14 shows annual mean average soil NO emission rates for these three options, with BEIS producing the least soil NO (1.07 Tg/yr) and BDSNP producing the most (2.99 Tg/yr). SEGA's annual total is closer to BEIS at 1.21 Tg/yr, but with notably higher values over California and across much of the Midwest's cropland. SEGA's seasonal cycle has a stronger peak than BEIS that occurs in June. BDSNP's July peak is much larger than SEGA or BEIS, and is later in the year, consistent with Huber et al. (2020). The variance in BDSNP's seasonal cycle may be due to its sensitivity to a continuously updated soil nitrogen deposition reservoir that is affected by model spin up duration. The 12US1 CONUS domain's BDSNP module was not spun up for the entire year of 2021, unlike the 108HEMI BDSNP simulation.

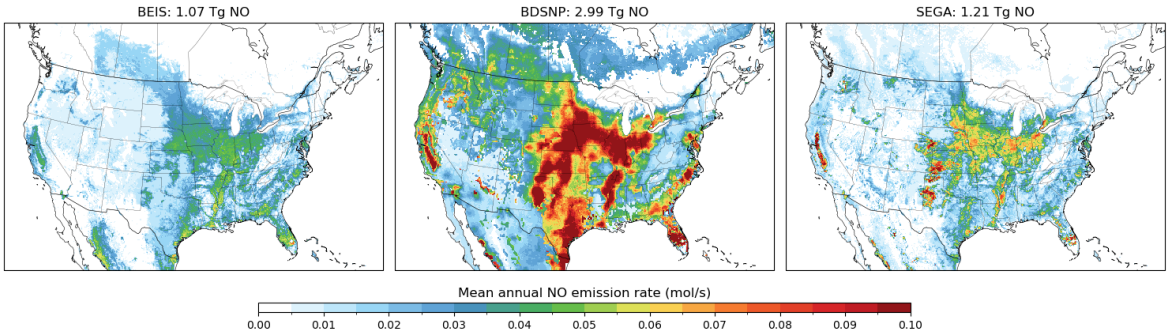

Figure 6-14 CONUS domain soil NO emissions for BEIS, BDSNP, and SEGA.

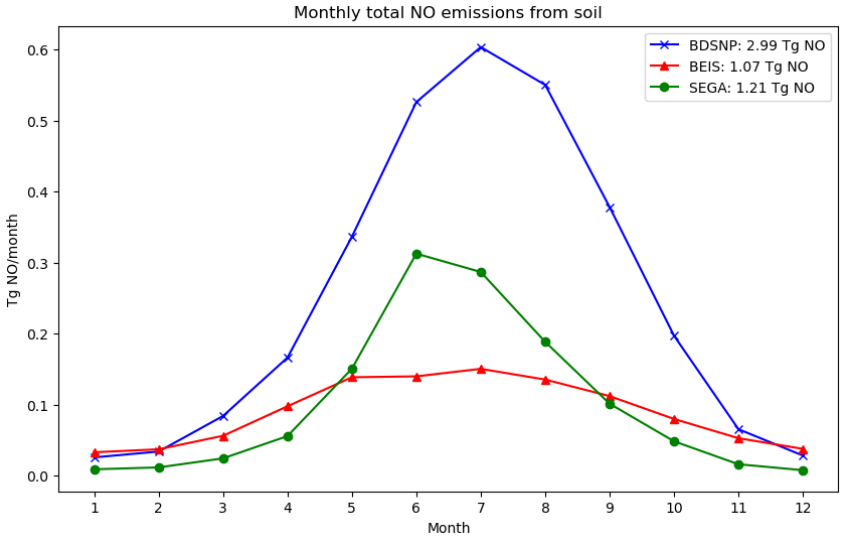

Figure 6-15 Time series of soil NO emissions with different science options used in the 12US1 simulations.

The effect of soil NO parameterization on hemispheric and CONUS ozone is shown in Figure 6-16 and Figure 6-17. BDSNP's large emissions increase mean surface ozone concentrations over agricultural regions relative to CAMS, with increases of 5 ppb over Africa and 2 ppb over North America. SEGA increases surface ozone over Northern Africa and the Middle East relative to CAMS, but the annually averaged ozone response over CONUS is small, and concentrations decrease over sub-Saharan Africa. Boundary conditions generated from hemispheric simulations using SEGA are likely to resemble those generated from hemispheric simulations using CAMS. For the CONUS domain the most common soil NO option selected is BEIS. Both BDSNP and SEGA contribute more soil NO to the domain than BEIS, and the ozone response is significant. Using BDSNP instead of BEIS results in domain-wide increases in ozone over 5 ppb in the annual average. SEGA likewise produces more ozone than BEIS with a similar spatial pattern to BDSNP, but with smaller magnitudes. Figure 6-18 shows BEIS and SEGA seasonal normalized mean 8-hr max ozone biases for each region. For most regions and seasons the surface ozone bias is not sensitive to the choice of BEIS or SEGA for soil NO, but several regions have a larger high bias in summer with SEGA.

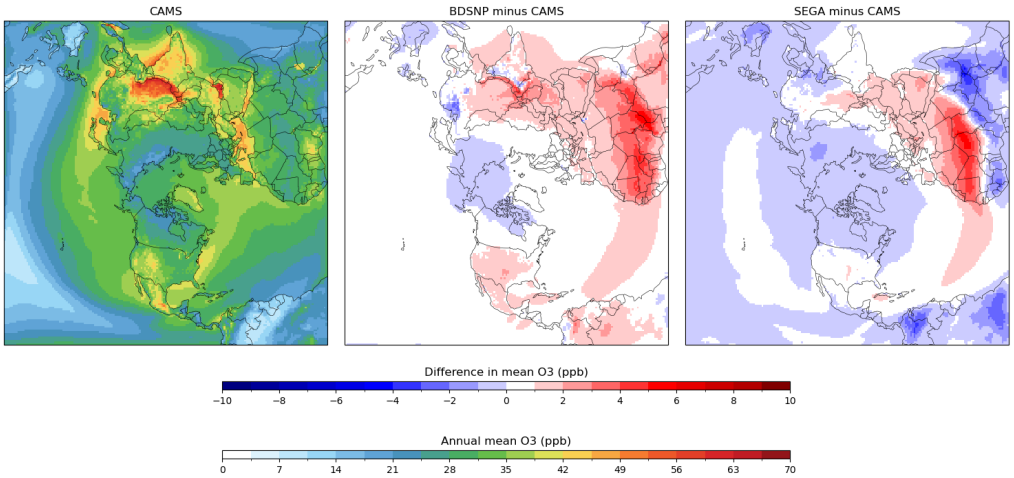

Figure 6-16 BASE case annual average ozone from CAMS, and difference from BASE when using BDSNP or SEGA soil NO options.

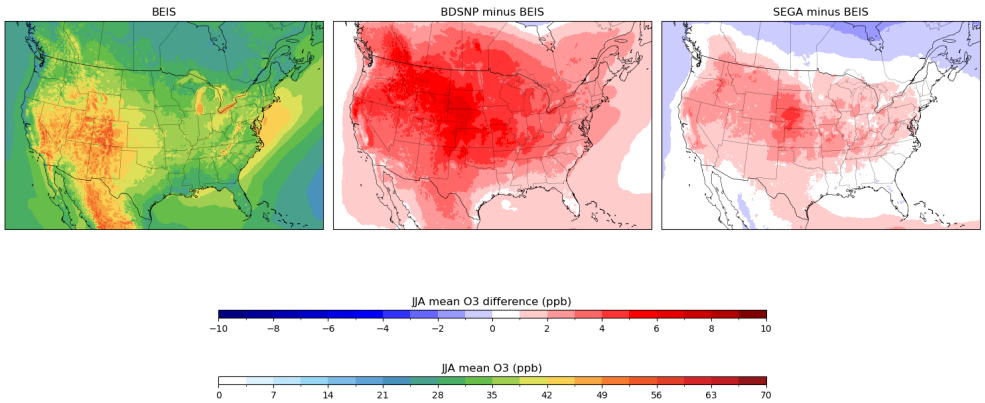

Figure 6-17 BASE case summertime average ozone from BEIS, and difference from BASE when using BDSNP or SEGA soil NO options.

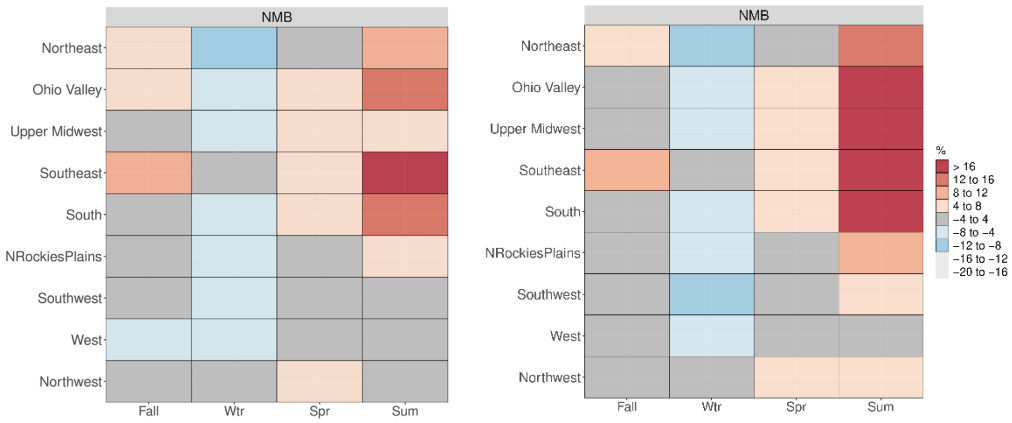

Figure 6-18 Normalized mean bias in 8-hr max O_3 by season and region for 12 km CONUS BASE with BEIS (left) and SEGA (right) soil NO.

6.2.3 Lightning NOx Emissions

Updates were made to the online lightning module to include an additional method to estimate lightning NOx emissions. In the CMAQv5.5 and CMAQv6.0 base model, lightning NOx emissions are estimated from ground-based observations that measure lightning flashes, which are then parameterized to estimate NOx emissions both spatially and temporally. The new method uses GOES Lightning Mapper (GLM) and the World Wide Lightning Location Network (WWLLN) strike energy data (Wu et al., 2023; Cheng et al., 2024; Kang et al., 2026). Both datasets are normalized to account for differences in their means of detection and adjusted by a factor to account for the ratio of inter-cloud and cloud-to-ground strikes.

In the June – August average (Figure 6-19), when surface ozone and lightning activity are both near their annual maximum, the new lightning emission option generally decreases NOx emissions over the 12 km gridded modeling domain with resulting decreases of simulated NO_2 column. The new option decreases simulated surface level ozone by as much as 1 ppb in the high elevation regions of the southwest US and generates more moderate decreases elsewhere, except over parts of California and the northwest where the simulation modestly increases ozone via transport from the western boundary. The impacts on annual-average surface-level nitrate $PM_{2.5}$ are small, no larger than 0.01 μg m^{-3} (not shown).

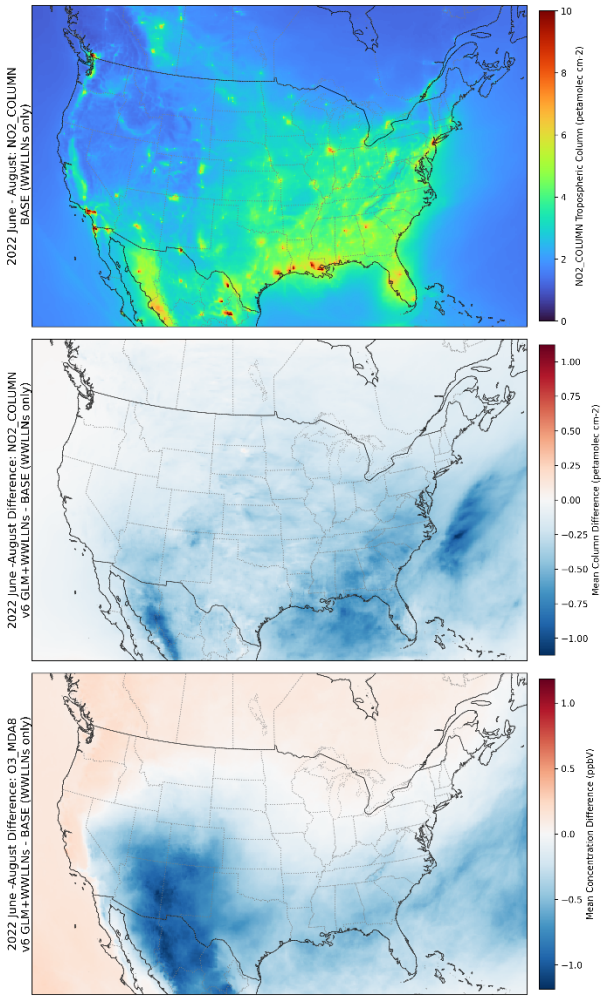

Figure 6-19 June – August average NO_2 column for base model (top) and impact of new science option for model lightning NOx emission on NO_2 column (middle) and on surface MDA8 ozone (bottom). The base model lightning NOx emission option did not change between CMAQv5.5 and CMAQv6.0.

6.3 Dry Deposition Incremental Testing

Updates to dry deposition in CMAQv6.0 are described in detail in Section 2.3. Both the M3DRY and STAGE dry deposition models have been updated with revised relative reactivities for trace organic species. Other than this update to relative reactivities, M3DRY has not been further updated in CMAQv6.0. STAGE has been further updated in CMAQv6.0, and the specific updates are described in Section 2.3. Here we show the impact of the STAGE updates on seasonal average ozone and $PM_{2.5}$ concentrations. The impacts of STAGE updates are shown as the difference in concentrations between a simulation in which STAGE updates were included and one in which STAGE updates were not included. Results for both the hemispheric (108NHEMI) and CONUS (12US1) domains are shown. For CONUS simulations, the results also include effects of STAGE updates in the 108NHEMI simulations as inherited through the lateral boundary conditions.

For the northern hemisphere (Figure 6-20), there are large (up to 10 ppb) decreases in ozone at northern latitudes during winter, spring, and fall. These decreases are due to a bugfix related to deposition to snow covered land which increased deposition when snow is present. An increase in ozone concentrations is seen in all seasons along most coastal areas due to a change in how LAI is represented in coastal areas. Otherwise, changes in seasonal average MDA8 ozone are generally within +/- 1 ppb.

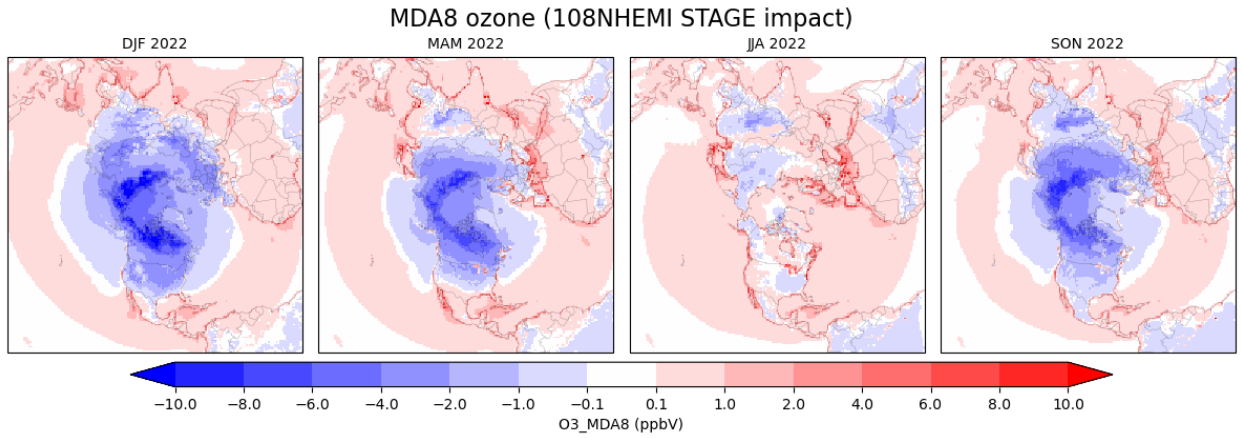

Figure 6-20 Seasonal average impact on surface layer MDA8 ozone due to STAGE updates for the 108NHEMI domain.

For the ozone effects within the CONUS domain, the STAGE incremental impact simulations presented here do not distinguish between effects on the CONUS domain that come from changes in the large scale background concentration of ozone that depends on the hemispheric simulations vs. effects that are from differences at the CONUS scale. However, the pattern of ozone impacts within the CONUS domain largely follows the pattern seen in the hemispheric simulations. Ozone is decreased over much of the domain during winter, spring, and fall. In the

spring, ozone is slightly increased in the southwestern US. In the summer, ozone is slightly increased in the western US and slightly decreased in the eastern US.

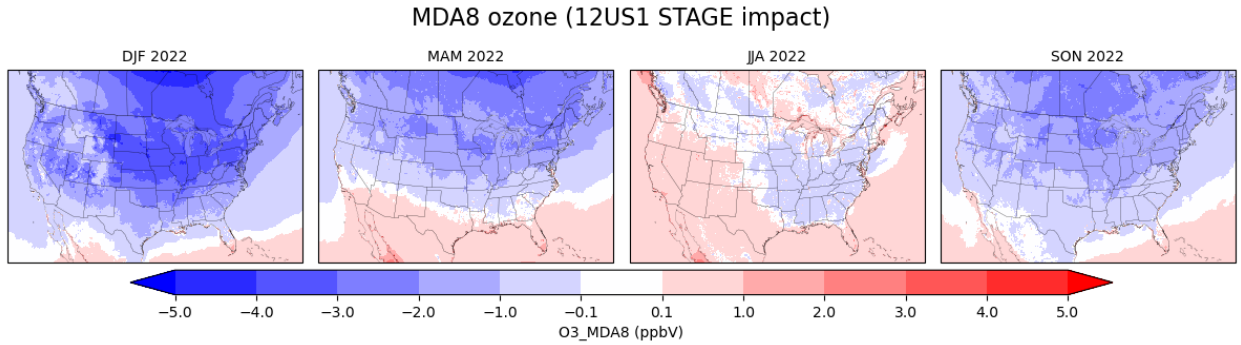

Figure 6-21 Seasonal average impact on surface layer MDA8 ozone due to STAGE updates for the 12US1 domain.

For $PM_{2.5}$, The largest effects of the STAGE updates are seen over China and the Indian subcontinent, particularly during winter and fall. $PM_{2.5}$ is decreased in these areas due to reductions in soluble gas-phase precursor species such as SO_2, NOy, NH_3, and organic gases that result from changes to the treatment of canopy water content in STAGE. In other regions, the STAGE deposition updates do not have large effects on $PM_{2.5}$, with changes smaller than +/- 1 $\mu g/m^3$.

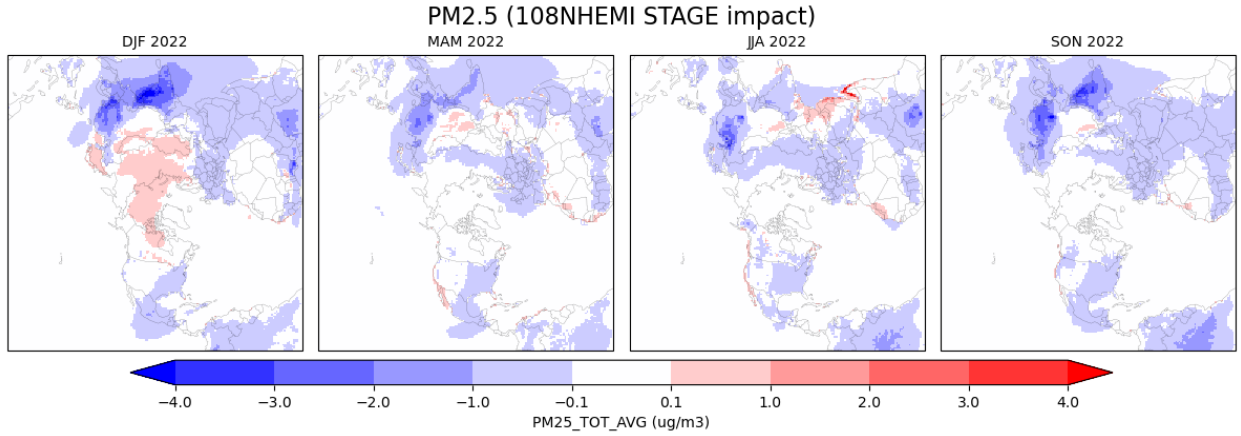

Figure 6-22 Seasonal average impact on surface layer $PM_{2.5}$ due to STAGE updates for the 108NHEMI domain.

Over the CONUS domain, the STAGE updates lead to small reductions in $PM_{2.5}$ over the eastern US across all seasons. In winter and fall, $PM_{2.5}$ is also decreased in the Central Valley of California and in western Washington and Oregon. The decreases in $PM_{2.5}$ are mostly due to

decreases in organic aerosol and decreases in SO_4 to a lesser extent. As discussed for the hemispheric results, these reductions are due to decreases in precursor concentrations resulting from changes to the treatment of canopy water content in STAGE.

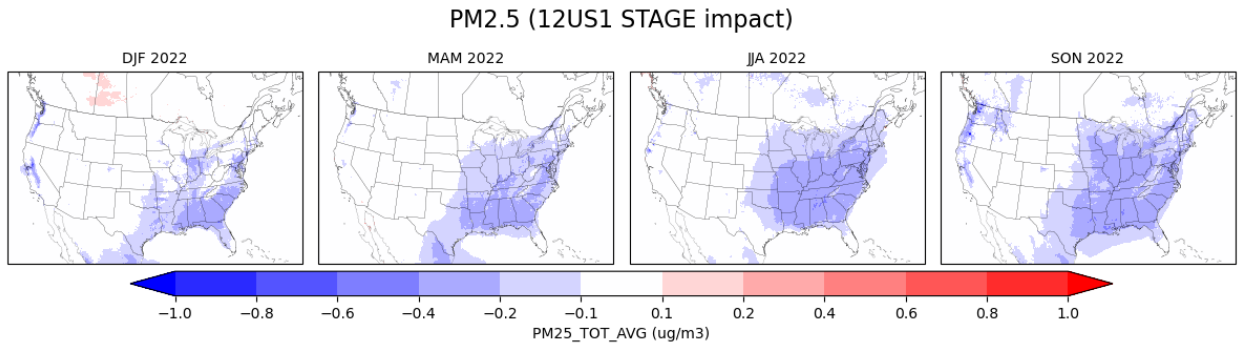

Figure 6-23 Seasonal average impact on surface layer $PM_{2.5}$ due to STAGE updates for the 12US1 domain.

6.4 Meteorology and Urban Mixing Incremental Testing

As introduced in section 2.4, the most significant meteorological update for CMAQ version 6.0 is an update to the near-surface vertical diffusion in cold conditions.

Minimum vertical eddy diffusivity (Kz_{min}) is a lower bound on the rate of mixing in the lower atmosphere. This value can have a large effect on nighttime concentrations of pollutants such as NO_x, ozone, and PM, particularly in very stable conditions. The urban heat island effect is poorly represented at common CMAQ grid resolutions, and anthropogenic heating is not parameterized in WRF configurations that are typically used for air quality modeling. The Kz_{min} assumptions in CMAQ had been designed to compensate for a lack of urban heating by allowing a minimum magnitude of mixing up to 500 meters, even if the reported WRF PBL height was much lower, as is the case in stable conditions during extremely cold nights. The value of Kz_{min} between the surface and 500 meters is calculated as:

$$Kz_{min} = Kz_L + (Kz_u - Kz_L) * \text{Urban_Fraction}$$

where $Kz_L = 0.01$and $Kz_U = 1.0$. These values (Kz_L and Kz_U) correspond to the lower and upper bounds of the minimum vertical eddy diffusivity, respectively. Urban fraction ranges from 0 to 1 and represents the developed fraction of the grid cell. Findings from Desai et al. (2024) motivated revisiting the Kz_{min} assumptions in CMAQ, as high values of nighttime ozone were attributed to NOx underestimates from excessive mixing of fresh air above the boundary layer. In CMAQ version 6.0 the urban-weighted value of Kz_{min} no longer applies to all layers under 500

m. The urban-weighted minimum vertical eddy diffusivity now only applies up to WRF's PBL height, which is often lower than 500 m in cold conditions. This change allows for consistency between CMAQ and WRF, but results in a weaker vertical mixing at night in cold conditions, which can lead to higher concentrations of precursors, pollutants, or oxidants near the surface (Figure 6-24).

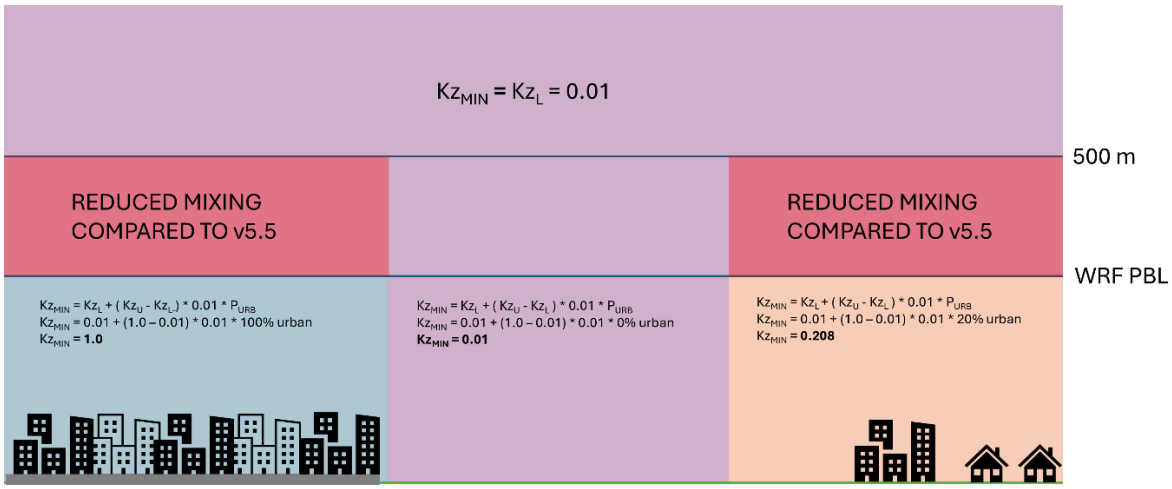

Figure 6-24 Cartoon depicting Kz_{min} calculations for urban, rural, and suburban grid cells (from left to right). The red boxes highlight the areas that will experience reduced mixing in CMAQ version 6.0, which occurs when the WRF PBL height is below the previously fixed value of 500 m.

A sensitivity simulation was conducted for 12km CONUS using both the previous (CMAQ version 5.5) and new Kz_{min} assumptions. The results confirm that this change has negligible effects on 8hr-max ozone and $PM_{2.5}$ (Figure 6-25 and Figure 6-26). Model ozone performance degrades with the new Kz_{min} approach for fall in the Northeast, but in Western winter the model ozone performance improves. There are no category changes for $PM_{2.5}$ in any region or season. Overall, the seasonally-averaged performance metrics for ozone and $PM_{2.5}$ are not sensitive to the new Kz_{min} behavior.

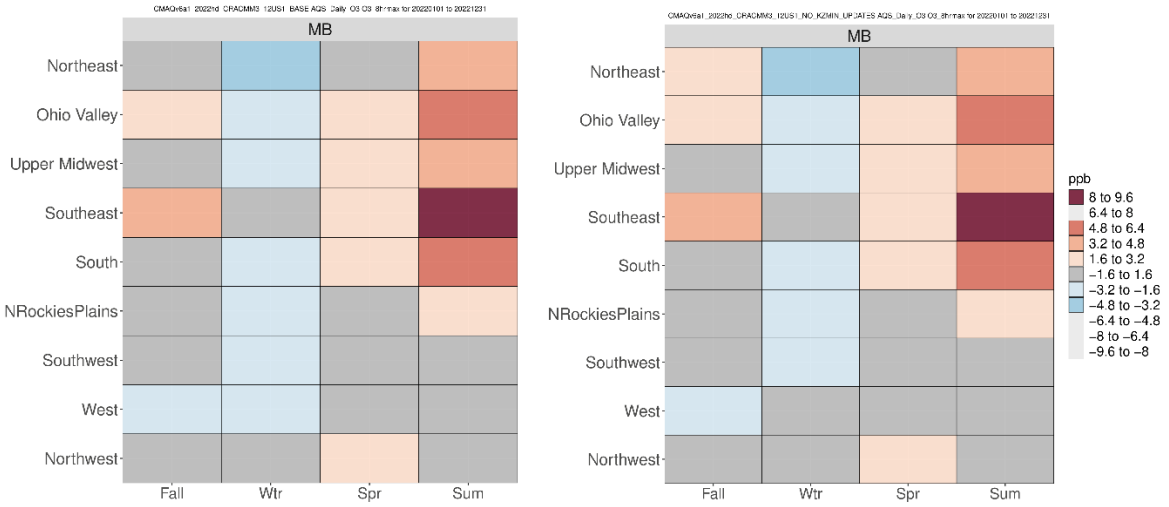

Figure 6-25 Seasonal plots of mean ozone bias for the Base CB6 case (left) and Kz_{min} sensitivity test (right).

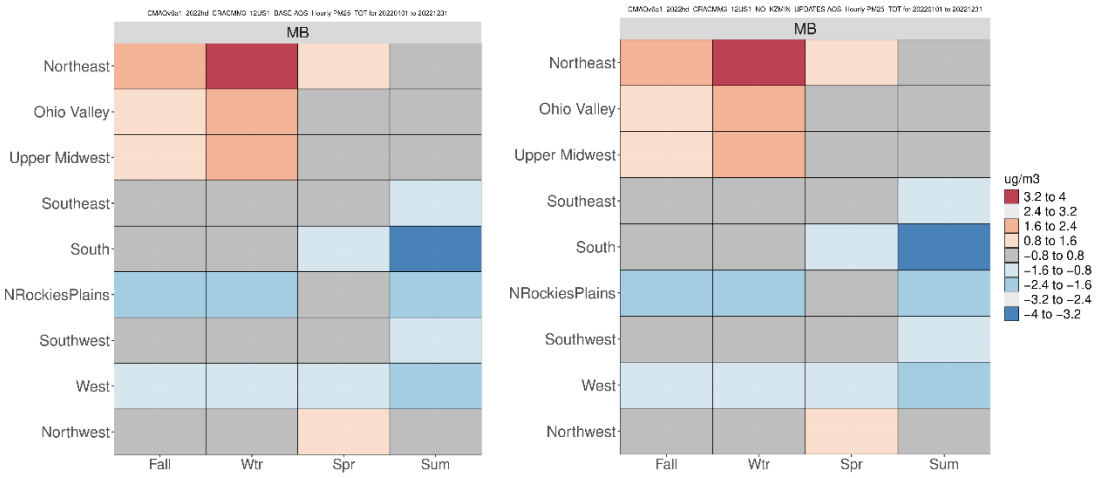

Figure 6-26 Seasonal plots of mean $PM_{2.5}$ bias for the Base CB6 case (left) and Kz_{min} sensitivity test (right).

While seasonal performance is not sensitive to the Kz_{min} update, CMAQ 5.5 suffered from an overprediction of PM in the Northeast in winter (Figure 6-26). The change in Kz_{min} assumptions has a made this PM performance issue worse on high-PM winter days in the Northeast, as shown by an event in January of the modeled year 2022 (Figure 6-27). This period (January 12th through 14th) coincides with a cold bias in the model (not shown), and weak vertical mixing at night allows for the buildup of PM near the surface. Applications like this may benefit from modifying the behavior of Kz_{min} to account for a missing anthropogenic heating effect. We have added a

new runtime option to accommodate bounding the urban-weighted portion of the Kz_{min} calculation. The option is set in the run script as:

```
setenv KZU_CUSTOM  1.0   #> Use a custom value for KZmin
```

and allows users to replicate performance comparable to simulations using CMAQ version 5.5's Kz_{min} assumptions.

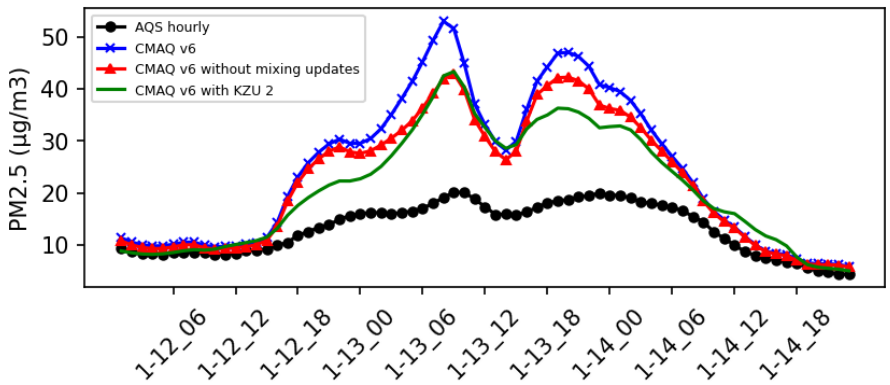

Figure 6-27 Case study of Northeast $PM_{2.5}$ prediction from Jan 12, 2022 through Jan 14, 2022. Lines represent the base configuration (blue), base configuration without Kz_{min} without updates (red), and KZU_CUSTOM equal to 2.0 (green).

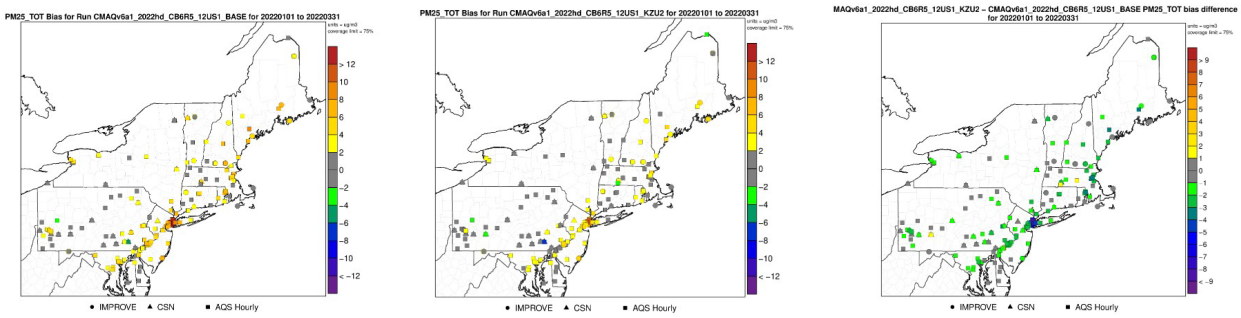

Figure 6-28 $PM_{2.5}$ bias for January through March in the v6.0 base simulation (left), simulation with KZU_CUSTOM = 2.0 (middle), and the difference in bias (right). Cool colors in the rightmost panel indicate improved model performance.

Setting the KZU_CUSTOM environment variable to a value over the default of 1.0 will result in stronger vertical diffusion over urban areas. Prior to the CMAQ version 5.0 release in 2012 the default value for KZU was 2.0. Setting KZU_CUSTOM to 2.0 results in significantly reduced

bias for the case study shown in Figure 6-27, even improving performance relative to the CMAQ version 5.5 implementation. Figure 6-28 shows that setting KZU_CUSTOM to 2.0 results in a nearly monotonic reduction in JFM average bias in Northeastern $PM_{2.5}$. Increasing KZU_CUSTOM to 2.0 does not significantly affect ozone for any region or season (not shown). It is reasonable to conclude that values up to 2.0 are warranted in certain applications that include large urban areas in strongly stable conditions. Future development may include the addition of an anthropogenic heating parameterization to the P-X land surface model to reduce the need for Kz_u customization.

7. Appendix

7.1 Summary of Model Performance Statistics

Model performance statistics for CMAQv6.0 are provided for $PM_{2.5}$, $PM_{2.5}$ species, and ozone in Tables 7-1 to 7-11. The CMAQv6.0 simulation used for developing the model performance statistics is based on a slightly newer version of the 2022 modeling platform emissions than were available for the simulations described in the main text above. The emissions updates have very small influence on model performance results and were used here to allow for direct comparison with model performance statistics recently reported for the 2022 modeling platform based on these emissions with an earlier version of CMAQ (US EPA, 2026).

The model performance statistics for CMAQv6.0 using 2022he emissions (US EPA, 2025b) are generally within the range of those reported in 2022v1 regulatory platform (US EPA, 2026). The 2022 platform used CMAQv5.4 for 12US2 with:

1. Initial and boundary conditions from customized CMAQv5.4+ with aerosol nitrate photolysis
2. CB6R5 chemical mechanism
3. AERO7 aerosol module with non-volatile primary organic aerosol (POA)
4. STAGE deposition module
5. Ammonia bi-directional flux activated
6. BEIS biogenic emissions
7. Inline lightning NO_x emissions (based on scaled WWLLNs data)
8. Windblown dust turned off

Table 7-1 Performance statistics for **$PM_{2.5}$** at AQS Sites in 2022 using CMAQv6.0 CB6R5 with 2022he emissions consistent with 2022v2 air quality modeling platform.

Region	Season	N	AvgObs (µg m^{-3})	AvgMod (µg m^{-3})	MB	NMB	NME	RMSE	r
Northeast	All	94803	6.9	9.0	2.2	31.5	53.6	6.16	0.61
	Winter	22620	8.1	12.7	4.6	56.3	67.0	8.69	0.65
	Spring	24144	6.0	8.1	2.1	34.8	51.8	5.24	0.60
	Summer	24631	7.1	6.6	-0.5	-7.3	36.3	3.67	0.52
	Fall	23408	6.2	8.9	2.7	43.4	59.5	6.19	0.62
Southeast	All	73423	7.7	7.7	0.0	0.2	37.1	4.06	0.58
	Winter	17747	7.9	9.2	1.3	16.5	41.8	4.79	0.63
	Spring	18413	7.8	7.9	0.1	1.4	34.6	4.00	0.61
	Summer	18996	7.6	6.4	-1.3	-16.5	35.2	3.62	0.51
	Fall	18267	7.3	7.3	0.0	-0.3	37.1	3.77	0.58
Ohio Valley	All	87586	8.2	9.3	1.1	12.9	36.7	4.40	0.63
	Winter	21179	8.9	11.2	2.3	26.0	40.6	4.98	0.69
	Spring	22061	7.3	8.5	1.2	16.3	37.5	3.81	0.69
	Summer	22341	8.7	8.0	-0.7	-7.6	31.2	4.07	0.46
	Fall	22005	8.1	9.6	1.5	18.3	37.8	4.67	0.68
Upper Midwest	All	50413	7.3	8.0	0.7	9.4	38.0	4.30	0.69
	Winter	12399	8.3	10.5	2.1	25.3	39.8	5.00	0.71
	Spring	12210	6.3	7.1	0.7	11.8	39.1	4.11	0.64
	Summer	12422	6.8	5.5	-1.3	-19.1	35.8	3.47	0.46
	Fall	13382	7.8	9.0	1.2	14.9	37.2	4.47	0.78
South	All	50911	8.6	7.6	-1.1	-12.4	41.5	5.46	0.40
	Winter	12261	7.4	8.1	0.7	9.8	42.5	4.97	0.50
	Spring	12861	9.1	8.2	-0.9	-9.5	37.8	5.19	0.51
	Summer	12952	9.5	5.6	-3.9	-41.3	50.5	7.09	0.25
	Fall	12837	8.4	8.3	-0.1	-1.3	34.3	4.12	0.57
Southwest	All	40373	6.4	6.3	-0.1	-2.3	55.0	5.58	0.37
	Winter	9912	8.0	8.0	0.0	-0.2	61.2	7.60	0.37
	Spring	10299	6.0	6.7	0.8	13.2	53.5	4.89	0.30
	Summer	10111	5.9	4.1	-1.8	-30.6	50.5	4.35	0.15
	Fall	10051	5.9	6.3	0.4	7.4	52.5	4.95	0.44
Northern Rockies & Plains	All	25372	5.7	4.4	-1.3	-22.7	48.0	4.56	0.62
	Winter	6135	5.3	4.2	-1.1	-20.4	49.7	4.61	0.43
	Spring	6286	4.1	4.2	0.1	1.4	45.1	2.66	0.47
	Summer	6522	5.7	3.3	-2.5	-43.3	51.6	4.06	0.32
	Fall	6429	7.5	5.9	-1.6	-21.0	45.5	6.19	0.72
Northwest	All	52038	7.6	8.0	0.4	5.6	70.6	15.20	0.56
	Winter	12806	8.1	8.3	0.1	1.7	86.0	10.90	0.21
	Spring	13327	3.8	5.5	1.7	44.7	83.7	6.76	0.20
	Summer	13174	5.2	5.0	-0.2	-4.3	55.7	10.10	0.42
	Fall	12731	13.5	13.5	0.0	0.2	63.4	25.80	0.60
West	All	72477	8.0	7.3	-0.7	-9.3	46.8	7.38	0.52
	Winter	18018	9.3	9.0	-0.3	-3.4	53.1	8.12	0.58
	Spring	18145	6.9	7.0	0.1	1.1	43.5	4.79	0.42
	Summer	17956	7.1	5.3	-1.9	-26.4	42.2	7.33	0.46
	Fall	18358	8.6	7.7	-0.9	-10.0	46.5	8.65	0.54

Table 7-2 Performance statistics for **$PM_{2.5}$** SO_4^{2-} at CSN Sites in 2022 using CMAQv6.0 CB6R5 with 2022he emissions consistent with 2022v2 air quality modeling platform.

Region	Season	N	AvgObs (µg m-3)	AvgMod (µg m-3)	MB	NMB	NME	RMSE	r
Northeast	All	3034	0.81	0.75	-0.06	-7.8	35.8	0.51	0.45
	Winter	732	0.83	0.79	-0.04	-4.6	34.8	0.47	0.41
	Spring	781	0.76	0.87	0.10	13.6	32.0	0.40	0.61
	Summer	784	0.99	0.65	-0.34	-33.9	39.3	0.68	0.55
	Fall	737	0.67	0.69	0.02	3.2	36.0	0.43	0.46
Southeast	All	1788	0.86	0.81	-0.06	-6.7	34.2	0.42	0.43
	Winter	444	0.81	0.84	0.03	3.9	34.8	0.37	0.49
	Spring	451	0.91	0.92	0.00	0.4	31.4	0.40	0.49
	Summer	461	0.97	0.68	-0.29	-29.8	37.3	0.53	0.39
	Fall	432	0.76	0.79	0.03	4.3	32.8	0.35	0.53
Ohio Valley	All	2117	1.04	0.91	-0.13	-12.8	33.7	0.56	0.57
	Winter	518	1.04	0.91	-0.13	-12.2	33.8	0.53	0.52
	Spring	550	1.01	1.01	0.00	0.5	32.2	0.52	0.61
	Summer	547	1.25	0.87	-0.38	-30.1	37.7	0.73	0.57
	Fall	502	0.87	0.84	-0.03	-3.3	29.0	0.36	0.72
Upper Midwest	All	1029	0.84	0.78	-0.07	-7.9	32.2	0.47	0.65
	Winter	250	0.92	0.84	-0.08	-8.4	29.7	0.42	0.63
	Spring	265	0.84	0.86	0.02	2.2	32.9	0.50	0.69
	Summer	266	0.87	0.64	-0.23	-26.4	35.6	0.57	0.63
	Fall	248	0.73	0.76	0.03	4.0	30.2	0.33	0.76
South	All	1032	1.15	1.01	-0.14	-11.9	41.2	0.73	0.48
	Winter	254	0.94	0.98	0.04	3.9	43.4	0.61	0.64
	Spring	275	1.32	1.14	-0.19	-14.1	39.2	0.90	0.61
	Summer	256	1.34	0.83	-0.51	-37.9	44.0	0.78	0.32
	Fall	247	0.95	1.08	0.13	13.4	38.2	0.58	0.44
Southwest	All	1083	0.52	0.55	0.03	6.7	42.3	0.30	0.38
	Winter	259	0.45	0.47	0.02	4.2	52.4	0.36	0.12
	Spring	267	0.49	0.69	0.20	41.5	49.3	0.28	0.74
	Summer	276	0.68	0.51	-0.17	-25.6	33.9	0.33	0.46
	Fall	281	0.45	0.55	0.09	21.0	38.4	0.22	0.58
Northern Rockies & Plains	All	520	0.54	0.55	0.01	2.0	42.2	0.37	0.61
	Winter	130	0.50	0.48	-0.02	-3.7	45.6	0.31	0.58
	Spring	125	0.52	0.63	0.12	22.2	47.6	0.39	0.63
	Summer	134	0.60	0.48	-0.11	-18.6	36.9	0.38	0.66
	Fall	131	0.54	0.60	0.06	11.8	40.1	0.39	0.65
Northwest	All	542	0.49	0.60	0.12	23.8	51.2	0.44	0.36
	Winter	143	0.40	0.52	0.12	29.7	60.3	0.32	0.33
	Spring	149	0.41	0.59	0.18	45.0	55.2	0.28	0.55
	Summer	133	0.63	0.67	0.04	6.5	51.8	0.74	0.16
	Fall	117	0.54	0.66	0.11	21.1	38.6	0.26	0.74
West	All	1868	0.91	0.79	-0.12	-12.6	43.1	0.71	0.50
	Winter	462	0.62	0.66	0.04	5.8	62.7	0.62	0.34
	Spring	466	0.86	0.84	-0.02	-2.5	40.5	0.51	0.58
	Summer	473	1.28	0.87	-0.41	-32.3	40.5	1.06	0.42
	Fall	467	0.85	0.80	-0.05	-6.4	35.6	0.49	0.66

Table 7-3 Performance statistics for **$PM_{2.5}$** SO_4^{2-} at IMPROVE Sites in 2022 using CMAQv6.0 CB6R5 with 2022he emissions consistent with 2022v2 air quality modeling platform.

Region	Season	N	AvgObs (µg m-3)	AvgMod (µg m-3)	MB	NMB	NME	RMSE	r
Northeast	All	1952	0.58	0.53	-0.05	-9.0	34.1	0.30	0.69
	Winter	484	0.61	0.56	-0.04	-7.1	27.2	0.23	0.69
	Spring	486	0.53	0.62	0.09	16.4	31.5	0.22	0.77
	Summer	487	0.73	0.46	-0.27	-37.4	42.7	0.47	0.79
	Fall	495	0.46	0.48	0.02	4.0	32.8	0.20	0.77
Southeast	All	1619	0.81	0.68	-0.12	-15.3	35.3	0.41	0.51
	Winter	390	0.74	0.70	-0.04	-5.1	35.9	0.44	0.49
	Spring	408	0.84	0.81	-0.03	-4.1	30.6	0.36	0.56
	Summer	416	0.95	0.59	-0.36	-37.5	40.7	0.49	0.59
	Fall	405	0.69	0.63	-0.06	-8.2	32.8	0.31	0.59
Ohio Valley	All	939	0.88	0.75	-0.12	-14.0	33.9	0.42	0.65
	Winter	222	0.76	0.71	-0.04	-5.6	33.3	0.35	0.62
	Spring	239	0.81	0.82	0.00	0.2	31.9	0.42	0.64
	Summer	241	1.18	0.77	-0.41	-34.7	38.3	0.57	0.72
	Fall	237	0.75	0.72	-0.03	-4.3	29.4	0.31	0.75
Upper Midwest	All	938	0.57	0.54	-0.03	-5.6	33.1	0.31	0.76
	Winter	229	0.64	0.61	-0.04	-5.7	29.4	0.26	0.73
	Spring	232	0.57	0.58	0.01	1.1	35.4	0.43	0.70
	Summer	241	0.58	0.42	-0.16	-26.8	35.0	0.29	0.91
	Fall	236	0.50	0.56	0.06	12.1	33.0	0.22	0.84
South	All	1138	0.87	0.75	-0.12	-14.1	43.8	0.60	0.46
	Winter	275	0.59	0.66	0.07	12.3	47.1	0.52	0.57
	Spring	281	0.98	0.90	-0.08	-8.3	41.9	0.71	0.52
	Summer	292	1.17	0.66	-0.52	-43.9	47.0	0.71	0.39
	Fall	290	0.74	0.78	0.05	6.4	38.6	0.39	0.53
Southwest	All	3639	0.41	0.48	0.07	15.8	51.6	0.33	0.51
	Winter	891	0.29	0.35	0.06	19.5	69.6	0.39	0.26
	Spring	897	0.41	0.64	0.22	54.3	66.5	0.35	0.57
	Summer	927	0.58	0.45	-0.13	-22.5	34.8	0.29	0.70
	Fall	924	0.36	0.47	0.12	32.4	48.6	0.26	0.72
Northern Rockies & Plains	All	1858	0.35	0.39	0.04	12.1	47.5	0.25	0.64
	Winter	446	0.31	0.32	0.01	2.9	57.7	0.27	0.72
	Spring	462	0.35	0.48	0.13	37.0	57.2	0.26	0.59
	Summer	483	0.37	0.33	-0.04	-10.5	33.2	0.21	0.66
	Fall	467	0.37	0.44	0.07	19.7	45.1	0.27	0.69
Northwest	All	1926	0.26	0.38	0.11	43.4	65.6	0.27	0.47
	Winter	445	0.16	0.27	0.12	76.2	104.0	0.20	0.49
	Spring	495	0.23	0.40	0.17	74.6	84.2	0.24	0.57
	Summer	502	0.33	0.40	0.07	20.6	51.2	0.39	0.28
	Fall	484	0.33	0.43	0.10	30.7	50.6	0.22	0.68
West	All	2231	0.45	0.48	0.04	8.3	50.7	0.32	0.52
	Winter	539	0.26	0.32	0.07	26.0	80.0	0.35	0.53
	Spring	607	0.49	0.63	0.14	28.1	51.5	0.32	0.53
	Summer	565	0.61	0.51	-0.11	-17.3	43.0	0.36	0.35
	Fall	520	0.41	0.45	0.04	10.2	43.3	0.23	0.62

Table 7-4 Performance statistics for **$PM_{2.5}$** NO_3^- at CSN Sites in 2022 using CMAQv6.0 CB6R5 with 2022he emissions consistent with 2022v2 air quality modeling platform.

Region	Season	N	AvgObs (µg m-3)	AvgMod (µg m-3)	MB	NMB	NME	RMSE	r
Northeast	All	3032	0.82	1.03	0.20	24.7	60.1	0.88	0.82
	Winter	731	1.63	2.52	0.89	54.4	66.2	1.58	0.74
	Spring	781	0.80	0.82	0.02	2.9	46.5	0.56	0.78
	Summer	783	0.30	0.12	-0.19	-61.0	78.5	0.33	0.19
	Fall	737	0.60	0.72	0.13	21.0	52.6	0.52	0.84
Southeast	All	1787	0.39	0.60	0.21	54.9	96.5	0.69	0.73
	Winter	444	0.73	1.46	0.73	99.8	116.0	1.19	0.66
	Spring	451	0.32	0.35	0.03	9.4	64.8	0.31	0.35
	Summer	460	0.21	0.15	-0.06	-28.9	76.6	0.22	0.27
	Fall	432	0.31	0.48	0.17	54.8	97.0	0.61	0.60
Ohio Valley	All	2117	1.14	1.18	0.04	3.3	43.7	0.80	0.85
	Winter	518	2.41	2.77	0.37	15.2	37.2	1.24	0.76
	Spring	550	0.94	0.88	-0.06	-6.0	45.0	0.65	0.82
	Summer	547	0.40	0.15	-0.25	-63.1	75.8	0.41	0.30
	Fall	502	0.85	0.97	0.12	13.8	44.9	0.66	0.89
Upper Midwest	All	1028	1.30	1.28	-0.03	-1.9	38.0	0.82	0.88
	Winter	250	2.54	2.91	0.37	14.4	30.9	1.18	0.82
	Spring	265	1.31	1.07	-0.24	-18.3	40.5	0.86	0.85
	Summer	265	0.42	0.17	-0.25	-59.8	74.6	0.47	0.27
	Fall	248	1.00	1.05	0.05	5.1	36.4	0.63	0.93
South	All	1031	0.62	0.57	-0.05	-8.2	56.8	0.54	0.74
	Winter	253	1.11	1.22	0.11	9.6	43.1	0.69	0.74
	Spring	275	0.60	0.41	-0.19	-31.0	53.9	0.46	0.75
	Summer	256	0.34	0.18	-0.16	-47.0	71.4	0.30	0.42
	Fall	247	0.45	0.50	0.05	10.4	84.4	0.65	0.54
Southwest	All	1083	1.11	0.51	-0.61	-54.6	68.7	1.87	0.67
	Winter	259	2.99	1.06	-1.93	-64.5	68.7	3.66	0.63
	Spring	267	0.53	0.43	-0.10	-19.5	57.2	0.49	0.38
	Summer	276	0.30	0.17	-0.13	-42.9	94.4	0.36	0.05
	Fall	281	0.74	0.40	-0.34	-46.4	66.2	0.93	0.68
Northern Rockies & Plains	All	519	0.60	0.44	-0.16	-26.7	54.9	0.63	0.71
	Winter	130	1.08	0.93	-0.15	-13.6	48.3	0.93	0.68
	Spring	125	0.54	0.40	-0.14	-25.6	49.7	0.44	0.76
	Summer	133	0.24	0.08	-0.16	-66.9	74.1	0.24	0.57
	Fall	131	0.57	0.36	-0.20	-35.7	64.1	0.68	0.52
Northwest	All	541	0.90	1.30	0.40	44.1	112.0	1.71	0.36
	Winter	143	1.64	1.91	0.28	16.8	99.0	2.37	0.19
	Spring	148	0.46	0.88	0.42	90.8	131.0	1.04	0.42
	Summer	133	0.27	1.04	0.77	280.0	310.0	1.41	0.54
	Fall	117	1.28	1.39	0.11	8.5	76.3	1.75	0.48
West	All	1867	1.94	0.76	-1.18	-60.8	68.3	2.61	0.59
	Winter	462	3.54	1.57	-1.97	-55.6	64.1	3.88	0.59
	Spring	465	1.35	0.66	-0.69	-50.8	65.8	1.45	0.32
	Summer	473	0.93	0.30	-0.63	-68.1	71.2	1.03	0.60
	Fall	467	1.98	0.53	-1.45	-73.2	76.2	3.02	0.53

Table 7-5 Performance statistics for **$PM_{2.5}$** NO_3^- at IMPROVE Sites in 2022 using CMAQv6.0 CB6R5 with 2022he emissions consistent with 2022v2 air quality modeling platform.

Region	Season	N	AvgObs (µg m-3)	AvgMod (µg m-3)	MB	NMB	NME	RMSE	r
Northeast	All	1953	0.35	0.64	0.29	81.5	108.0	0.71	0.77
	Winter	486	0.68	1.54	0.86	126.0	129.0	1.25	0.74
	Spring	486	0.29	0.47	0.17	59.4	95.0	0.50	0.61
	Summer	486	0.16	0.15	-0.01	-3.3	89.8	0.24	0.42
	Fall	495	0.28	0.41	0.13	45.7	78.3	0.38	0.78
Southeast	All	1619	0.31	0.44	0.13	40.4	93.0	0.54	0.72
	Winter	390	0.55	1.07	0.52	94.3	118.0	0.93	0.70
	Spring	408	0.29	0.30	0.01	2.5	63.0	0.26	0.49
	Summer	416	0.18	0.11	-0.07	-39.1	70.2	0.18	0.46
	Fall	405	0.23	0.30	0.07	29.9	93.6	0.48	0.59
Ohio Valley	All	939	0.59	0.75	0.16	26.9	67.4	0.71	0.79
	Winter	222	1.34	2.02	0.68	51.0	70.3	1.26	0.69
	Spring	239	0.42	0.44	0.02	5.0	58.9	0.42	0.74
	Summer	241	0.21	0.05	-0.16	-74.7	81.8	0.26	0.19
	Fall	237	0.45	0.58	0.13	28.4	60.5	0.52	0.88
Upper Midwest	All	936	0.58	0.64	0.06	9.9	48.8	0.54	0.87
	Winter	229	1.29	1.59	0.30	23.6	45.6	0.87	0.86
	Spring	231	0.49	0.43	-0.06	-12.3	50.9	0.49	0.72
	Summer	241	0.13	0.05	-0.08	-62.2	79.2	0.15	0.55
	Fall	235	0.44	0.51	0.07	16.8	46.5	0.41	0.94
South	All	1138	0.45	0.40	-0.05	-10.5	62.0	0.45	0.79
	Winter	275	0.75	0.90	0.15	20.2	51.9	0.59	0.81
	Spring	281	0.51	0.38	-0.13	-26.0	48.7	0.34	0.87
	Summer	292	0.26	0.04	-0.23	-85.0	88.5	0.30	0.22
	Fall	290	0.30	0.32	0.02	8.1	84.2	0.50	0.62
Southwest	All	3638	0.23	0.13	-0.10	-44.4	76.1	0.39	0.45
	Winter	891	0.37	0.17	-0.20	-53.1	75.2	0.69	0.50
	Spring	897	0.22	0.23	0.00	1.2	65.5	0.22	0.44
	Summer	927	0.17	0.03	-0.14	-81.7	88.9	0.20	0.16
	Fall	923	0.15	0.08	-0.07	-47.8	79.0	0.25	0.50
Northern Rockies & Plains	All	1858	0.22	0.21	-0.01	-4.3	67.9	0.29	0.70
	Winter	446	0.33	0.39	0.06	18.4	69.0	0.41	0.66
	Spring	462	0.23	0.22	-0.02	-7.0	54.8	0.25	0.76
	Summer	482	0.10	0.03	-0.08	-72.8	79.9	0.13	0.61
	Fall	468	0.22	0.21	0.00	-0.8	74.4	0.31	0.68
Northwest	All	1911	0.22	0.24	0.03	11.8	106.0	0.63	0.45
	Winter	440	0.34	0.39	0.05	13.5	106.0	0.81	0.42
	Spring	489	0.14	0.20	0.06	40.2	104.0	0.35	0.52
	Summer	498	0.10	0.14	0.04	38.3	168.0	0.52	0.57
	Fall	484	0.30	0.26	-0.04	-12.7	86.7	0.74	0.51
West	All	2230	0.45	0.19	-0.26	-56.9	71.1	0.93	0.75
	Winter	538	0.63	0.30	-0.34	-53.2	64.0	1.31	0.85
	Spring	607	0.44	0.28	-0.17	-37.7	64.7	0.53	0.46
	Summer	565	0.25	0.05	-0.20	-79.3	85.4	0.31	0.30
	Fall	520	0.48	0.15	-0.34	-69.7	79.4	1.22	0.75

Table 7-6 Performance statistics for **$PM_{2.5}$** OC at CSN Sites in 2022 using CMAQv6.0 CB6R5 with 2022he emissions consistent with 2022v2 air quality modeling platform.

Region	Season	N	AvgObs (µg m-3)	AvgMod (µg m-3)	MB	NMB	NME	RMSE	r
Northeast	All	2951	1.61	3.17	1.57	97.5	107.0	2.94	0.37
	Winter	707	1.30	3.69	2.38	183.0	186.0	3.76	0.44
	Spring	760	1.35	3.01	1.66	123.0	128.0	2.86	0.45
	Summer	781	2.18	2.83	0.65	29.9	48.7	1.71	0.49
	Fall	703	1.56	3.22	1.66	107.0	113.0	3.16	0.46
Southeast	All	1724	2.25	3.12	0.87	38.6	60.4	1.97	0.52
	Winter	427	2.09	3.25	1.16	55.4	71.2	2.17	0.63
	Spring	423	2.29	3.22	0.93	40.4	60.6	2.08	0.53
	Summer	445	2.21	2.89	0.69	31.0	54.6	1.67	0.41
	Fall	429	2.42	3.14	0.72	29.6	56.5	1.93	0.45
Ohio Valley	All	2116	1.90	2.70	0.80	42.1	54.5	1.47	0.65
	Winter	535	1.49	2.87	1.38	92.7	99.0	1.93	0.55
	Spring	549	1.75	2.51	0.76	43.6	55.0	1.36	0.75
	Summer	525	2.37	2.74	0.37	15.7	31.0	1.00	0.72
	Fall	507	2.01	2.68	0.67	33.5	48.0	1.45	0.71
Upper Midwest	All	1162	1.61	2.53	0.92	56.9	74.7	1.96	0.45
	Winter	289	1.25	3.31	2.07	166.0	166.0	2.82	0.58
	Spring	288	1.27	2.15	0.89	69.9	81.2	1.69	0.53
	Summer	303	1.98	1.93	-0.04	-2.2	33.6	0.93	0.50
	Fall	282	1.95	2.76	0.81	41.3	55.5	1.97	0.62
South	All	936	2.18	2.55	0.36	16.6	48.9	2.84	0.29
	Winter	223	1.96	2.81	0.85	43.3	61.9	1.87	0.53
	Spring	233	1.81	2.20	0.39	21.8	46.2	1.37	0.67
	Summer	250	1.89	2.05	0.16	8.4	45.0	1.32	0.49
	Fall	230	3.10	3.18	0.08	2.7	45.2	5.07	0.18
Southwest	All	1110	1.68	2.58	0.91	54.1	78.8	2.24	0.38
	Winter	282	2.36	3.92	1.56	66.3	94.8	3.34	0.24
	Spring	280	1.14	2.00	0.86	75.7	85.6	1.52	0.40
	Summer	276	1.40	1.58	0.19	13.4	48.6	0.87	0.31
	Fall	272	1.81	2.81	1.00	55.3	76.5	2.40	0.32
Northern Rockies & Plains	All	488	1.46	1.16	-0.30	-20.2	57.8	1.84	0.65
	Winter	116	1.12	1.03	-0.09	-8.2	82.8	2.07	0.14
	Spring	113	0.68	0.79	0.11	16.5	58.5	0.60	0.53
	Summer	129	1.61	0.90	-0.71	-44.1	51.6	1.14	0.30
	Fall	130	2.29	1.87	-0.42	-18.3	51.1	2.69	0.78
Northwest	All	530	2.21	5.46	3.26	148.0	166.0	5.16	0.45
	Winter	143	1.92	5.96	4.04	211.0	218.0	5.34	0.51
	Spring	148	1.13	4.72	3.59	318.0	319.0	5.29	0.56
	Summer	134	1.67	4.45	2.78	167.0	177.0	4.08	0.44
	Fall	105	4.80	7.12	2.32	48.4	82.5	5.90	0.54
West	All	1232	2.75	3.75	1.00	36.6	60.7	3.49	0.48
	Winter	309	3.78	6.09	2.31	61.2	75.4	4.62	0.64
	Spring	306	1.81	2.66	0.85	46.9	59.2	1.67	0.59
	Summer	312	1.95	1.97	0.01	0.8	38.9	1.06	0.39
	Fall	305	3.46	4.31	0.85	24.6	57.9	4.87	0.36

Table 7-7 Performance statistics for **$PM_{2.5}$** OC at IMPROVE Sites in 2022 using CMAQv6.0 CB6R5 with 2022he emissions consistent with 2022v2 air quality modeling platform.

Region	Season	N	AvgObs (µg m-3)	AvgMod (µg m-3)	MB	NMB	NME	RMSE	r
Northeast	All	1830	0.86	1.70	0.85	99.2	118.0	3.17	0.33
	Winter	458	0.67	2.09	1.43	214.0	217.0	2.16	0.73
	Spring	451	0.65	1.81	1.16	177.0	184.0	5.76	0.28
	Summer	458	1.26	1.30	0.04	3.1	42.3	0.81	0.71
	Fall	463	0.84	1.61	0.78	92.5	104.0	1.42	0.78
Southeast	All	1727	1.31	1.83	0.51	39.1	60.6	2.04	0.58
	Winter	420	1.24	2.05	0.81	65.6	80.1	2.20	0.61
	Spring	437	1.35	2.09	0.74	54.6	73.3	3.15	0.47
	Summer	438	1.31	1.61	0.30	22.6	47.4	1.00	0.77
	Fall	432	1.34	1.56	0.22	16.1	43.3	0.94	0.80
Ohio Valley	All	930	1.23	1.86	0.63	51.3	63.7	1.34	0.70
	Winter	221	0.92	1.76	0.84	91.1	95.8	1.45	0.63
	Spring	236	1.19	1.88	0.69	58.4	70.1	1.70	0.79
	Summer	236	1.50	2.01	0.51	34.2	48.0	1.10	0.71
	Fall	237	1.29	1.78	0.49	38.1	54.6	1.01	0.72
Upper Midwest	All	1036	0.89	1.23	0.35	38.9	66.1	0.92	0.66
	Winter	253	0.63	1.46	0.83	132.0	133.0	1.20	0.85
	Spring	253	0.64	0.99	0.34	53.5	67.8	0.71	0.79
	Summer	266	1.23	1.03	-0.20	-16.4	39.4	0.62	0.58
	Fall	264	1.02	1.45	0.43	42.4	57.9	1.03	0.75
South	All	1142	1.08	1.35	0.27	24.6	52.5	1.22	0.69
	Winter	274	0.75	1.21	0.46	61.9	73.2	1.19	0.68
	Spring	290	1.23	1.63	0.40	32.3	58.1	1.86	0.77
	Summer	293	1.18	1.11	-0.07	-6.2	39.7	0.72	0.62
	Fall	285	1.16	1.45	0.29	25.3	46.9	0.78	0.73
Southwest	All	3637	0.66	0.65	-0.01	-1.9	52.4	0.70	0.66
	Winter	886	0.67	0.67	-0.01	-0.8	61.0	1.00	0.65
	Spring	894	0.58	0.77	0.19	32.5	56.9	0.68	0.78
	Summer	932	0.74	0.50	-0.24	-32.4	47.3	0.52	0.58
	Fall	925	0.65	0.66	0.01	1.8	45.9	0.52	0.70
Northern Rockies & Plains	All	1935	1.06	0.91	-0.15	-14.4	61.0	3.36	0.46
	Winter	462	0.31	0.53	0.22	71.6	93.3	0.90	0.25
	Spring	474	0.34	0.51	0.17	50.0	80.7	0.80	0.26
	Summer	504	1.16	0.69	-0.48	-41.0	58.1	1.59	0.23
	Fall	495	2.36	1.87	-0.49	-20.6	55.8	6.35	0.47
Northwest	All	1877	1.39	1.65	0.26	19.0	81.1	3.48	0.67
	Winter	430	0.51	1.02	0.52	102.0	149.0	1.93	0.46
	Spring	470	0.33	0.79	0.45	136.0	159.0	1.70	0.62
	Summer	500	1.09	1.18	0.09	8.3	74.4	1.75	0.44
	Fall	477	3.52	3.55	0.03	0.8	67.1	6.20	0.68
West	All	2185	1.02	1.04	0.03	2.7	62.1	2.78	0.43
	Winter	526	0.74	0.84	0.10	13.0	63.8	0.99	0.81
	Spring	584	0.68	0.74	0.06	9.4	47.7	0.54	0.62
	Summer	552	1.30	1.23	-0.07	-5.4	67.6	4.73	0.37
	Fall	523	1.38	1.40	0.02	1.6	63.8	2.72	0.58

Table 7-8 Performance statistics for **$PM_{2.5}$** EC at CSN Sites in 2022 using CMAQv6.0 CB6R5 with 2022he emissions consistent with 2022v2 air quality modeling platform.

Region	Season	N	AvgObs (µg m-3)	AvgMod (µg m-3)	MB	NMB	NME	RMSE	r
Northeast	All	2952	0.58	0.41	-0.16	-28.2	44.7	0.44	0.47
	Winter	707	0.60	0.52	-0.08	-13.0	41.0	0.48	0.47
	Spring	761	0.53	0.39	-0.14	-26.9	42.7	0.42	0.52
	Summer	781	0.57	0.31	-0.26	-45.0	50.5	0.43	0.35
	Fall	703	0.62	0.45	-0.17	-27.3	44.4	0.44	0.52
Southeast	All	1725	0.76	0.36	-0.40	-52.7	60.6	0.69	0.39
	Winter	428	0.85	0.43	-0.42	-49.8	57.0	0.74	0.43
	Spring	423	0.77	0.35	-0.42	-54.7	59.9	0.69	0.48
	Summer	445	0.56	0.28	-0.29	-50.8	61.2	0.52	0.08
	Fall	429	0.85	0.38	-0.47	-55.1	64.3	0.77	0.31
Ohio Valley	All	2116	0.70	0.36	-0.34	-48.7	51.8	0.50	0.55
	Winter	535	0.64	0.42	-0.21	-33.1	42.7	0.45	0.42
	Spring	549	0.68	0.33	-0.36	-52.2	54.1	0.52	0.64
	Summer	525	0.71	0.30	-0.41	-58.1	58.6	0.54	0.47
	Fall	507	0.76	0.38	-0.38	-49.9	50.9	0.49	0.76
Upper Midwest	All	1164	0.50	0.35	-0.15	-30.6	47.9	0.34	0.50
	Winter	290	0.46	0.47	0.01	2.3	44.0	0.33	0.45
	Spring	289	0.40	0.30	-0.10	-25.4	44.3	0.25	0.54
	Summer	303	0.49	0.24	-0.25	-51.3	54.9	0.34	0.39
	Fall	282	0.64	0.38	-0.26	-41.1	47.2	0.43	0.65
South	All	936	0.68	0.40	-0.28	-41.0	47.8	1.29	0.25
	Winter	223	0.84	0.51	-0.33	-39.0	43.5	0.55	0.72
	Spring	233	0.52	0.33	-0.20	-37.4	41.6	0.32	0.73
	Summer	250	0.41	0.29	-0.11	-27.8	47.8	0.26	0.47
	Fall	230	0.98	0.49	-0.50	-50.5	54.7	2.50	0.08
Southwest	All	1110	0.63	0.42	-0.22	-34.1	47.1	0.56	0.56
	Winter	282	1.13	0.63	-0.50	-44.0	53.7	0.96	0.39
	Spring	280	0.36	0.32	-0.04	-11.9	38.2	0.21	0.61
	Summer	276	0.33	0.26	-0.07	-20.0	37.0	0.16	0.54
	Fall	272	0.71	0.45	-0.26	-36.2	45.6	0.49	0.48
Northern Rockies & Plains	All	488	0.40	0.16	-0.24	-59.0	65.6	0.70	0.31
	Winter	116	0.49	0.17	-0.32	-65.5	76.0	1.14	0.06
	Spring	113	0.20	0.12	-0.08	-40.5	51.5	0.19	0.44
	Summer	129	0.35	0.11	-0.24	-67.9	68.1	0.30	0.22
	Fall	130	0.55	0.25	-0.30	-54.1	60.2	0.72	0.52
Northwest	All	530	0.71	0.77	0.06	8.9	61.8	0.68	0.48
	Winter	143	0.86	0.79	-0.07	-8.2	49.9	0.58	0.51
	Spring	148	0.47	0.64	0.17	37.1	75.2	0.53	0.49
	Summer	134	0.47	0.74	0.27	57.6	88.2	0.56	0.57
	Fall	105	1.15	0.98	-0.17	-15.0	52.5	1.03	0.48
West	All	1232	0.98	0.52	-0.45	-46.4	49.7	0.81	0.74
	Winter	309	1.68	0.85	-0.83	-49.4	52.0	1.13	0.69
	Spring	306	0.61	0.39	-0.23	-36.9	44.1	0.38	0.69
	Summer	312	0.49	0.29	-0.20	-40.0	44.2	0.36	0.42
	Fall	305	1.14	0.57	-0.57	-49.7	51.7	1.04	0.67

Table 7-9 Performance statistics for **$PM_{2.5}$** EC at IMPROVE Sites in 2022 using CMAQv6.0 CB6R5 with 2022he emissions consistent with 2022v2 air quality modeling platform.

Region	Season	N	AvgObs (µg m-3)	AvgMod (µg m-3)	MB	NMB	NME	RMSE	r
Northeast	All	1823	0.18	0.19	0.01	5.4	47.6	0.15	0.70
	Winter	455	0.19	0.27	0.08	42.3	59.6	0.18	0.71
	Spring	449	0.15	0.19	0.03	22.9	51.3	0.16	0.67
	Summer	458	0.20	0.12	-0.08	-38.6	43.3	0.12	0.78
	Fall	461	0.20	0.20	0.00	1.9	38.1	0.12	0.83
Southeast	All	1724	0.29	0.17	-0.12	-41.1	48.5	0.24	0.78
	Winter	420	0.32	0.22	-0.09	-29.4	41.0	0.21	0.80
	Spring	437	0.30	0.18	-0.12	-39.2	49.0	0.29	0.74
	Summer	435	0.23	0.12	-0.11	-49.4	54.4	0.19	0.77
	Fall	432	0.32	0.16	-0.15	-48.2	51.1	0.26	0.83
Ohio Valley	All	930	0.25	0.16	-0.09	-34.6	42.6	0.14	0.67
	Winter	221	0.24	0.20	-0.04	-14.8	34.6	0.12	0.59
	Spring	236	0.24	0.16	-0.08	-32.9	40.6	0.13	0.76
	Summer	236	0.24	0.11	-0.13	-53.1	54.9	0.16	0.64
	Fall	237	0.28	0.18	-0.10	-36.3	40.2	0.15	0.77
Upper Midwest	All	1033	0.20	0.13	-0.06	-32.2	47.4	0.14	0.72
	Winter	252	0.18	0.19	0.01	4.8	36.1	0.10	0.81
	Spring	253	0.16	0.11	-0.05	-29.1	42.8	0.11	0.79
	Summer	266	0.21	0.08	-0.12	-60.0	61.6	0.17	0.76
	Fall	262	0.25	0.16	-0.09	-35.9	46.0	0.18	0.77
South	All	1135	0.20	0.13	-0.07	-37.3	49.6	0.21	0.47
	Winter	274	0.19	0.13	-0.05	-28.8	39.5	0.12	0.73
	Spring	290	0.22	0.17	-0.05	-24.8	53.6	0.29	0.61
	Summer	286	0.16	0.07	-0.09	-54.3	56.6	0.12	0.48
	Fall	285	0.23	0.13	-0.10	-44.5	48.8	0.24	0.34
Southwest	All	3606	0.16	0.09	-0.07	-45.3	57.0	0.26	0.68
	Winter	876	0.24	0.10	-0.14	-57.0	63.3	0.46	0.73
	Spring	878	0.12	0.10	-0.02	-17.6	50.3	0.14	0.73
	Summer	928	0.11	0.06	-0.05	-44.8	56.0	0.09	0.66
	Fall	924	0.17	0.09	-0.08	-48.5	53.9	0.22	0.68
Northern Rockies & Plains	All	1913	0.14	0.11	-0.03	-22.0	61.8	0.29	0.50
	Winter	450	0.07	0.07	-0.01	-10.4	63.2	0.15	0.20
	Spring	470	0.06	0.06	0.00	0.3	65.6	0.13	0.18
	Summer	498	0.13	0.07	-0.06	-48.1	69.2	0.21	0.15
	Fall	495	0.27	0.22	-0.05	-17.7	57.1	0.50	0.52
Northwest	All	1855	0.20	0.18	-0.02	-9.0	69.6	0.68	0.48
	Winter	415	0.13	0.13	0.00	3.5	76.8	0.20	0.70
	Spring	472	0.07	0.10	0.03	35.4	87.0	0.20	0.59
	Summer	494	0.14	0.14	0.00	2.2	79.0	0.24	0.68
	Fall	474	0.44	0.34	-0.10	-23.3	61.7	1.30	0.50
West	All	2145	0.17	0.11	-0.06	-36.4	56.3	0.27	0.70
	Winter	512	0.20	0.11	-0.09	-44.3	60.2	0.24	0.82
	Spring	573	0.10	0.09	-0.02	-17.1	46.4	0.09	0.69
	Summer	537	0.16	0.10	-0.06	-36.5	55.9	0.28	0.61
	Fall	523	0.24	0.14	-0.09	-39.2	58.1	0.40	0.71

Table 7-10 Performance statistics MDA8 O_3 at AQS Sites in 2022 using CMAQv6.0 CB6R5 with 2022he emissions consistent with 2022v2 air quality modeling platform.

Region	Season	N	AvgObs (ppb)	AvgMod (ppb)	MB	NMB	NME	RMSE	r
Northeast	All	52703	39.8	40.8	1.0	2.4	11.6	6.00	0.81
	Winter	7926	33.9	32.9	-1.0	-3.0	10.7	4.82	0.75
	Spring	16165	42.5	42.9	0.4	0.9	10.1	5.48	0.70
	Summer	16222	44.8	46.5	1.7	3.8	11.5	6.70	0.79
	Fall	12390	33.5	35.5	2.0	6.0	14.9	6.35	0.74
Southeast	All	48275	39.4	41.5	2.1	5.2	13.5	6.84	0.76
	Winter	6842	36.7	35.6	-1.1	-3.1	12.6	5.77	0.70
	Spring	15220	43.9	43.6	-0.3	-0.7	10.3	5.80	0.79
	Summer	14520	37.9	43.2	5.4	14.2	17.9	8.39	0.80
	Fall	11693	37.2	40.0	2.9	7.7	13.5	6.53	0.77
Ohio Valley	All	60934	41.6	43.6	2.1	5.0	13.0	6.91	0.78
	Winter	5499	30.9	31.0	0.0	0.1	12.7	5.05	0.79
	Spring	20427	42.7	44.1	1.4	3.4	11.5	6.28	0.65
	Summer	20107	46.4	49.7	3.4	7.2	13.3	7.71	0.73
	Fall	14901	37.4	39.3	1.9	5.1	14.9	7.17	0.72
Upper Midwest	All	24294	40.2	41.9	1.7	4.2	11.8	6.12	0.81
	Winter	1492	33.3	34.1	0.8	2.4	8.8	3.81	0.82
	Spring	8201	42.0	44.0	2.0	4.7	10.1	5.40	0.75
	Summer	8620	43.4	44.9	1.5	3.6	11.7	6.57	0.79
	Fall	5981	34.8	36.6	1.8	5.2	15.5	6.79	0.74
South	All	45543	40.5	41.0	0.4	1.1	14.2	7.31	0.80
	Winter	9623	33.7	31.9	-1.7	-5.1	14.9	6.28	0.77
	Spring	12336	44.2	44.1	-0.2	-0.4	12.7	7.21	0.72
	Summer	12064	41.3	44.3	3.1	7.4	16.4	8.43	0.82
	Fall	11520	41.5	41.6	0.1	0.2	13.1	6.96	0.83
Southwest	All	46368	47.8	46.9	-0.9	-1.9	11.2	7.08	0.77
	Winter	10532	39.1	36.4	-2.6	-6.8	13.6	6.92	0.66
	Spring	12012	50.9	50.4	-0.5	-1.0	9.5	6.48	0.60
	Summer	12353	55.7	55.2	-0.4	-0.8	11.4	8.35	0.50
	Fall	11471	44.1	44.0	-0.1	-0.3	11.0	6.31	0.73
Northern Rockies & Plains	All	16891	42.1	42.8	0.8	1.8	10.1	5.55	0.78
	Winter	4042	38.0	37.5	-0.5	-1.3	9.9	4.94	0.70
	Spring	4278	44.6	45.2	0.7	1.5	8.1	4.79	0.68
	Summer	4335	47.1	48.9	1.8	3.9	11.0	6.54	0.68
	Fall	4236	38.3	39.3	1.0	2.5	11.4	5.71	0.76
Northwest	All	6337	37.7	38.2	0.6	1.5	13.3	6.73	0.78
	Winter	803	32.3	33.9	1.6	4.9	16.9	7.15	0.74
	Spring	1672	39.1	40.2	1.2	3.0	10.3	5.25	0.71
	Summer	2521	39.1	38.7	-0.3	-0.9	13.6	7.28	0.80
	Fall	1341	36.5	37.4	0.9	2.5	14.8	7.02	0.76
West	All	60629	44.5	42.5	-2.0	-4.4	13.0	7.58	0.83
	Winter	13437	34.9	33.9	-1.1	-3.1	15.6	6.88	0.66
	Spring	15970	47.4	45.4	-2.0	-4.3	10.7	6.72	0.74
	Summer	16392	49.8	47.1	-2.7	-5.5	13.6	8.80	0.84
	Fall	14830	44.2	42.2	-1.9	-4.4	12.9	7.61	0.80

Table 7-11 Performance statistics for MDA8 O_3 at CASTNET Sites in 2022 using CMAQv6.0 CB6R5 with 2022he emissions consistent with 2022v2 air quality modeling platform.

Region	Season	N	AvgObs (ppb)	AvgMod (ppb)	MB	NMB	NME	RMSE	r
Northeast	All	4265	39.9	39.8	-0.1	-0.2	10.5	5.51	0.80
	Winter	1113	35.4	33.8	-1.6	-4.6	9.8	4.58	0.75
	Spring	1183	43.9	43.6	-0.3	-0.8	9.1	5.14	0.70
	Summer	978	45.1	46.3	1.2	2.7	11.0	6.58	0.73
	Fall	991	35.1	35.7	0.7	1.9	12.7	5.75	0.71
Southeast	All	4006	39.7	40.0	0.2	0.6	12.9	6.56	0.72
	Winter	982	37.1	34.4	-2.8	-7.4	14.3	6.57	0.69
	Spring	1067	45.4	43.8	-1.6	-3.6	10.0	5.70	0.77
	Summer	971	38.1	42.7	4.6	12.1	16.4	7.94	0.77
	Fall	986	37.7	38.7	1.0	2.6	11.7	5.86	0.71
Ohio Valley	All	5596	40.1	40.6	0.5	1.2	12.5	6.38	0.77
	Winter	1407	33.7	32.4	-1.4	-4.0	12.9	5.62	0.74
	Spring	1550	44.5	44.5	0.0	0.0	10.6	6.05	0.63
	Summer	1307	44.6	47.6	3.0	6.8	13.5	7.28	0.74
	Fall	1332	37.3	37.9	0.6	1.5	13.7	6.57	0.70
Upper Midwest	All	1765	38.1	38.9	0.7	1.9	10.7	5.42	0.82
	Winter	436	34.7	34.9	0.3	0.7	7.4	3.33	0.82
	Spring	454	42.9	44.2	1.3	3.0	9.1	4.89	0.76
	Summer	442	40.9	41.6	0.7	1.8	11.9	6.35	0.82
	Fall	433	33.9	34.5	0.6	1.8	14.9	6.51	0.71
South	All	2034	41.4	40.9	-0.5	-1.1	13.4	6.89	0.77
	Winter	517	36.0	33.4	-2.6	-7.3	15.5	6.80	0.75
	Spring	536	45.9	45.1	-0.8	-1.8	10.9	6.36	0.73
	Summer	501	42.3	45.0	2.7	6.3	15.3	8.04	0.79
	Fall	480	41.1	40.2	-0.9	-2.3	12.3	6.24	0.80
Southwest	All	4235	48.8	47.7	-1.1	-2.2	9.6	5.92	0.77
	Winter	1060	43.7	39.0	-4.7	-10.8	12.1	6.18	0.74
	Spring	1075	52.3	51.4	-0.9	-1.8	8.0	5.33	0.64
	Summer	1056	54.3	55.4	1.1	2.1	9.2	6.66	0.51
	Fall	1044	44.7	44.9	0.3	0.6	9.5	5.40	0.71
Northern Rockies & Plains	All	2476	44.2	45.9	1.7	3.8	10.4	6.08	0.72
	Winter	609	40.8	40.4	-0.4	-0.9	11.2	6.07	0.59
	Spring	634	47.1	47.6	0.5	1.0	6.9	4.22	0.72
	Summer	624	47.8	52.0	4.2	8.8	11.5	6.82	0.75
	Fall	609	40.8	43.2	2.4	5.8	12.4	6.87	0.67
Northwest	All	1050	40.3	42.3	1.9	4.8	10.7	5.87	0.74
	Winter	256	36.6	39.8	3.2	8.7	15.0	7.64	0.39
	Spring	268	42.4	43.8	1.4	3.3	8.0	4.36	0.77
	Summer	267	44.0	45.0	1.0	2.4	9.0	5.20	0.81
	Fall	259	38.2	40.3	2.1	5.5	11.8	5.87	0.76
West	All	2443	49.4	45.5	-3.9	-7.9	12.2	7.88	0.76
	Winter	597	41.7	39.0	-2.6	-6.3	12.1	6.08	0.55
	Spring	607	50.9	47.5	-3.4	-6.7	10.4	6.63	0.72
	Summer	630	56.7	51.1	-5.6	-9.8	13.8	10.20	0.67
	Fall	609	48.1	44.1	-4.0	-8.2	12.1	7.91	0.69

References

ADEC: Fairbanks PM2.5 Moderate State Implementation Plan: http://dec.alaska.gov/air/anpms/communities/fbks-pm2-5-moderate-sip/, 2014, last access: July 24, 2026.

Andersen, S. T., Carpenter, L. J., Reed, C., Lee, J. D., Chance, R., Sherwen, T., Vaughan, A. R., Stewart, J., Edwards, P. M., Bloss, W. J., Sommariva, R., Crilley, L. R., Nott, G. J., Neves, L., Read, K., Heard, D. E., Seakins, P. W., Whalley, L. K., Boustead, G. A., Fleming, L. T., Stone, D., and Fomba, K. W.: Extensive field evidence for the release of HONO from the photolysis of nitrate aerosols, Science Advances, 9, eadd6266, https://doi.org/10.1126/sciadv.add6266, 2023.

Bash, J. O., Walker, J. T., Wu, Z., Rumsey, I. C., Murphy, B., Hogrefe, C., Fahey, K. M., Pye, H. O. T., Jones, M. R., Appel, K. W., Shephard, M., Alnsour, N. I., and Cady-Periera, K. E.: Evaluation of HNO3, SO2, and NH3 in the Surface Tiled Aerosol and Gaseous Exchange (STAGE) option in the Community Multiscale Air Quality Model version 5.3.2 against field-scale, in situ and satellite observations, EGUsphere, 2026, 1-29, https://doi.org/10.5194/egusphere-2025-3536, 2026.

Byun, D. and Schere, K. L.: Review of the Governing Equations, Computational Algorithms, and Other Components of the Models-3 Community Multiscale Air Quality (CMAQ) Modeling System, Applied Mechanics Reviews, 59, 51-77, https://doi.org/10.1115/1.2128636, 2006.

Byun, D. W., Pleim, J. E., Tang, R. T., and Bourgeois, A.: Science Algorithms of the EPA Models-3 Community Multiscale Air Quality (CMAQ) Modeling System Chapter 12 Meteorology-Chemistry Interface Processor (MCIP) for Models-3 Community Multiscale Air Quality (CMAQ) Modeling System: https://www.cmascenter.org/cmaq/science_documentation/, 1999, last access: July 24, 2026.

CAMS: Soil N emissions for 2000-present: https://atmosphere.copernicus.eu/sites/default/files/2019-11/25_CAMS81_2017SC1_D81.3.6.1-201810_APPROVED_Ver1.pdf, 2018, last access: July 24, 2026.

Carter, W. P. L.: Development of the SAPRC-07 chemical mechanism, Atmospheric Environment, 44, 5324-5335, https://doi.org/10.1016/j.atmosenv.2010.01.026, 2010a.

Carter, W. P. L.: Development of a condensed SAPRC-07 chemical mechanism, Atmospheric Environment, 44, 5336-5345, https://doi.org/10.1016/j.atmosenv.2010.01.024, 2010b.

Chen, N., Yu, K., Jia, R., Teng, J., and Zhao, C.: Biocrust as one of multiple stable states in global drylands, Science Advances, 6, eaay3763, doi:10.1126/sciadv.aay3763, 2020.

Cheng, P., Pour-Biazar, A., Wu, Y., Kuang, S., McNider, R. T., and Koshak, W. J.: Utility of Geostationary Lightning Mapper-derived lightning NO emission estimates in air quality modeling studies, Atmos. Chem. Phys., 24, 41-63, 10.5194/acp-24-41-2024, 2024.

Crippa, M., Guizzardi, D., Butler, T., Keating, T., Wu, R., Kaminski, J., Kuenen, J., Kurokawa, J., Chatani, S., Morikawa, T., Pouliot, G., Racine, J., Moran, M. D., Klimont, Z., Manseau, P. M., Mashayekhi, R., Henderson, B. H., Smith, S. J., Suchyta, H., Muntean, M., Solazzo, E., Banja, M., Schaaf, E., Pagani, F., Woo, J. H., Kim, J., Monforti-Ferrario, F., Pisoni, E., Zhang, J., Niemi, D., Sassi, M., Ansari, T., and Foley, K.: The HTAP_v3 emission mosaic: merging regional and global monthly emissions (2000–2018) to support air quality modelling and policies, Earth Syst. Sci. Data, 15, 2667-2694, https://doi.org/10.5194/essd-15-2667-2023, 2023.

Delaria, E. R., Place, B. K., Liu, A. X., and Cohen, R. C.: Laboratory measurements of stomatal NO2 deposition to native California trees and the role of forests in the NOx cycle, Atmos. Chem. Phys., 20, 14023-14041, 10.5194/acp-20-14023-2020, 2020.

Desai, N. S., Moore, A. C., Mouat, A. P., Liang, Y., Xu, T., Takeuchi, M., Pye, H. O. T., Murphy, B., Bash, J., Pollack, I. B., Peischl, J., Ng, N. L., and Kaiser, J.: Impact of Heatwaves and Declining NOx on Nocturnal Monoterpene Oxidation in the Urban Southeastern United States, Journal of Geophysical Research: Atmospheres, 129, e2024JD041482, https://doi.org/10.1029/2024JD041482, 2024.

Emerson, E. W., Hodshire, A. L., DeBolt, H. M., Bilsback, K. R., Pierce, J. R., McMeeking, G. R., and Farmer, D. K.: Revisiting particle dry deposition and its role in radiative effect estimates, Proceedings of the National Academy of Sciences, 117, 26076-26082, https://doi.org/10.1073/pnas.2014761117, 2020.

Farrell, S. L., Pye, H. O. T., Gilliam, R., Pouliot, G., Huff, D., Sarwar, G., Vizuete, W., Briggs, N., Duan, F., Ma, T., Zhang, S., and Fahey, K.: Predicted impacts of heterogeneous chemical pathways on particulate sulfur over Fairbanks (Alaska), the Northern Hemisphere, and the Contiguous United States, Atmos. Chem. Phys., 25, 3287-3312, https://doi.org/10.5194/acp-25-3287-2025, 2025.

Finney, D. L., Doherty, R. M., Wild, O., Young, P. J., and Butler, A.: Response of lightning NOx emissions and ozone production to climate change: Insights from the Atmospheric Chemistry and Climate Model Intercomparison Project, Geophysical Research Letters, 43, 5492-5500, https://doi.org/10.1002/2016GL068825, 2016.

Foroutan, H., Young, J., Napelenok, S., Ran, L., Appel, K. W., Gilliam, R. C., and Pleim, J. E.: Development and evaluation of a physics-based windblown dust emission scheme implemented in the CMAQ modeling system, Journal of Advances in Modeling Earth Systems, 9, 585-608, https://doi.org/10.1002/2016MS000823, 2017.

Gantt, B., Kelly, J. T., and Bash, J. O.: Updating sea spray aerosol emissions in the Community Multiscale Air Quality (CMAQ) model version 5.0.2, Geosci. Model Dev., 8, 3733-3746, https://doi.org/10.5194/gmd-8-3733-2015, 2015.

Guenther, A., Jiang, X., Shah, T., Huang, L., Kemball-Cook, S., and Yarwood, G.: Model of Emissions of Gases and Aerosol from Nature Version 3 (MEGAN3) for Estimating Biogenic Emissions, in: Mensink, C., Gong, W., Hakami, A. (eds) Air Pollution Modeling and its Application XXVI, ITM 2018, Ottawa, Canada, 187-192, https://doi.org/10.1007/978-3-030-22055-6_29,

Guenther, A. B., Jiang, X., Heald, C. L., Sakulyanontvittaya, T., Duhl, T., Emmons, L. K., and Wang, X.: The Model of Emissions of Gases and Aerosols from Nature version 2.1 (MEGAN2.1): an extended and updated framework for modeling biogenic emissions, Geosci. Model Dev., 5, 1471-1492, https://doi.org/10.5194/gmd-5-1471-2012, 2012.

Huang, X. and Foroutan, H.: Effects of Non-Photosynthetic Vegetation on Dust Emissions, Journal of Geophysical Research: Atmospheres, 127, e2021JD035243, https://doi.org/10.1029/2021JD035243, 2022.

Huber, D. E., Steiner, A. L., and Kort, E. A.: Daily Cropland Soil NOx Emissions Identified by TROPOMI and SMAP, Geophysical Research Letters, 47, e2020GL089949, https://doi.org/10.1029/2020GL089949, 2020.

Hudman, R. C., Moore, N. E., Mebust, A. K., Martin, R. V., Russell, A. R., Valin, L. C., and Cohen, R. C.: Steps towards a mechanistic model of global soil nitric oxide emissions: implementation and space based-constraints, Atmos. Chem. Phys., 12, 7779-7795, https://doi.org/10.5194/acp-12-7779-2012, 2012.

Hutzell, W. T., Luecken, D. J., Appel, K. W., and Carter, W. P. L.: Interpreting predictions from the SAPRC07 mechanism based on regional and continental simulations, Atmospheric Environment, 46, 417-429, https://doi.org/10.1016/j.atmosenv.2011.09.030, 2012.

Jenkin, M. E., Saunders, S. M., Wagner, V., and Pilling, M. J.: Protocol for the development of the Master Chemical Mechanism, MCM v3 (Part B): tropospheric degradation of aromatic volatile organic compounds, Atmos. Chem. Phys., 3, 181-193, https://doi.org/10.5194/acp-3-181-2003, 2003.

Kang, D., Wu, Y., Pour-Biazar, A., Mathur, R., Wong, D., and Appel, W.: Development and Assessment of an Energy-Based Lightning NOx Model by Synergizing Satellite and Ground-Based Lightning Datasets for Air Quality Modeling, in: Mensink, C., Im, U. (eds) Air Pollution Modeling and Its Application XXX, ITM 2024, Copenhagen, Denmark, 329-335, https://doi.org/10.1007/978-3-032-02971-3_41, 2026.

Kang, D., Hogrefe, C., Sarwar, G., East, J. D., Madden, J. M., Mathur, R., and Henderson, B. H.: Assessing the Impact of Lightning NOx Emissions in CMAQ Using Lightning Flash Data from WWLLN over the Contiguous United States, Atmosphere, 13, 1248, https://doi.org/10.3390/atmos13081248, 2022.

Kelly, J. T., Bhave, P. V., Nolte, C. G., Shankar, U., and Foley, K. M.: Simulating emission and chemical evolution of coarse sea-salt particles in the Community

Multiscale Air Quality (CMAQ) model, Geosci. Model Dev., 3, 257-273, https://doi.org/10.5194/gmd-3-257-2010, 2010.

Kim, M. and Or, D.: Microscale pH variations during drying of soils and desert biocrusts affect HONO and NH3 emissions, Nature Communications, 10, 3944, 10.1038/s41467-019-11956-6, 2019.

Malm, W. C., Sisler, J. F., Huffman, D., Eldred, R. A., and Cahill, T. A.: Spatial and seasonal trends in particle concentration and optical extinction in the United States, Journal of Geophysical Research: Atmospheres, 99, 1347-1370, https://doi.org/10.1029/93JD02916, 1994.

Mansouri, K., Grulke, C. M., Judson, R. S., and Williams, A. J.: OPERA models for predicting physicochemical properties and environmental fate endpoints, Journal of Cheminformatics, 10, 10, https://doi.org/10.1186/s13321-018-0263-1, 2018.

Mathur, R., Xing, J., Gilliam, R., Sarwar, G., Hogrefe, C., Pleim, J., Pouliot, G., Roselle, S., Spero, T. L., Wong, D. C., and Young, J.: Extending the Community Multiscale Air Quality (CMAQ) modeling system to hemispheric scales: overview of process considerations and initial applications, Atmos. Chem. Phys., 17, 12449-12474, https://doi.org/10.5194/acp-17-12449-2017, 2017.

Nault, B. A., Laughner, J. L., Wooldridge, P. J., Crounse, J. D., Dibb, J., Diskin, G., Peischl, J., Podolske, J. R., Pollack, I. B., Ryerson, T. B., Scheuer, E., Wennberg, P. O., and Cohen, R. C.: Lightning NOx Emissions: Reconciling Measured and Modeled Estimates With Updated NOx Chemistry, Geophysical Research Letters, 44, 9479-9488, https://doi.org/10.1002/2017GL074436, 2017.

Oikawa, P. Y., Ge, C., Wang, J., Eberwein, J. R., Liang, L. L., Allsman, L. A., Grantz, D. A., and Jenerette, G. D.: Unusually high soil nitrogen oxide emissions influence air quality in a high-temperature agricultural region, Nature Communications, 6, 8753, 10.1038/ncomms9753, 2015.

Otte, T. L. and Pleim, J. E.: The Meteorology-Chemistry Interface Processor (MCIP) for the CMAQ modeling system: updates through MCIPv3.4.1, Geosci. Model Dev., 3, 243-256, https://doi.org/10.5194/gmd-3-243-2010, 2010.

Place, B. K., Hutzell, W. T., Appel, K. W., Farrell, S., Valin, L., Murphy, B. N., Seltzer, K. M., Sarwar, G., Allen, C., Piletic, I. R., D'Ambro, E. L., Saunders, E., Simon, H., Torres-Vasquez, A., Pleim, J., Schwantes, R. H., Coggon, M. M., Xu, L., Stockwell, W. R., and Pye, H. O. T.: Sensitivity of northeastern US surface ozone predictions to the representation of atmospheric chemistry in the Community Regional Atmospheric Chemistry Multiphase Mechanism (CRACMMv1.0), Atmos. Chem. Phys., 23, 9173-9190, https://doi.org/10.5194/acp-23-9173-2023, 2023.

Pleim, J. and Ran, L.: Surface Flux Modeling for Air Quality Applications, Atmosphere, 2, 271-302, https://doi.org/10.3390/atmos2030271, 2011.

Pleim, J. E., Ran, L., Appel, W., Shephard, M. W., and Cady-Pereira, K.: New Bidirectional Ammonia Flux Model in an Air Quality Model Coupled With an Agricultural Model, Journal of Advances in Modeling Earth Systems, 11, 2934-2957, https://doi.org/10.1029/2019MS001728, 2019.

Pleim, J. E., Ran, L., Saylor, R. D., Willison, J., and Binkowski, F. S.: A New Aerosol Dry Deposition Model for Air Quality and Climate Modeling, Journal of Advances in Modeling Earth Systems, 14, e2022MS003050, https://doi.org/10.1029/2022MS003050, 2022.

Potter, P., Ramankutty, N., Bennett, E. M., and Donner, S. D.: Characterizing the Spatial Patterns of Global Fertilizer Application and Manure Production, Earth Interactions, 14, 1-22, https://doi.org/10.1175/2009EI288.1, 2010.

Pye, H. O. T., Place, B. K., Murphy, B. N., Seltzer, K. M., D'Ambro, E. L., Allen, C., Piletic, I. R., Farrell, S., Schwantes, R. H., Coggon, M. M., Saunders, E., Xu, L., Sarwar, G., Hutzell, W. T., Foley, K. M., Pouliot, G., Bash, J., and Stockwell, W. R.: Linking gas, particulate, and toxic endpoints to air emissions in the Community Regional Atmospheric Chemistry Multiphase Mechanism (CRACMM), Atmos. Chem. Phys., 23, 5043-5099, https://doi.org/10.5194/acp-23-5043-2023, 2023.

Pye, H. O. T., Hutzell, W. T., Fann, N. L., Skipper, T. N., Pye, M. J., Beidler, J., Allen, C., Murphy, B. N., D'Ambro, E. L., Lin, S., Talgo, K., Reynolds, L., Kang, D., Bash, J., Seltzer, K. M., Farrell, S. L., Appel, K. W., Brehme, K., Gilliam, R. C., Henderson, B. H., and Chan, A. W. H.: The Risks to Human Health of Air Toxics, PM2.5, and Ozone from the 2023 Canadian Wildfires, Environmental Science & Technology Letters, 13, 268-274, 10.1021/acs.estlett.5c01181, 2026a.

Pye, H. O. T., Hogrefe, C., Sarwar, G., Murphy, B. N., Skipper, T. N., Sidi, F., Foley, K. M., Hutzell, W. T., Fahey, K. M., Stockwell, W. R., Bash, J. O., Seltzer, K. M., Schwantes, R. H., Farrell, S. L., Yu, C. M., Kang, D., Saiz-Lopez, A., D'Ambro, E. L., Willison, J., Henderson, B. H., Pouliot, G., Baker, K., Beidler, J., Gilliam, R., Mallard, M., Napelenok, S. L., Nolte, C. G., Pleim, J., Spero, T., Wong, D. C., Appel, K. W., Pinder, R., and Mathur, R.: A coupled representation of ozone and PM2.5 across the U.S. and Northern Hemisphere from CRACMM version 3 (in prep), 2026b.

Sarwar, G., Simon, H., Bhave, P., and Yarwood, G.: Examining the impact of heterogeneous nitryl chloride production on air quality across the United States, Atmos. Chem. Phys., 12, 6455-6473, https://doi.org/10.5194/acp-12-6455-2012, 2012.

Sarwar, G., Gantt, B., Schwede, D., Foley, K., Mathur, R., and Saiz-Lopez, A.: Impact of Enhanced Ozone Deposition and Halogen Chemistry on Tropospheric Ozone over the Northern Hemisphere, Environmental Science & Technology, 49, 9203-9211, https://doi.org/10.1021/acs.est.5b01657, 2015.

Sarwar, G., Kang, D., Henderson, B. H., Hogrefe, C., Appel, W., and Mathur, R.: Examining the Impact of Dimethyl Sulfide Emissions on Atmospheric Sulfate over the Continental U.S, Atmosphere, 14, 660, https://doi.org/10.3390/atmos14040660, 2023.

Sarwar, G., Hogrefe, C., Henderson, B. H., Mathur, R., Gilliam, R., Callaghan, A. B., Lee, J., and Carpenter, L. J.: Impact of particulate nitrate photolysis on air quality over the Northern Hemisphere, Science of The Total Environment, 917, 170406, https://doi.org/10.1016/j.scitotenv.2024.170406, 2024.

Sarwar, G., Sidi, F., Simon, H., Henderson, B. H., Willison, J., Gilliam, R., Hogrefe, C., Foley, K., Mathur, R., and Appel, W.: Representing particulate nitrate photolysis over seawater improves CMAQ ozone predictions over the contiguous United States, Science of The Total Environment, 970, 178968, https://doi.org/10.1016/j.scitotenv.2025.178968, 2025.

Sarwar, G., Gantt, B., Foley, K., Fahey, K., Spero, T. L., Kang, D., Mathur, R., Foroutan, H., Xing, J., Sherwen, T., and Saiz-Lopez, A.: Influence of bromine and iodine chemistry on annual, seasonal, diurnal, and background ozone: CMAQ simulations over the Northern Hemisphere, Atmospheric Environment, 213, 395-404, https://doi.org/10.1016/j.atmosenv.2019.06.020, 2019.

Sarwar, G., Hutzell, W. T., Wong, D., Gilliam, R., Hogrefe, C., Sidi, F., Nash Skipper, T., Pye, H., Mathur, R., Willison, J., Murphy, B., Henderson, B., Talgo, K., Stockwell, W. R., and Saiz-Lopez, A.: Implementing Halogen Chemistry and Photolysis of Particulate Nitrate into the CRACMM and Examining Their Impacts on Springtime Ozone Using CMAQ Over the Northern Hemisphere, in: Mensink, C., Im, U. (eds) Air Pollution Modeling and Its Application XXX, ITM 2024, Copenhagen, Denmark, 31-38, https://doi.org/10.1007/978-3-032-02971-3_5, 2026.

Schumann, U. and Huntrieser, H.: The global lightning-induced nitrogen oxides source, Atmos. Chem. Phys., 7, 3823-3907, https://doi.org/10.5194/acp-7-3823-2007, 2007.

Shah, V., Jacob, D. J., Dang, R., Lamsal, L. N., Strode, S. A., Steenrod, S. D., Boersma, K. F., Eastham, S. D., Fritz, T. M., Thompson, C., Peischl, J., Bourgeois, I., Pollack, I. B., Nault, B. A., Cohen, R. C., Campuzano-Jost, P., Jimenez, J. L., Andersen, S. T., Carpenter, L. J., Sherwen, T., and Evans, M. J.: Nitrogen oxides in the free troposphere: implications for tropospheric oxidants and the interpretation of satellite NO2 measurements, Atmos. Chem. Phys., 23, 1227-1257, https://doi.org/10.5194/acp-23-1227-2023, 2023.

Simpson, W. R., Mao, J., Fochesatto, G. J., Law, K. S., DeCarlo, P. F., Schmale, J., Pratt, K. A., Arnold, S. R., Stutz, J., Dibb, J. E., Creamean, J. M., Weber, R. J., Williams, B. J., Alexander, B., Hu, L., Yokelson, R. J., Shiraiwa, M., Decesari, S., Anastasio, C., D'Anna, B., Gilliam, R. C., Nenes, A., St. Clair, J. M., Trost, B., Flynn, J. H., Savarino, J., Conner, L. D., Kettle, N., Heeringa, K. M., Albertin, S., Baccarini, A., Barret, B., Battaglia, M. A., Bekki, S., Brado, T. J., Brett, N., Brus, D., Campbell, J. R., Cesler-Maloney, M., Cooperdock, S., Cysneiros de Carvalho, K., Delbarre, H., DeMott, P. J., Dennehy, C. J. S., Dieudonné, E., Dingilian, K. K., Donateo, A., Doulgeris, K. M., Edwards, K. C., Fahey, K., Fang, T., Guo, F., Heinlein, L. M. D., Holen, A. L., Huff, D., Ijaz, A., Johnson, S., Kapur, S., Ketcherside, D. T., Levin, E., Lill, E., Moon, A. R., Onishi, T., Pappaccogli, G., Perkins, R., Pohorsky, R., Raut, J.-C., Ravetta, F., Roberts,

T., Robinson, E. S., Scoto, F., Selimovic, V., Sunday, M. O., Temime-Roussel, B., Tian, X., Wu, J., and Yang, Y.: Overview of the Alaskan Layered Pollution and Chemical Analysis (ALPACA) Field Experiment, ACS ES&T Air, 1, 200-222, https://doi.org/10.1021/acsestair.3c00076, 2024.

Sindelarova, K., Granier, C., Bouarar, I., Guenther, A., Tilmes, S., Stavrakou, T., Müller, J. F., Kuhn, U., Stefani, P., and Knorr, W.: Global data set of biogenic VOC emissions calculated by the MEGAN model over the last 30 years, Atmos. Chem. Phys., 14, 9317-9341, https://doi.org/10.5194/acp-14-9317-2014, 2014.

Skamarock, W. C., Klemp, J. B., Dudhia, J., Gill, D. O., Liu, Z., Berner, J., Wang, W., Powers, J. G., Duda, M. G., Barker, D. M., and Huang, X.-Y.: A Description of the Advanced Research WRF Model Version 4: https://opensky.ucar.edu/system/files/2024-08/technotes_576.pdf, 2019, last access: July 24, 2026.

Skipper, T. N., D'Ambro, E. L., Wiser, F. C., McNeill, V. F., Schwantes, R. H., Henderson, B. H., Piletic, I. R., Baublitz, C. B., Bash, J. O., Whitehill, A. R., Valin, L. C., Mouat, A. P., Kaiser, J., Wolfe, G. M., St. Clair, J. M., Hanisco, T. F., Fried, A., Place, B. K., and Pye, H. O. T.: Role of chemical production and depositional losses on formaldehyde in the Community Regional Atmospheric Chemistry Multiphase Mechanism (CRACMM), Atmos. Chem. Phys., 24, 12903-12924, https://doi.org/10.5194/acp-24-12903-2024, 2024.

Stark, J. M.: Modeling the temperature response of nitrification, Biogeochemistry, 35, 433-445, 10.1007/BF02183035, 1996.

Steinkamp, J. and Lawrence, M. G.: Improvement and evaluation of simulated global biogenic soil NO emissions in an AC-GCM, Atmos. Chem. Phys., 11, 6063-6082, 10.5194/acp-11-6063-2011, 2011.

US EPA: Modeling Guidance for Demonstrating Attainment of Air Quality Goals for Ozone, PM2.5, and Regional Haze: https://www.epa.gov/sites/default/files/2020-10/documents/o3-pm-rh-modeling_guidance-2018.pdf, 2018, last access: July 29, 2026.

US EPA: Meteorological Model Performance for Annual 2022 Simulation WRF v4.4.2: https://www.epa.gov/system/files/documents/2024-03/wrf_2022_tsd.pdf, 2024, last access: July 24, 2026.

US EPA: Technical Support Document (TSD): Preparation of Emissions Inventories for the 2022v1 North American Emissions Modeling Platform https://www.epa.gov/system/files/documents/2025-12/2022v1_emismod_tsd_base_and_2026_may2025_508.pdf, 2025a, last access: July 24, 2026.

US EPA: Technical Support Document (TSD): Preparation of Emissions Inventories for the 2022v2 North American Emissions Modeling Platform https://www.epa.gov/system/files/documents/2025-12/2022v2_emismod_tsd_base_december2025.pdf, 2025b, last access: July 24, 2026.

US EPA: Technical Support Document (TSD): 2022 Regulatory Modeling Platform: Air Quality Modeling Version 1: https://www.epa.gov/system/files/documents/2026-04/2022-v1-modeling-platform-aq-model-tsd_final_version.pdf, 2026, last access: July 24, 2026.

Vannucci, P. F., Foley, K., Murphy, B. N., Hogrefe, C., Cohen, R. C., and Pye, H. O. T.: Temperature-Dependent Composition of Summertime PM2.5 in Observations and Model Predictions across the Eastern U.S, ACS Earth and Space Chemistry, 8, 381-392, 10.1021/acsearthspacechem.3c00333, 2024.

Wang, Y., Li, Q., Wang, Y., Ren, C., Saiz-Lopez, A., Xue, L., and Wang, T.: Increasing soil nitrous acid emissions driven by climate and fertilization change aggravate global ozone pollution, Nature Communications, 16, 2463, 10.1038/s41467-025-57161-6, 2025.

Weber, B., Wu, D., Tamm, A., Ruckteschler, N., Rodríguez-Caballero, E., Steinkamp, J., Meusel, H., Elbert, W., Behrendt, T., Sörgel, M., Cheng, Y., Crutzen, P. J., Su, H., and Pöschl, U.: Biological soil crusts accelerate the nitrogen cycle through large NO and HONO emissions in drylands, Proceedings of the National Academy of Sciences, 112, 15384-15389, doi:10.1073/pnas.1515818112, 2015.

Weng, H., Lin, J., Martin, R., Millet, D. B., Jaeglé, L., Ridley, D., Keller, C., Li, C., Du, M., and Meng, J.: Global high-resolution emissions of soil NOx, sea salt aerosols, and biogenic volatile organic compounds, Scientific Data, 7, 148, 10.1038/s41597-020-0488-5, 2020.

Wennberg, P. O., Bates, K. H., Crounse, J. D., Dodson, L. G., McVay, R. C., Mertens, L. A., Nguyen, T. B., Praske, E., Schwantes, R. H., Smarte, M. D., St Clair, J. M., Teng, A. P., Zhang, X., and Seinfeld, J. H.: Gas-Phase Reactions of Isoprene and Its Major Oxidation Products, Chemical Reviews, 118, 3337-3390, https://doi.org/10.1021/acs.chemrev.7b00439, 2018.

Wiedinmyer, C., Kimura, Y., McDonald-Buller, E. C., Emmons, L. K., Buchholz, R. R., Tang, W., Seto, K., Joseph, M. B., Barsanti, K. C., Carlton, A. G., and Yokelson, R.: The Fire Inventory from NCAR version 2.5: an updated global fire emissions model for climate and chemistry applications, Geosci. Model Dev., 16, 3873-3891, https://doi.org/10.5194/gmd-16-3873-2023, 2023.

Wiser, F., Place, B. K., Sen, S., Pye, H. O. T., Yang, B., Westervelt, D. M., Henze, D. K., Fiore, A. M., and McNeill, V. F.: AMORE-Isoprene v1.0: a new reduced mechanism for gas-phase isoprene oxidation, Geosci. Model Dev., 16, 1801-1821, https://doi.org/10.5194/gmd-16-1801-2023, 2023.

Wu, Y., Pour-Biazar, A., Koshak, W. J., and Cheng, P.: LNOx Emission Model for Air Quality and Climate Studies Using Satellite Lightning Mapper Observations, Journal of Geophysical Research: Atmospheres, 128, e2022JD037406, https://doi.org/10.1029/2022JD037406, 2023.

Xie, Y., Paulot, F., Carter, W. P. L., Nolte, C. G., Luecken, D. J., Hutzell, W. T., Wennberg, P. O., Cohen, R. C., and Pinder, R. W.: Understanding the impact of recent advances in isoprene photooxidation on simulations of regional air quality, Atmos. Chem. Phys., 13, 8439-8455, https://doi.org/10.5194/acp-13-8439-2013, 2013.

Xing, J., Mathur, R., Pleim, J., Hogrefe, C., Wang, J., Gan, C. M., Sarwar, G., Wong, D. C., and McKeen, S.: Representing the effects of stratosphere–troposphere exchange on 3-D O3 distributions in chemistry transport models using a potential vorticity-based parameterization, Atmos. Chem. Phys., 16, 10865-10877, https://doi.org/10.5194/acp-16-10865-2016, 2016.

Yarwood, G., Shi, Y., and Beardsley, R.: Impact of CB6r5 Mechanism Changes on Air Pollutant Modeling in Texas: https://wayback.archive-it.org/414/20210529064250/https:/www.tceq.texas.gov/assets/public/implementation/air/am/contracts/reports/pm/5822011221014-20200730-Ramboll-CB6r5MechanismChanges.pdf, 2020, last access: July 24, 2026.

Yienger, J. J. and Levy, H.: Empirical model of global soil-biogenic NOχ emissions, Journal of Geophysical Research: Atmospheres, 100, 11447-11464, https://doi.org/10.1029/95JD00370, 1995.

Zhao, J., Sarwar, G., Gantt, B., Foley, K., Henderson, B. H., Pye, H. O. T., Fahey, K. M., Kang, D., Mathur, R., Zhang, Y., Li, Q., and Saiz-Lopez, A.: Impact of dimethylsulfide chemistry on air quality over the Northern Hemisphere, Atmospheric Environment, 244, 117961, https://doi.org/10.1016/j.atmosenv.2020.117961, 2021.